University of Bath

UNIVERSITY OF BATH

PHD

Gypsy moth modelling with an application of optimal control theory

Whittle, Andrew John

Award date:
2004

Awarding institution:
University of Bath

[Link to publication](#)

Gypsy Moth modelling with an application of Optimal Control Theory

submitted by

Andrew John Whittle

for the degree of Doctor of Philosophy

of the

University of Bath
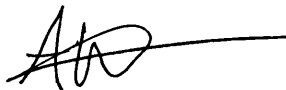
Department of Mathematical Sciences

December 2004

COPYRIGHT

Signature of Author ....

Andrew John Whittle

UMI Number: U191115

UMI®

Dissertation Publishing

ProQuest®

Acknowledgements

I would like to thank the following people:

- My supervisor, Dr Jane White, for her support, encouragement and perseverance with me during my time at Bath University

- EPSRC for funding, without which I would not have begun a PhD

- Neha and my parents for correcting my poor grammar

- Computer Support and the School Office, in particular Mary for sending off numerous versions of chapters to Jane for me.

- Professor Suzanne Lenhart and Dr Hem Raj Joshi for my visit to Knoxville and their help with Optimal Control Theory. Also to Suzanne for her return visit to Bath and allowing me the opportunity to continue my work in Knoxville

- My friends and office mates, James Coughlan, Matt Dorey, Kwabena Doku-Amponsah, Lorina Varvaruca, Viveka Vivekanandan, Ceridwyn Fiddes and Sarah Mitchell. Special thanks go to Damien Harwin, JF Williams, Joerg Berns-Muller, Steven White and Fas Yousaf who have always been able to solve all my MATLAB and LATEX problems. Also every member of the postgrad football team

- Lastly, I'd like to thank a very special person which without their help this thesis would never have been completed

Abstract

The gypsy moth has long been a pest in the forests of North America. Historically, population levels have displayed cyclic behaviour with outbreaks observed every 5-12 years. A number of different attempts have been made to eradicate or control gypsy moth outbreaks; however, gypsy moths continue to expand across the United States.

This thesis proposes a mathematical model as a tool for explaining and predicting population changes of gypsy moths, and to devise control strategies. Advantages of this modelling approach is that it is relatively less costly and time-consuming than experiments.

It has been suggested that there are two causes for the decline phase in gypsy moth population dynamics. These are, diseases caused by the Nuclear Polyhedrosis Virus (NPV), and a decrease in plant food quality (leaf quality). But previous modelling has not included the full impact of plant food quality. Foster, Schultz & Hunter (1992) considered gypsy moth and NPV interactions at different levels of leaf quality over a hundred year period. Others have focused solely on the host-pathogen interactions of the gypsy moth-NPV system and ignored plant food quality effects.

In this thesis we extend the Foster-Schultz-Hunter model (Foster et al. 1992) by including leaf quality into the dynamics of the system. First, we develop this model to include leaf quality as a changeable (dynamic) value. The potential complexities of field investigations into gypsy moth, NPV and leaf quality interactions makes modelling the system mathematically a more convenient approach for initial understanding.

Previously modelling has been based on an Anderson & May (1981) continuous time model. We extend this by considering a discrete time structure. This is because gypsy moth life cycles are annual and have distinct non-overlapping generations and hence forms a discrete time population system. Due to this we turn our attention to building a gypsy moth model using a more appropriate discrete time approach. We later introduce a spatial component to the model.

Once a good understanding of how gypsy moths interact with NPV and leaf quality is achieved then control strategies to contain outbreaks can be developed. In the latter part of the thesis we will study the model incorporating a control mechanism (by spraying areas with a biological control agent) with the intention to prevent major outbreaks, and optimal control strategies will be suggested to minimise costs.

ii

Contents

List of Figures

xi

List of Tables

Chapter 1

Introduction

The gypsy moth is a forest pest, which has caused extensive defoliation across the Northeastern United States over the past 130 years. Gypsy moths were brought from Europe to the United States in 1867 and have since caused millions of acres of deforestation which has harmed forest ecosystems. Gypsy moths in the US have not only affected forests, but recreational and urban vegetation as well.

There is a long history of attempts to eradicate, suppress or at least slow down the spread of the gypsy moths. These attempts have had varying degrees of success (Chapter 2, section 2.1.3). Despite these attempts the gypsy moth population continues to grow and spread to the south and west of the United States. Since the early 20th century, numerous predators and parasites have been introduced into the US in an attempt to control gypsy moth infestations. Over twenty of these parasites and predators have established themselves yet they have been unable to control gypsy moth population levels in the long term (Campbell 1981).

Gypsy moths are an irruptive pest whose population levels remain low for a number of years before suddenly exploding to reach maximum (outbreak) levels within 1-2 years. Fortunately outbreak levels are often unable to sustain themselves and a crash usually occurs within 2-3 years. This process was described as bimodal by Campbell (1981) and gypsy moth populations each year were described to be in one of four phases; innocuous, release, outbreak or decline (Figure 1-1). These phases are now well used terms in the literature. The population is said to be bimodal because there are two relatively stable population levels, innocuous and outbreak. The cause of the transition from one level to another is not completely understood, although extensive research seems to indicate that a decrease in predation is the catalyst for the release phase (Elkinton, Healy, Buonaccorsi, Boettner, Hazzard, Smith & Leibhold 1996) and a combination of Nuclear Polyhedrosis Virus (NPV) and plants' defence mechanism cause

1

a sharp decline phase (Foster et al. 1992). Disease of gypsy moth population levels from NPV initiated the development and production of a biological pesticide called Gypchek. This pesticide is now used by the United States Department of Agriculture (USDA) to fight infested areas and to prevent gypsy moths invading nearby uninfested areas. Gypchek is applied by spraying aerially in forest regions and on the ground in urban areas.
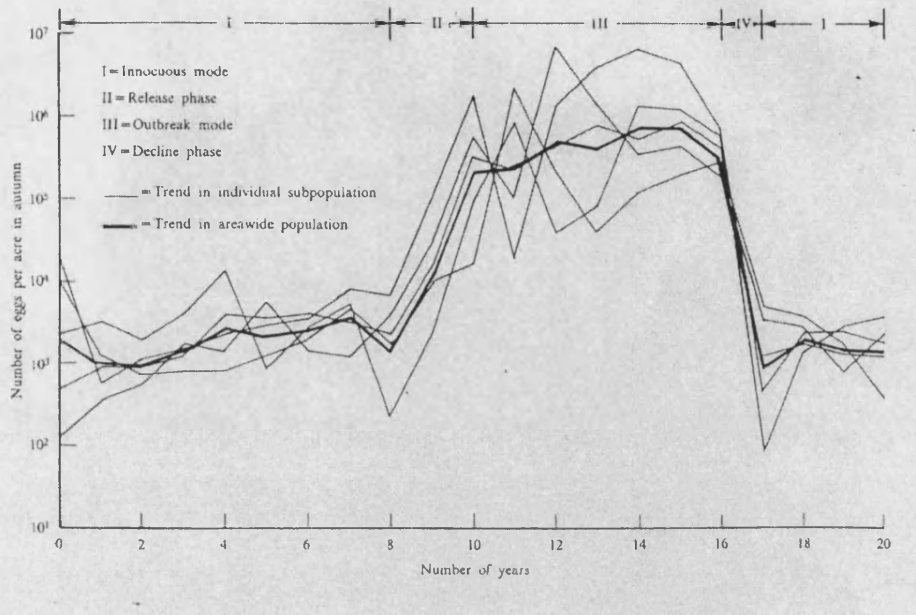
Figure 1-1: Four phases of gypsy moth populations: innocuous, release, outbreak and decline (source Campbell (1981)).

Spraying large areas is a costly process for the USDA. Gypsy moths are continuing to spread further across the United States and this is likely to continue. Residents are not always in favour of having their land and surroundings sprayed, due to irritation caused to eyes and skin, therefore heavy spraying is not an option in urban or recreational areas. This leads to the question of whether it is worthwhile continuing with an expensive spraying program. This is a question that can only be answered by management strategists.

Further to this it has been suggested that tannin, a chemical produced in plants, can affect the gypsy moth susceptibility to NPV. High levels of tannin in plants are caused by extensive defoliation of the plant and this results in food which is less favourable to gypsy moths. High tannin levels also reduce fecundity, however this is to a lesser extent

than the decrease in susceptibility. Therefore, we have a positive feedback system:
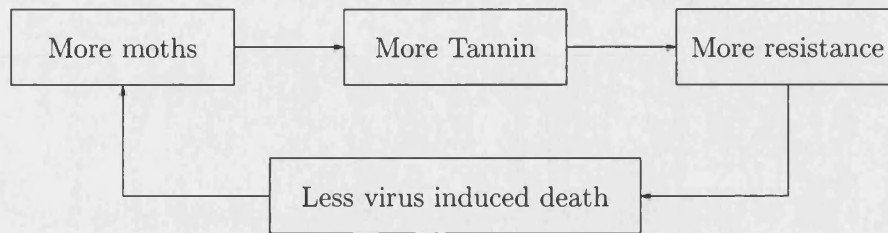
Figure 1-2: Positive feedback created by plants defence mechanism against severe defoliation by gypsy moths.

This system is important to consider when using NPV as a biocontrol agent.

The purpose of this thesis is first to formulate a mathematical model to forecast gypsy moth population levels. Mathematical modelling is a less costly and time-consuming approach than experiments in understanding the gypsy moths interaction with NPV and plant food quality. This model is then examined to see if and how outbreaks can be controlled via the use of the biological pesticide Gypchek. We can then optimise a control strategy in order to minimise the amount of spray, and consequently cost, required. This would reduce the unfavourable effects of excessive virus spraying on humans, as well as the high cost of the pest to society.

The thesis therefore aims to answer the following questions:

- How does tannin affect the dynamics of gypsy moth-NPV interactions?

- Can a discrete time system predict realistic gypsy moth population dynamics, and how does this compare with the continuous time model?

- Can spatial differences occur in gypsy moth population levels?

- How quickly are gypsy moths spreading across the US and can this spread rate be reduced?

- Will spraying help reduce gypsy moth outbreaks?

- What is the optimum strategy to reduce the combined costs of environmental and economic damage by gypsy moths and spray?

1.1 Layout of thesis

In Chapter 2 we look at the background of the gypsy moth problem and the ways in which mathematics can help answer the questions raised in the previous section. The chapter is split into two sections. The first begins with the reasons why gypsy moths are a pest in North America. This is followed by the history of gypsy moths in North America and a description of its life cycle and how it disperses. Many predators and parasites from Europe have been introduced to try to regulate gypsy moth population levels. These are discussed along with the influence that one pathogen has on gypsy moth growth - the NPV. Plant food quality, in particular tannin levels in leaves, plays a role in changing the vital rates of gypsy moths and also affects the resistance of gypsy moths to NPV infection. A discussion of this concludes the first section.

The second section concerns mathematical modelling and its applicability to biological systems. It examines previous continuous time modelling for gypsy moth-NPV interactions. The Foster et al. (1992) modelling system which incorporates plant food quality is described and compared with other models in the literature. Discrete time models for host pathogen systems have a long history beginning with the model of Nicholson & Bailey (1935). We discuss some of these models and why this type of modelling system is relevant. Following on from this we look at how discrete time models can be extended to include space using integrodifference equations. Integrodifference equations allow space to be continuous whilst populations remain discrete. Many studies have used integrodifference equations recently and we will discuss some of these. Optimal control has been applied several times to spatial PDE ecological models. Yet for hybrid systems, such as integrodifference models, optimal control is a newly developing area. We review one of the first studies in this field.

Chapter 3 examines the only known work to have modelled the combined effect of NPV and leaf quality on gypsy moth populations, i.e. Foster-Hunter-Schultz model (Foster et al. 1992). This models the gypsy moth-NPV interaction using continuous time differential equations. Leaf quality is included only in the sense that it changes parameter values, such as fecundity and disease induced mortality.

We extend this approach to incorporate tannin as a dynamic variable. This gives a more realistic representation of the system. Simulations are carried out to determine behaviours at various parameter sets. This model is simplified to consider a special case where the abundance of NPV has little effect on the level of infected eggs. This simplification enables us to perform some mathematical analysis and hence better understand the system. The chapter concludes with the interpretation of results and a comparison to the Foster et al. (1992) study.

Chapter 4 takes a different approach to model the system. Instead of using a continuous time model we develop a discrete time model. This approach is deemed to be a more appropriate due to the yearly non-overlapping generations formed in the gypsy moth life cycle (see Chapter 2, Section 1.2). We begin by building a model looking solely at gypsy moth populations, i.e. without any influence of NPV or plant food quality. This base model aids the understanding of how gypsy moths will grow for different fecundities and carrying capacities. NPV is then introduced into the system, and later plant food quality, comparing each of these stages with the original base model. The complete system is complex thus it is simulated numerically. One component of the complete system is the density dependent growth rate of gypsy moths. This component has a limiting effect on the population when approaching high density levels. This corresponds to overcrowding, where gypsy moths compete for limited resources. However, several authors have reported that despite high densities of gypsy moths there appears to be little mortality due to starvation (Doane 1970, Campbell 1981). They report instead that the NPV was the sole determinant in reducing the rate of growth of gypsy moth outbreaks. For this case, we look at a reduced system without density dependent growth. This reduced model is much simpler and some analysis can be carried out.

Chapter 5 considers the incorporation of Gypchek into the model system presented in Chapter 4. Gypchek is a biological control agent (ie. NPV) used against gypsy moth infestations. It should be noted that Gypchek is a very costly control method, however, there is an economic gain in reducing gypsy moth outbreaks. We therefore create a bioeconomic model consisting of the cost of control plus the cost of damage by gypsy moth infestations. We then seek an optimal control strategy to minimise the total cost. Simulations of the results are presented along with alternative strategies which are compared to the optimum.

Also following on from Chapter 4, Chapter 6 extends the model to include spatial effects. This is formulated using a system of integrodifference equations, which contain two components or stages. The first stage is the difference equations given in Chapter 4. The second is the dispersal or movement stage. This addition allows us to predict spatial patterns or patchiness formed by the system using bifurcation analysis. This will be important in determining spray strategies which are discussed in the subsequent chapter. Spatial effects also allow us to determine the rate of spread in virgin forests using travelling waves. We investigate the differences in travelling wave speeds for different spatial modelling systems, reaction diffusion and integrodifference equations. We then apply this information to consider the use of NPV as a barrier to slow the spread rate of gypsy moths.

5

Chapter 7 extends the spatial model to include control in a similar way to Chapter 5. We again create a bioeconomic model with the goal of minimising the total cost by seeking an optimal control strategy. The total cost consists of the cost of control by NPV (in the form of Gypchek) and the damage cost that gypsy moths cause to the economy at each spatial location. We prove the existence and uniqueness of the optimal control. Numerical results and interpretations are given.

Chapter 8 concludes by giving a summary of the achievements of the thesis as well as suggestions for future research. The bioeconomic model in Chapter 7 considers virus as a control input, however control by NPV may not be the only way to influence the gypsy moth system. New research is investigating the control of plant tannin levels. This would aid the control of gypsy moth infestations and brief discussion is given for future work.

Chapter 2

Background

2.1 Gypsy Moths - a problem

The problem is that gypsy moth populations historically outbreak to high levels every 7-12 years. Gypsy moths feed heavily on tree foliage during the caterpillar stage thus at outbreak levels, large number of caterpillars can cause extensive widespread defoliation. Trees can usually survive a year or two of partial defoliation, however either a longer period or more acute defoliation makes the trees become increasingly vulnerable to diseases. Consequently gypsy moths have contributed significantly to tree mortality in the United States. The loss of trees and forest areas have meant a huge drop in oak numbers throughout Northeastern United States. The gypsy moth population has had devastating effects and as Oak is one of the preferred hosts there is now a major concern over the potential loss of one Oak species, Querces spp. Furthermore deforestation has a knock on effect for local economies. The tourist industry is undoubtedly affected as well as industries such as timber. The gypsy moth also infests recreational and urban areas bringing undesirable results. Hence, the need for the United States Department of Agriculture (USDA) to become involved in controlling the pest.

Figure 2-1: Gypsy moth larva.

2.1.1 History of Gypsy Moth in America

The Gypsy Moth was first brought to the USA in 1868/9 by Ettiane Leopald Trouvelot from France. Trouvelot settled in Medford, near Boston, Massachusetts after fleeing France, his native homeland, during the coup d'etat in 1852. He was an artist and amateur entomologist whose main interest was in silkworms for the use in silk production. In the late 1860's, after visiting France, Trouvelot brought back some gypsy moth egg masses to his house at 27 Martle Street in Medford. There, it is said, he either cultivated them on trees in the back garden where some of them escaped or they were blown from a window sill. He notified the local entomologists yet nothing was done. Trouvelot returned home to France prior to the first outbreak of gypsy moths which occurred on the street where he had lived, in 1889. Over the past 115 years, gypsy moths have spread, first locally, then throughout the state, into neighbouring states and beyond. They have now established themselves throughout the Northeastern USA and continue to spread to the west, south-west and into Canada.

The first attempts to eradicate gypsy moths were made in 1890. These attempts were launched by the State and Federal Governments by poisoning gypsy moths whilst in the caterpillar stage. However this initiative failed as the insecticide damaged leaves and spraying was not effective. When the outbreak naturally subsided the funding was cut and the program was terminated. The next outbreak occurred in 1905 when the

gypsy moths had spread to several states. On this occasion, the government chose to import the gypsy moths natural enemies from Europe, but this also failed to reduce the population as predicted and funding was again cut. This program however, was ultimately effective in reducing the gypsy moth population by the 1920's.

Several attempts later, scientists introduced DDT which was found to be very effective against gypsy moths, as it was for many other insects. Over 3 million acres were treated with DDT by 1957. However, due to increasing health concerns, the program was abandoned and focus was directed to biological methods of control such as a pathogenic bacteria or NPV in the form of Gypchek. Initiative such as the Slow-the-Spread project have also been put in place to slow the spread of gypsy moths in the United States (Virginia Gypsy Moth Information Systems Lab).

2.1.2 The Gypsy Moth Life Cycle

The gypsy moth life cycle begins in late August or September each year when egg masses are laid. These egg masses remain in the egg stage over winter and are capable of survival at very low temperatures. The eggs hatch in the spring and the young larvae begin feeding immediately. Egg masses can on occasions become contaminated by free-living NPV during the winter. This can cause transovum vertical transmission of the disease as young larvae feed on their egg shells after hatching (Woods & Elkinton 1987).

The larvae go through either 5 or 6 instar stages of development. This period is when most feeding takes place and when the trees are first likely to suffer defoliation. Males go through 5 instar stages and are therefore lighter in mass which enables them to fly during adulthood. Females go through 6 instar stages and are too heavy to fly when adults, so dispersal or spread is not possible due to flight.

In early instar stages, the larvae are attracted to light and climb the trees to the crown. Once food is limited, the larvae hang by silken threads and are dispersed by the wind. Thus wind borne dispersal is one of the major reasons for gypsy moth spread across the country (Dwyer & Elkinton 1993). This type of dispersal is regarded as short range. The dispersal usually happens around the second or third instar stage and spraying is co-ordinated with this time. Another way the gypsy moths disperse is by human intervention, usually by accidental movement due to egg masses or larvae attaching themselves to motor vehicles. The egg masses and larvae can be carried very long distances; this method of dispersal is classified as long range.

After about 8 weeks of continuous feeding the larvae complete the instar stages and then pupate. The pupae are often found in bark crevices or located in other disguised locations. The pupa stage lasts for a few days before the adult moths hatch. Later in the season, adults reproduce. As females are unable to fly they attract a mate by

emitting a sex pheromone that male moths detect. After mating the female lays eggs in a single mass. The moths continue to live until late September when the cycle ends for this generation.
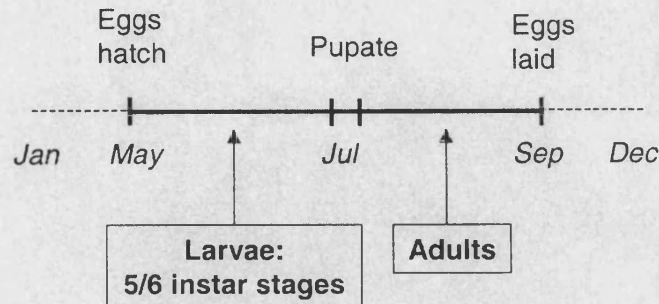
Figure 2-2: Gypsy moth life cycle.

2.1.3   Introduction of predators and parasites

Since the first outbreak considerable efforts have been made first to eradicate the gypsy moth and later just to control them. This started with the State and Federal Governments attempts to eradicate gypsy moths in the 1890's. This ultimately failed and gypsy moths continued to spread from Massachusetts into neighbouring states. Since then over 20 insects, parasites and predators have been introduced to try to dampen and control the growth and spread of gypsy moths. This has been described as one of the largest undertakings of its kind by authors such as Bess (1961), DeBach (1974) and May (1976). However, these introductions have come with different degrees of success. Small mammals perhaps have been one of the most important predators when gypsy moths are at sparse density levels, in particular white mice. It has also been reported that white mice may be a contributing factor for the release phase due to a decline in their predator numbers (Elkinton et al. 1996). However, these predators appear to play little role in the decline phase (Lauterschlager & Podewaite 1977). Many authors agree that disease plays a critical role when populations are at outbreak levels (Bess 1961), (Bess, Spurr & Littlefield 1947).

Doane (1970) and Kaya (1976) agree that NPV is a major component of infectious disease. The gypsy moth NPV is a naturally occurring baculovirus that is able to live freely in the environment. It infects gypsy moths by ingestion. Once ingested the virus replicates and kills its hosts within 14 days. Diseased gypsy moth canopes hang

from branches in an inverted V-shape releasing millions of NPV spores. Ultra-violet sunlight breaks down the virus, however some may survive by escaping the sunlight in shades or soils. These continue to be active and can infect gypsy moths for many years. Therefore, NPV induced disease is a critical factor in producing a decline phase in gypsy moth population levels. It is considered, however, to play only a minor role once gypsy moths are at innocuous modes again (Campbell 1981), since egg masses are sparse.

Figure 2-3: NPV infected gypsy moth larva.

2.1.4 The effects of plant food quality

Plant food quality has been reported as one of the main contributors to the collapse of gypsy moth outbreaks, yet has not had the same recognition when the system has been modelled. Plants are able to defend themselves when suffering extensive defoliation by changing their biochemical composition in order to make itself less appealing to its host. This is an attempt to reduce the plants consumption. The different biological composition of leaves affects the development of gypsy moths that feed on them (Edel'man 1963). Gypsy moths that were fed on different plants were found to have different rates of fecundity and survival (Hough & Pimental 1978). More recently tannin, a chemical found in leaves, was found to affect fecundity and mortality rates of gypsy moths (Schultz, Foster & Montgomery 1990). Further work revealed that the level of tannin in leaves fed on gypsy moths had a positive effect on their resistance to NPV (Keating, Yendol & Schultz 1988, Keating, Hunter & Schultz 1990). This finding was contrary to previous theories that gypsy moths eating poor quality food would be more vulnerable to infectious diseases.

Biochemical responses in plants do not happen immediately (D'Amico, Elkinton, Dwyer, Willis & Montgomery 1998) and it is unlikely that increases in tannin will

11

have any effect on gypsy moth populations during the release phase. However, during an outbreak, defoliated plants may develop a higher level of tannin to defend themselves. This is supported by Camboni who concluded that delayed bud burst in cork oak was entirely due to defoliation from the previous year (Campbell 1981). Indeed newly infested areas, where presumably plant food quality is higher and therefore more favourable for gypsy moths, were found to have higher fecundity values. This indicates that after an outbreak, future year plants will have a high tannin level to combat the risk of further defoliation. Ultimately this results in leaving plants too weak to fight off disease. Due to the reduced fecundity and increased resistance caused by higher levels of tannin, the varying levels of plant food quality should be included in the dynamics of modelling gypsy moth populations.

2.2 Mathematics in population dynamics

There has been a long history of mathematicians fascination with the problems associated with the development of populations or population dynamics. Indeed due to this, Renshaw (1991) rates population biology as perhaps the most mathematically developed area in all ecology. The earliest studies focused on small mammals and laboratory controlled organisms as these populations could easily be formulated into simple mathematical systems (Renshaw 1991). With the development of computers, fairly sophisticated continuous and discrete time models have been developed (Freedman 1980) as well as stochastic models (Ludwig 1974). More recent population dynamical modelling has centred around multi-species systems and the inclusion of spatial effects on population growth.

So, what is a population and what is population biology? The definitions given by Hastings (1997) are that "a population is a group of individuals of some species that have a high probability of interacting with each other" and that "population biology is simply the study of biological populations". To study biological populations we need to understand how and why population levels change. In order to do this, we require mathematical models to explain and predict these changes. Mathematical models are used to simulate population behaviour and are a popular alternative to expensive and time consuming experiments. These models are able to show how a system can be controlled, which has great applications to wildlife management practices (Clark 1976). Therefore, "models of population dynamics are central to understanding and application of optimal control techniques for containing pest outbreaks" - (Hallam & Levin 1986).

Mathematical modelling has also been very important and very successful in the

theory of spread (Hastings 1997) - in predicting future rates of invasion of populations. This has been important in helping to control the spread by developing programs to prepare areas for invasion and to design measures to reduce the speed of an invasion.

2.2.1 Models for gypsy moths

There have been several attempts to model gypsy moth - NPV interactions. These have all primarily based their model on Anderson & May (1981) host-microparasite system with a free-living microparasite stage (see Anderson & May (1981) (Model G)). We will now review a selection of models which have provided insight into the research presented in the thesis.

Foster, Schultz & Hunter (1992)

One of the first to model gypsy moth population dynamics was Foster et al. (1992). They considered a host pathogen model based on the Anderson & May (1981) free living pathogen system. The Anderson-May model was extended to incorporate the transovum vertical transmission associated with gypsy moth dynamics. The Foster-Schultz-Hunter model is as follows

$$\frac{dX}{dt} = a(1 - q(W))X - bX - dXW \tag{2.1a}$$

$$\frac{dY}{dt} = aq(W)X - (b + \alpha)Y + dXW \tag{2.1b}$$

$$\frac{dW}{dt} = \lambda Y - (u + v(X + Y))W \tag{2.1c}$$

where X is the susceptible population size of the host, Y is the population size of infected gypsy moths, W is the population size of the free living virus and $q(W)$ represents the proportion of newly born gypsy moths contracting the disease. The parameters of the system are given by

$$
\begin{aligned}
a &= \text{fecundity of gypsy moths} \\
b &= \text{natural mortality rate of gypsy moths} \\
d &= \text{horizontal transmission coefficient} \\
\alpha &= \text{disease induced mortality} \\
\lambda &= \text{rate at which the free living virus enters the environment} \\
u &= \text{death rate of the free living virus} \\
v &= \text{ingestion rate by the host of the free living virus}
\end{aligned}
$$

13

Vertical transmission occurs by egg contamination overwinter by NPV (Murray & Elkinton 1989). This transmission has been shown to increase with levels of NPV (Woods, Elkinton & Podgewaite 1989). Therefore Foster et al. (1992) allow vertical transmission to be represented by

$$q = \sqrt{W} \text{x} 10^{-8}$$

This is consistent with $q = 0.01$ for low virus years (10^{12} NPV per 0.4ha) and $q = 0.3$ for high virus years (10^{15} NPV per 0.4ha), (Woods & Elkinton 1987).

Plant food quality, in particular tannin levels, is found to influence certain parameters of the system. There are two main effects of tannin on gypsy moth dynamics, firstly susceptibility to the virus decreases with tannin and secondly fecundity decreases with tannin. Although tannin decreases the effect on the susceptibility to the virus it is greater than its effects on fecundity of gypsy moths (Schultz et al. 1990).

They found that when numerical simulations were conducted, for moderately high tannin levels, long lived pathogen and low natural gypsy moth mortality, the solutions closely fitted with field data. The dynamics also agreed with the predictions of limit cycles by Anderson and May which occurred if the pathogen was long lived and if there was high pathogenicity relative to intrinsic growth rate of the prey. However, simulations revealed that gypsy moth populations were stable at low tannin levels which lead to their conclusion that an increase in tannin has a destabilising effect on the population of gypsy moths.

Dwyer & Elkinton (1993)

Other modelling attempts for gypsy moth population dynamics have been made by Dwyer & Elkinton (1993). They modelled the dynamics of gypsy moths and its interaction with NPV. They, like the Foster et al. (1992) model, adapted the Anderson & May (1981) model. However, instead of looking at long-term behaviour in population dynamics, they adapted the model to consider within-season dynamics, due to the availability of data (Woods & Elkinton 1987).

The Dwyer and Elkinton model is given by

$$\frac{dS}{dt} = -vPS$$
$$\frac{dI}{dt} = vPS - vP(t-\tau)S(t-\tau)$$
$$\frac{dP}{dt} = \lambda vP(t-\tau)S(t-\tau) - uP$$

14

where S is the population size of susceptible gypsy moths, I is the population size of infected gypsy moths, P represents the density of pathogen in the environment and τ is the time between infection and death of the host. The other parameters v, u, λ are as described in (2.1).

As Dwyer and Elkinton only model within-season dynamics, there are three main differences between their model and the Anderson-May model. These are

(1) No fecundity of the gypsy moth or mortality due to non-virus induced death.

(2) There is a constant time delay between the point where the gypsy moth becomes infected and when death occurs (Dwyer 1991).

(3) No loss of pathogen particles due to consumption by the host.

The system is computed and compared with field data. Whilst some field data agreed favourably with model predictions under appropriate parameter selections, those with low initial levels of gypsy moth population did not. They therefore concluded that their assumption of the linear virus transmission is only valid at high density of gypsy moth initial population.

Dwyer and Elkinton suggested that a possible cause for the underestimation of virus transmission rate in low initial densities was due to immigration. They also considered this could be due to food quality for the gypsy moths, however they dismissed this since low levels of gypsy moths would cause low levels of defoliation and hence low transmission (Keating & Yendol 1987).

Dwyer, Dushoff, Elkinton & Levin (2000)

Dwyer, Dushoff, Elkinton & Levin (2000) later derived a two-compartment model by including seasonality in host reproduction and heterogeneity among the host in their susceptibility to the virus. This extended model differs from the Dwyer & Elkinton (1993) model by allowing heterogeneity in susceptibility as well as including host reproduction.

Contaminated egg masses introduce the pathogen into the host population each year by the process,

$$
\begin{aligned}
S(v,0) &= N_t f(v) \exp(-v\rho Z_t) \\
P(0) &= N_t \int f(v)(1 - \exp(-v\rho Z_t)) dv
\end{aligned}
$$

where S is the density of uninfected insects, P is the density of infectious cadavers. v is the rate of horizontal transmission of the disease and ρ is the ratio of effectiveness of infection at the time of egg hatch relative to infection later in the season. N_t, Z_t are

the initial densities of the host and pathogen respectively at generation t.

The within season dynamics are given by,

$$\frac{\partial S}{\partial t} = -vPS$$

$$\frac{dP}{dt} = P(t - \tau) \int vS(v, t - \tau)dv - uP$$

with τ the time between infection and death, and u the breakdown rate of cadavers. At the end of the season the gypsy moths reproduce with fecundity λ. In order to simplify the model for computation, the model was discretised as follows

$$N_{t+1} = \lambda N_t(1 - I)$$

$$Z_{t+1} = \rho f N_t I + \gamma Z_t$$

$$1 - I = \left(1 + C^2(N_t I + \rho Z_t)\right)^{\frac{-1}{C^2}}$$

The Anderson-May model concluded that high pathogen survival was needed for cyclic behaviour in population dynamics. However Dwyer & Elkinton (1993) found in their model, that even low pathogen survival could cause such outbreaks, partly due to newly hatched insect larvae having higher average susceptibility than the older larvae.

2.2.2 Discrete Time models

One branch of host-pathogen modelling is based on a host-parasitoid model which dates back to Nicholson & Bailey (1935) who created a discrete time model. The Nicholson-Bailey model was based on two main assumptions

1. The number of encounters E that parasitoids P_t have with hosts N_t is directly proportional to the hosts' density. Hence,

$$E = aN_t P_t$$

where a represents the probability that a given parasitoid will encounter a given host during its lifetime. This is usually termed "the area of discovery".

2. The number of encounters are distributed randomly among hosts. Therefore the probability that a particular host will not be attacked is given by the zeroth term of the Poisson distribution,

$$Prob(\text{A host is not attacked}) = \exp(-E/N_t) = \exp(-aP_t)$$

After making these two assumptions the Nicholson-Bailey model is given by

$$N_{t+1} = rN_t \exp(-aP_t)$$
$$P_{t+1} = N_t[1 - \exp(-aP_t)]$$

where r denotes the net rate of increase of the host. This system is unstable as it gives rise to only one nontrivial fixed point which never satisfies stability criteria for positive parameter values. However, the model was stabilised by adding density dependent mortality (Hassell 1978).

$$N_{t+1} = N_t \exp(r(1 - N_t/K) - aP_t)$$
$$P_{t+1} = N_t[1 - \exp(-aP_t)]$$

When the stable equilibrium existed, it was found that increasing the carrying capacity, K, destabilised the steady state. This was due to the reduced effect of density dependence on the host population.

Regniere (1984) also studied a discrete time insect pathogen system in which the host reproduced seasonally and the pathogen was only transmitted by direct vertical transmission or by horizontal transmission. He found that the pathogen could regulate the host population in absence of self-regulation. This could lead to a stable equilibrium or limit cycles.

White & Wilson (1999) constructed a discrete host-pathogen system including hosts that were resistant to the disease. The host population was split into two categories, those that were susceptible and those that were resistant. The model system is given by

$$S_{i+1} = \Lambda_S f(N_i)N_i$$
$$R_{i+1} = \Lambda_R(1 - f(N_i))N_i$$
$$P_{i+1} = \sigma_P P_i + \lambda(\sigma_S(0) - \sigma_S(P_i))S_i$$

where

$$N_i = \sigma_S(P_i)S_i + \sigma_R R_i.$$

S is the population of susceptible host, R is the population of resistant host and P is

density of free living pathogen particles.

$$\begin{aligned}
\Lambda_S &= \text{number of susceptibles born per surviving individual} \\
\Lambda_R &= \text{number of resistants born per surviving individual} \\
\lambda &= \text{number of pathogen propagules produced per infected death} \\
f(N) &= \text{fraction of surviving individuals giving birth to susceptibles} \\
\sigma_S(P) &= \text{density-dependent survival of susceptibles} \\
\sigma_R &= \text{density-independent survival of resistants} \\
\sigma_P &= \text{density-independent survival of pathogen propagules}
\end{aligned}$$

When the model was analysed with and without the resistant class, it was found that the resistant class stabilised the host pathogen interactions even though disease acts as the population regulator. Also, when the function of offspring which were born susceptible ($f(N)$) was constant, then the system was more stable. If resistance to the disease was changed so that it was density dependent, then unstable population dynamics would be stabilised and the behaviours of the system became reliant on the initial conditions.

2.2.3 Spatial Integrodifference models

The models discussed previously only examined the interactions of the host and pathogens populations over time. It is also important to consider what role space plays in these interactions. Continuous time (reaction diffusion) models have been shown to be driven unstable when dispersal is included, such as Turing instability. Also dispersal-driven instabilities have been observed in discrete time integrodifference models which we will now discuss.

Neubert, Kot & Lewis (1995) investigated the dispersal-driven instabilities in discrete-time predator-prey models formulated as a system of integrodifference equations. This formulation gives a far broader set of ecological conditions than do reaction diffusion models. They performed detailed analysis on the following system

$$\begin{aligned}
N_{t+1} &= N_t \exp[r(1 - N_t - P_t)], \\
P_{t+1} &= cN_t P_t.
\end{aligned}$$

This system gives rise to three steady states

$$(0,0); \quad (1,0); \quad \left(\frac{1}{c}, 1 - \frac{1}{c}\right)$$

18

with the nontrivial steady state stable provided the following conditions on parameters hold

$$1 \; < c < \; 2,$$
$$0 \; < r < \; \frac{4c}{3-c}.$$

If $c < 1$ then the predators are no longer able to survive leaving the prey to reach its natural carrying capacity i.e. solutions go to the (1,0) steady state. If $c > 2$ then a Hopf bifurcation occurs resulting in sustained oscillations of predator and prey populations. Finally if $r > 4c/(3-c)$ then a plus-one transcritical bifurcation occurs. This causes the predator population to undergo a catastrophic collapse to extinction.

The addition of spatial effects are incorporated into the system by coupling the dynamics with a redistribution kernel. This yields the non-linear integrodifference equations

$$N_{t+1}(x) \;=\; \int k_1(x-y)N_t(y)\exp\left[r(1-N_t(y)-P_t(y))\right]dy,$$

$$P_{t+1}(x) \;=\; \int k_2(x-y)cN_t(y)P_t(y)dy.$$

Redistribution kernels are chosen to be either Laplace distributions or double-gamma distributions to determine which combinations of dispersal distribution can drive the stable steady state system to become unstable. It is then reported that in three of the four possible permutations (the exception being the two Laplace distributions) plus-one bifurcations occur when there is sufficiently high prey over-dispersal. In the case of a minus-one bifurcation this can be achieved when intrinsic growth rate of prey, r, is high and for sufficiently high predator dispersal relative to prey. The third and final condition would yield a Hopf bifurcation but due to the properties of redistribution this bifurcation can never occur in a 2-D system. So the example shows how integrodifference equations can exhibit dispersal-driven instability.

In addition, the inclusion of space allows populations to spread or invade. As in reaction diffusion systems, constant speed travelling waves may form in the integrodifference model. However this is not always the case as for some dispersal kernels, travelling waves may occur which are not constant and instead have asymptotically infinite speed. Furthermore, constant wave speeds vary depending on the chosen dispersal kernel. Kot, Lewis & van den Driessche (1996) discussed wave speeds for integrodifference equations which we now review.

Kot et al. (1996) examined dispersal data of Drosophila given in Taylor (1978) but collected by Dobzhansky & Wright (1943). Taylor (1978) fitted several dispersal curves

to Dobzhansky & Wright (1943) data, five of these curves were converted to dispersal kernels by Kot et al. (1996). Forming an integrodifference model using Beverton-Holt dynamics Kot et al. (1996) calculate wave speeds for each of the five different dispersal kernels. Four of the dispersal kernels gave rise to constant speed travelling waves each with a different speed. For the remaining dispersal kernel, an accelerating wave with asymptotically infinite speed of expansion occurred. This kernel was derived from the dispersal curve that had the best fit to the data. Following this work, Veit & Lewis (1996) used this to describe the accelerating spread of house finches across eastern North America. Further to this, Kot (2002) has classified travelling wave speeds into 3 categories as follows

1. Constant speed travelling waves. These occur when the dispersal kernel $k(x)$ has moment generating function

$$M(s) = \int K(x)e^{sx}dx$$

for some neighbourhood of s about zero.

2. Asymptotically infinite wave speed. These occur when the dispersal kernel has finite moment

$$\mu_n = \int x^n K(x)dx$$

of all orders n, but no moment generating function.

3. Populations that grow faster than any polynomial in time. These occur when the dispersal kernels have moments that are infinite.

2.2.4 Optimal control

There are several examples of optimal control applied to spatial ecological models (Lenhart & Bhat 1992, Bhat, Huffaker & Lenhart 1993, Neubert 2003) yet these have all focussed on continuous time systems. In Lenhart & Bhat (1992), a bioeconomic model for pest control is created for a beaver population. The beaver population causes damage and consequently a cost to the economy yet efforts to control the population also brings about a cost. A dilemma occurs which can be resolved by forming an optimal control problem which is solved by using an adjoint system. This method is described in Lions (1971).

Discrete time spatial systems, in particular integrodifference models, have not received the same attention. However Joshi, Lenhart & Gaff (in press) rectifies this with the first study of optimal control in an integrodifference population model. Here, Joshi et al. (in press) consider harvesting a crop with the goal of maximising profit by

controlling the amount of harvest. Existence and uniqueness of an optimal control is proved and using a combination of the discrete maximum principle (Clark 1990) and optimal control of infinite dimensional systems (see Lions (1971)) an adjoint system is derived. Numerical results are given that demonstrate how different dispersal kernels used to describe crop movement affect the optimal solution.

Chapter 3

Extending previous Gypsy Moth modelling

Many studies have considered how parasites or parasitoids may regulate their hosts population. Extensions to these studies have included hosts with multiple parasites (Dobson 1985, Hochberg & Holt 1990), parasites infecting multiple hosts (Bowers & Begon 1991, Holt & Pickering 1985) or a host-parasite-hyperparasite system (Hochberg, Hassell & May 1990). But there have been few studies on any effects that the hosts food source has on a host-pathogen system.

Population cycles of hosts have often been attributed to the interaction of purely the host and its pathogen. Studies, such as Anderson & May (1981) host-pathogen system show how as a hosts population grows a pathogens population follows. Once the pathogen population reaches high levels mass infection occurs and the host population decays. Due to this, the pathogen population subsequently decreases. This then allows the host population to grow again and thus the cycle continues.

Not all population cycles behave exactly like this though. Some host populations may increase to such high levels that their food source becomes depleted. In such a case, as with the gypsy moths (Schultz et al. 1990), plants invoke a natural response to protect themselves against severe defoliation. This response will influence the interaction between the gypsy moth and the virus. Furthermore, there is an added complication to this host-pathogen system. Namely, that the response by plants to prevent defoliation is also found to increase the resistance of gypsy moths to NPV infection (Keating et al. 1988, Keating et al. 1990). Foster et al. (1992) modelled this system as described in Chapter 2.

In this chapter, we build on the model presented by Foster et al. (1992). We do this by making two modifications. The first is to make a change to the vertical transmission

function, where gypsy moth larvae die several days after hatching due to overwinter contamination of egg masses by NPV. The second modification is to include tannin as a dynamic variable. This allows us to include the two essential effects of tannin, reduced fecundity and increased resistance to NPV infection, in a different way to the approach taken by Foster et al. (1992). The model is simulated numerically and compared to the simulations of Foster et al. (1992). Lastly, we make a simplification to the model in order to take a more detailed look at the effects of tannin on the system.

3.1 Overwinter contamination of egg masses by NPV

Overwinter contamination of egg masses is usually caused by laying egg masses on surfaces contaminated by NPV (Murray & Elkinton 1989). On hatching, gypsy moth larvae can become infected due to the presence of virus on the egg mass surface (Doane 1970). This was found to happen more frequently when virus populations were at high levels (Woods et al. 1989). Due to this, Foster et al. (1992) included a transmission term in their model that accounts for the increase in overwinter contamination seen at higher free-living virus levels.

The function chosen to represent this term was the square root function

$$Q(W) = \sqrt{W} \times 10^{-8} \tag{3.1}$$

where W is the amount of free-living virus in the environment and $Q(W)$ represents the proportion of egg masses that become infected over winter. This function displays the characteristics of increasing contamination with increasing virus levels and also compares well with estimates from the field by Woods & Elkinton (1987). Also simulations presented by Foster et al. (1992) display realistic behaviour of populations compared to field data. However, other parameter sets chosen give less plausible results due to the unboundedness of the function $Q(W)$. Therefore, in this section, we present an alternative function for the overwinter contamination term and compare the behaviour on the system of this alternative function to the behaviour of Foster et al. (1992).

3.1.1 Alternative function

We choose a simple alternative function to represent the overwinter contamination of egg masses

$$Q(W) = \frac{qW}{k + W} \tag{3.2}$$

where q is an upper bound for the overwinter contamination term and k determines the steepness of the function. This function (3.2) also displays the characteristics sought

for the vertical transmission term as well as being bounded. As q is an upper bound we select $q < 1$ to ensure the function $Q(W)$ remains as a probability for all $W \geq 0$. Figure 3-1(a) shows the square root function (3.1) plotted against the alternative function (3.2) for four different values of parameter k. We see that the alternative function is a good substitute for the square root function.

(a)   (b)
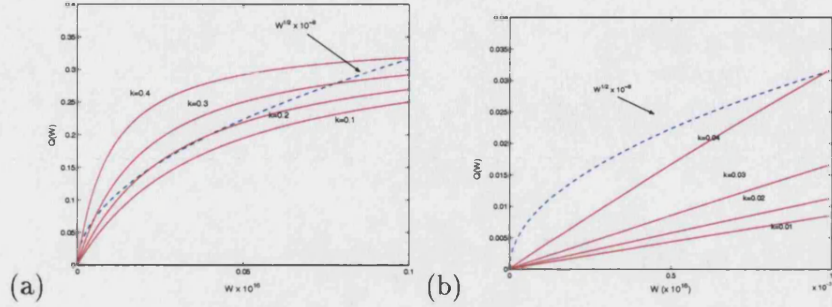
Figure 3-1: Plots show the square root function (3.1) against the alternative function (3.2). Figure (a) shows the alternative function for $q = 0.35$ and $k = 0.01 \times 10^{16}$, 0.02×10^{16}, 0.03×10^{16}, 0.04×10^{16}. Figure (b) shows the functions on a smaller scale.

Figure 3-1(b) magnifies the origin of Figure 3-1(a). Here we see that for the square root function, very small levels of virus have a considerable impact on the contamination of egg masses. The alternative function does not allow for such a large proportion to be infection. Hence the alternative functions finite growth at the origin causes significantly less egg masses contamination than the square root functions infinite growth at the origin. This is more realistic as using the square root function can cause problems with simulated behaviour of Foster et al. (1992) model because virus levels that could have died out may persist.

3.1.2 The model

The model we present in this section is a continuous-time differential system. The model is based on Foster et al. (1992) except it includes the alternative egg mass contamination term (3.2). The model is given by,

$$\frac{dH}{dt} = a(H - Y) - bH - \alpha Y \tag{3.3a}$$

$$\frac{dY}{dt} = a\frac{qW}{k + W}(H - Y) - (b + \alpha)Y + \beta W(H - Y) \tag{3.3b}$$

$$\frac{dW}{dt} = \lambda Y - (u + vH)W \tag{3.3c}$$

24

where H is the total population size of gypsy moths (susceptible + infecteds), Y is the population size of infected gypsy moths, W is the population size of the free-living virus and t is time. The model parameters are:

a = fecundity of susceptible hosts

b = natural mortality rate of gypsy moths

β = horizontal transmission coefficient

α = disease induced mortality

λ = rate at which the free-living virus enters the environment

u = death rate of the free-living virus

v = ingestion rate by gypsy moths of the free-living virus

Note that the first differential equation represents the rate of change of the total gypsy moth population. In Foster et al. (1992), the first equation represents the rate of change of only the susceptible gypsy moths. By a replacement of $H = X + Y$ we would obtain the same model form as Foster et al. (1992).

3.1.3 Model analysis

Steady state solutions occur when

$$
\begin{aligned}
H(t) &= H &&= \text{constant}, \\
Y(t) &= Y &&= \text{constant}, \\
W(t) &= W &&= \text{constant}.
\end{aligned}
$$

This gives rise to the set of simultaneous equations

$$
\begin{aligned}
0 &= a(H - Y) - bH - \alpha Y, &&\text{(3.4a)} \\
0 &= a\frac{qW}{k + W}(H - Y) - (b + \alpha)Y + \beta W(H - Y), &&\text{(3.4b)} \\
0 &= \lambda Y - (u + vH)W. &&\text{(3.4c)}
\end{aligned}
$$

Solving the equations (3.4) gives two biologically realistic steady state solutions. The first solution we call the trivial steady state and the second, the nontrivial steady state,

$$
(H^*, Y^*, W^*) = (0, 0, 0);
$$
$$
\left(\frac{u(a + \alpha)W^*}{\lambda(a - b) - v(a + \alpha)W^*}, \frac{u(a - b)W^*}{\lambda(a - b) - v(a + \alpha)W^*}, W^* \right)
$$

where W^* is a solution of the quadratic expression

$$
\beta(W^*)^2 + (a - aq - b - k\beta)W^* - k(a - b) = 0
$$

The only feasible solution of a quadratic expression is

$$W^* = \frac{a - aq - b - k\beta + \sqrt{(a - aq - b - k\beta)^2 + 4\beta k(a - b)}}{2\beta}. \tag{3.5}$$

as the other root always remains negative. The existence of the nontrivial steady state only occurs if it satisfies the two conditions

$$a > b, \tag{3.6a}$$

$$\lambda(a - b) > v(a + \alpha)W^*. \tag{3.6b}$$

The first inequality (3.6a) is that the birth rate of gypsy moths is greater than its mortality rate. If this were untrue, then the gypsy moths would become extinct. The second inequality (3.6b) is likely to hold as parameter estimates indicate that the left hand side of the inequality is several orders of magnitude higher than the right hand side.

We can find conditions for stability of the steady states from the Jacobian matrix of the system (3.3)

$$J = \begin{pmatrix} a - b & -(a + \alpha) & 0 \\ a\frac{qW}{k+W} + \beta W & -a\frac{qW}{k+W} - (b + \alpha) - \beta W & \left[\beta - a\frac{qk}{(k+W)^2}\right](H - Y) \\ -vW & \lambda & -(u + vH) \end{pmatrix}.$$

Linear stability for the two steady states are determined by the eigenvalues of the Jacobian matrix at the steady state. For the trivial state, the eigenvalues are

$$\sigma_1 = a - b,$$
$$\sigma_2 = -(b + \alpha),$$
$$\sigma_3 = -u.$$

As σ_2 and σ_3 are always negative, the stability depends only on the first eigenvalue σ_1. Hence, for stability of the trivial steady state we have just one condition

$$a < b. \tag{3.7}$$

Therefore for (3.7), if the birth rate of gypsy moths is less than the death rate, the gypsy moth population will die out. Conversely, if the condition does not hold (the birth rate is greater than the death rate) then the gypsy moth population will persist.

For the nontrivial steady state, the Jacobian gives three conditions. Two of these

conditions are always satisfied (see Appendix A). This leaves the remaining condition which determines stability of the steady state

$$\left(b + \alpha + u + \frac{vu(a + \alpha)W^*}{\lambda(a - b) - v(a + \alpha)W^*} \right)$$
$$\left(\frac{\lambda(a - b)(k + W^*) - \lambda[d(W^*)^2 + k(a - b)]}{\lambda(a - b) - v(a + \alpha)W^*} \right) \leq d(W^*)^2 + k(a - b)$$

where W^* is given in (3.5). This inequality is much more complex and it is not easy to see if it is likely to hold true. In fact as shown next, we see that the condition is sensitive to parameter estimates.

3.1.4 Comparisons

Foster et al. (1992) simulated model behaviour at various tannin levels where model parameters were dependent on the tannin level. We look at parameter sets where their model produced similar behaviour of population levels to that seen in the field. These occurred for low natural mortality rate for gypsy moths, long lived free-living virus and moderate to high tannin levels. We compare this with behaviour for the alternative function (3.2).

From simulations, we see similar fluctuating population cycles as described by Foster et al. (1992). Figures 3-2, 3-3 and 3-4 show these population cycles for different q and k parameters. Other parameter values are taken from estimates given in Foster et al. (1992). From extensive numerical simulations, we find that oscillatory behaviour was easily observed at low values of q ($q = 0.10$, $q = 0.30$). At these low values of q, a wide range of k values display similar oscillatory behaviour to that found by Foster et al. (1992).
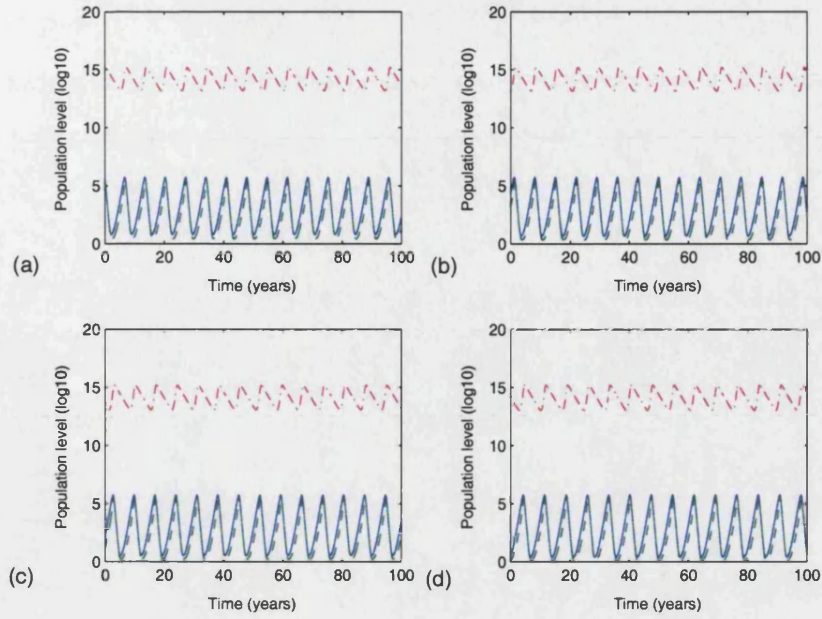
Figure 3-2: Plots show similar behaviour of populations using the alternative function for overwinter contamination of egg masses (gypsy moths - blue, infected gypsy moths - green, NPV - red). For Figure (a) $k = 0.01 \times 10^{16}$, Figure (b) $k = 0.02 \times 10^{16}$, Figure (c) $k = 0.03 \times 10^{16}$, Figure (d) $k = 0.04 \times 10^{16}$. Other parameters are $a = 6.0$, $q = 0.1$, $b = 3$, $\beta = 10^{-14}$, $\alpha = 5$, $\lambda = 1.49 \times 10^{10}$, $u = 1$, $v = 10^{-14}$.

For higher values of q ($q = 0.35$, $q = 0.4$), oscillatory behaviour was observed but only for a limited range of k values.
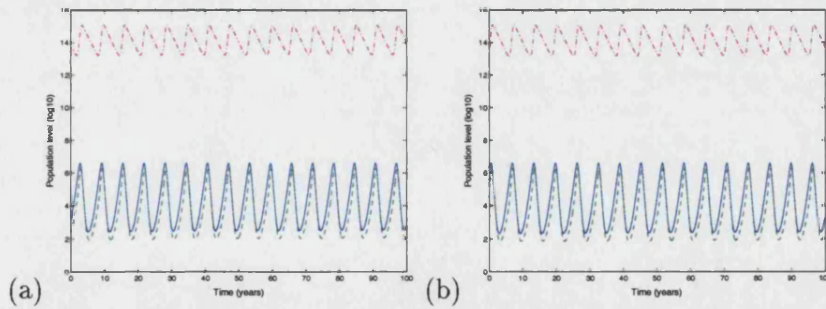
Figure 3-3: Plots show population behaviours for the alternative function for higher upper bounds (gypsy moths - blue, infected gypsy moths - green, NPV - red). Figure (a) $q = 0.35$, $k = 0.058 \times 10^{16}$ & Figure (b) $q = 0.4$, $k = 0.07 \times 10^{16}$. Other parameters are $a = 6.0$, $b = 3$, $\beta = 10^{-14}$, $\alpha = 5$, $\lambda = 1.49 \times 10^{10}$, $u = 1$, $v = 10^{-14}$.

28

For much smaller values of k, smaller oscillations or a nontrivial steady state occur. On the other hand, for larger values of k much bigger unrealistic oscillations appear. These are shown in Figure 3-4 where k varies showing behaviour from small oscillations through to very large oscillations.
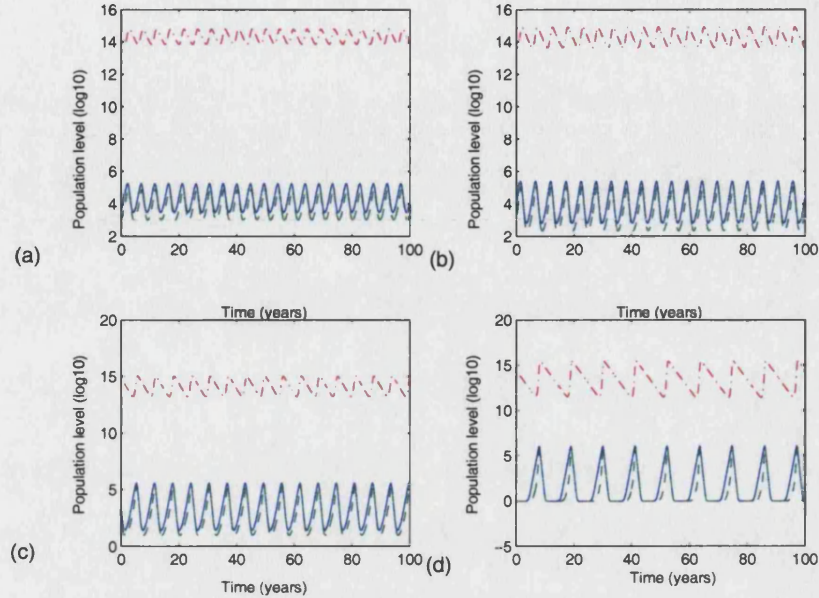
Figure 3-4: Plots show behaviour of populations using the alternative function for overwinter contamination of egg masses (gypsy moths - blue, infected gypsy moths - green, NPV - red). For Figure (a) $k = 0.01 \times 10^{16}$, Figure (b) $k = 0.02 \times 10^{16}$, Figure (c) $k = 0.03 \times 10^{16}$, Figure (d) $k = 0.04 \times 10^{16}$. Other parameters are $a = 6.0$, $q = 0.3$, $b = 3$, $\beta = 10^{-14}$, $\alpha = 5$, $\lambda = 1.49 \times 10^{10}$, $u = 1$, $v = 10^{-14}$.

In summary, we have discovered parameter values of the alternative function (3.2) that give the same behaviour as Foster et al. (1992) found. Nonetheless, this model like Foster et al. (1992) only describes outcomes when tannin is held constant over time.

3.2 The inclusion of tannin as a dynamic variable

Foster et al. (1992) considered behaviours of gypsy moth virus interactions over a set time period for different tannin levels. In this section, we adapt the model to incorporate tannin as a dynamic variable allowing tannin levels to change during the time period. This affects the birth rate, a, and we replace this with a function which is dependent on tannin levels, $a(T)$. The function is then changeable over time i.e.

$T = T(t)$ where t is time. We choose a decreasing function in tannin levels

$$a(T) = \frac{a}{1 + dT}.$$ (3.8)

where a is the birth rate when no tannin is present and d is a tannin coefficient that determines the amount of decay tannin causes on the birth rate. The function has an upper bound value, a, which it obtains when tannin levels are zero.

We also let the gypsy moth susceptibility to viral infection be dependent on the level of tannin. For the susceptibility, we use the function

$$\beta(T) = \frac{\beta}{1 + cT}.$$ (3.9)

where β is the transmission rate of the virus to the gypsy moth and c is a tannin coefficient that determines the amount of decay tannin causes on the susceptibility to infection. This is a decreasing function in tannin so the resistance to infection increases as tannin levels increase.

3.2.1 The model

The model is based on the model approach presented by Foster et al. (1992). However, tannin has been incorporated into the ordinary differential equation (ODE) system as discussed above. Then a fourth ODE is added to describe the rate of change of tannin. Levels of tannin increase as a response to an increase in the number of gypsy moths. It is assumed that tannin will decrease exponentially. The model is expressed by

$$\frac{dH}{dt} = \frac{a}{1 + dT}(H - Y) - bH - \alpha Y$$ (3.10a)

$$\frac{dY}{dt} = \frac{a}{1 + dT}Q(W)(H - Y) - (b + \alpha)Y + \frac{\beta W(H - Y)}{1 + cT}$$ (3.10b)

$$\frac{dW}{dt} = \lambda Y - (u + vH)W$$ (3.10c)

$$\frac{dT}{dt} = rH - sT$$ (3.10d)

where H is the total population size of gypsy moths (susceptible + infecteds), Y is the population size of infected gypsy moths, W is the population size of the free living virus, T is a measure of tannin level and t represents time. The model parameters are as given in (3.3) with the additional parameters:

c = tannin coefficient representing the impact of tannin on susceptibility to infection

d = tannin coefficient representing the impact of tannin on gypsy moth fecundity

r = the production rate of tannin per gypsy moth

s = the decay rate of tannin

As discussed in the previous section, we represent the proportion of offspring infected at egg hatch by a bounded increasing function

$$Q(W) = \frac{qW}{k + W} \tag{3.11}$$

3.2.2 Numerical simulations

The model (3.10) with the overwinter contamination of egg masses term (3.11) was simulated numerically. Simulations were run over a time period of 100 years. Typical population behaviours are shown in Figures 3-5 & 3-6
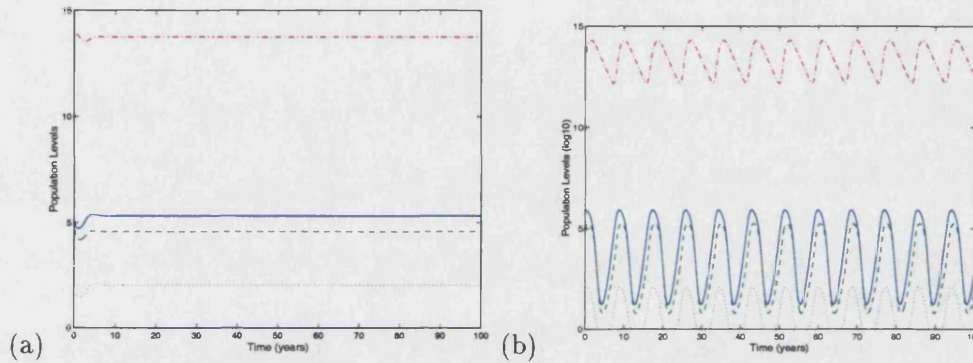
Figure 3-5: Plots show typical dynamic behaviour for realistic parameter values (gypsy moths - blue, infected gypsy moths - green, NPV - red, tannin - aqua). Figure (a) shows a stable steady state solution ($s = 2.0$). Figure (b) shows oscillatory population cycles ($s = 7.0$). Parameters are; $a = 6; b = 2; \beta = 10^{-14}; k = 2 * 10^{14}; \alpha = 5; \lambda = 1.49 * 10^{10}; u = 1.0; v = 10^{-14}; q = 0.4; r = 0.1; c = 0.1; d = 0.0067$.

We find that the dynamic behaviours fall into 4 categories; stable steady state, oscillatory cycles, extinction or gypsy moth persistence and virus extinction. In Figure 3-5(a) a stable steady state solution occurs for slow decay rate of tannin ($s = 2.0$) and slow production rate of tannin ($r = 0.1$). For a faster decay rate of tannin ($s = 7.0$) the population behaviour changes to oscillatory population cycles, Figure 3-5(b). Similarly, it was observed that a reduction in the production of tannin also caused population levels to become oscillatory.

31

(a)   (b)
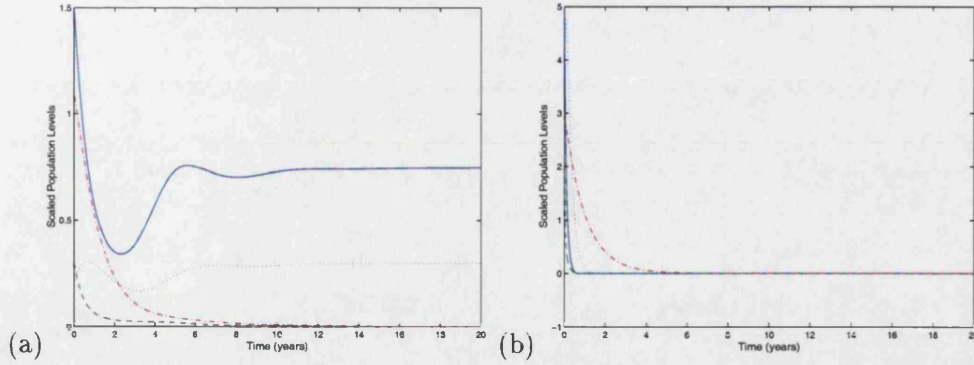
Figure 3-6: Plots show dynamic behaviour for the gypsy moth-NPV-tannin model (gypsy moths - blue, infected gypsy moths - green, NPV - red, tannin - aqua). Figure (a) shows the persistence of gypsy moth population when NPV dies out ($b = 2$, $\alpha = 5$, $r = 0.6$, $s = 0.4$). Figure (b) shows the decay of gypsy moth, NPV and tannin ($b = 3.5$, $\alpha = 25$, $r = 0.1$, $s = 5.0$). Parameters are; $a = 6$; $\beta = 10^{-14}$; $k = 2\text{x}10^{14}$; $\lambda = 1.49\text{x}10^{10}$; $u = 1.0$; $v = 10^{-14}$; $q = 0.4$; $c = 0.1$; $d = 0.0067$.

Furthermore, for very high production rate and low decay rate of tannin, the virus population died out leaving tannin as the only regulator of the gypsy moth population (Figure 3-6(a)). We also observe, in Figure 3-6(b), extinction of gypsy moths when the natural death rate of gypsy moths, b, and the disease induced mortality rate, α, are large.

Therefore, the new model, with the inclusion of tannin as a dynamic variable, still displays the same behaviour as the Foster-Schultz-Hunter model. We see, in Figure 3-5(b), that when the production rate of tannin is low and the decay rate of tannin is high the population behaviour is oscillatory. This behaviour compares well with Foster et al. (1992) findings and with realistic gypsy moth population estimates from field data. In addition, we found that oscillatory populations can be stabilised by either a reduction in the decay rate of tannin or by an increase in the production rate of tannin.

In the next section, we investigate further by considering a simplified version of the gypsy moth model.

3.3 Simplified model system

The previous section gave numerical simulations to show the behaviour of the gypsy moth-NPV interactions with tannin as a dynamic variable. In this section, we take a more detailed look at a simpler version of the model. We analyse this simplified

32

model to find steady states and stability conditions for two cases; tannin included as a dynamic variable and when tannin remains constant (i.e. no influence on the gypsy moth-NPV interactions). We look at these two cases to compare the dynamic tannin model presented in the last section with constant tannin levels in the Foster et al. (1992) model.

3.3.1 The model

We need to simplify the model in order to analyse the system to more easily compare constant tannin levels with tannin as a dynamic variable. We do this by making the following simplifications. Firstly, we consider the major impact that tannin has on the gypsy moth-NPV interaction i.e. we include the decrease in susceptibility of gypsy moths to NPV infection when tannin levels are high. The reduction in fecundity is shown to have lesser effect than the decrease in susceptibility (Schultz et al. 1990). Secondly, we let the proportion of overwinter contamination of egg masses, q, remain constant. Making these simplifications to model (3.10), we obtain the following

$$\frac{dH}{dt} = a(H - Y) - bH - \alpha Y, \tag{3.12a}$$

$$\frac{dY}{dt} = aq(H - Y) - (b + \alpha) Y + \frac{\beta}{1 + cT} W(H - Y), \tag{3.12b}$$

$$\frac{dW}{dt} = \lambda Y - (u + vH) W, \tag{3.12c}$$

$$\frac{dT}{dt} = rH - sT. \tag{3.12d}$$

As before, H represents the total population size of gypsy moths, Y represents the population size of infected gypsy moths, W represents the amount of free living virus and T represents the tannin level. The parameters of the system are as given in the model (3.10).

3.3.2 Model analysis

We analyse the model for the following cases. In the first case, we suppose tannin levels are constant and in the second case, we allow tannin to be a dynamic variable.

Case (i): Constant level of tannin

To analyse the model for a constant level of tannin we set $r = 0$, $s = 0$ and $c = 0$ in (3.12). By setting

$$
\begin{aligned}
H(t) &= H &&= constant \\
Y(t) &= Y &&= constant \\
W(t) &= W &&= constant
\end{aligned}
$$

we find the steady state solutions from the following simultaneous equations

$$0 = a(H - Y) - bH - \alpha Y \tag{3.13a}$$

$$0 = aq(H - Y) - (b + \alpha) Y + \beta W (H - Y) \tag{3.13b}$$

$$0 = \lambda Y - (u + vH) W. \tag{3.13c}$$

Solving (3.13) results in two steady state solutions

$$(H^*, Y^*, W^*) = (0, 0, 0); \quad \left(H^*, \frac{a - b}{a + \alpha} H^*, \frac{a - aq - b}{\beta} \right) \tag{3.14}$$

where

$$H^* = \frac{u(a + \alpha)(a - aq - b)}{\beta \lambda (a - b) - v(a + \alpha)(a - aq - b)}$$

The first solution in (3.14) is the trivial solution and this solution exists for all parameter values. The second solution of (3.14) is the nontrivial steady state and this only occurs if the parameter set satisfies the inequalities

$$\beta \lambda (a - b) \geq v(a + \alpha)(a - aq - b) \geq 0. \tag{3.15}$$

Parameter estimates for a, b, q and α have similar orders of magnitude. β and v have similar orders of magnitude as well. As λ is large, then (3.15) is likely to hold and the nontrivial steady state will exist.

The stability of the steady states are found from the Jacobian matrix

$$
J = \begin{pmatrix}
a - b & -a - \alpha & 0 \\
aq + \beta W & -aq - b - \alpha - \beta W & \beta(H - Y) \\
-vW & \lambda & -(u + vH)
\end{pmatrix} \tag{3.16}
$$

at $(H, Y, W) = (H^*, Y^*, W^*)$. For the trivial steady state, the eigenvalues of (3.16) are

$$
\begin{aligned}
\sigma_1 &= a - aq - b, \\
\sigma_2 &= -(b + \alpha), \\
\sigma_3 &= -u.
\end{aligned}
$$

Stability occurs if the real part of all the eigenvalues are negative. As the eigenvalues σ_2 and σ_3 are always negative, the stability of the trivial steady state relies on just one σ_2 and σ_3 are always negative, the stability of the trivial steady state relies on just one condition

$$
a - aq < b.
$$

That is, if the effective birth rate, $a - aq$, of gypsy moths is less then its death rate, b, then extinction will occur. For the nontrivial steady state, the Jacobian gives the following characteristic polynomial

$$
\chi^3 + A\chi^2 + B\chi + C = 0
$$

where

$$
\begin{aligned}
A &= b + \alpha + u + vH, \\
B &= (b + \alpha)(u + vH) - \beta\lambda(H - Y), \\
C &= (H - Y)[\beta\lambda(a - b) - v(a + \alpha)(a - aq - b)].
\end{aligned}
$$

Stability can be found from the characteristic polynomial by the Routh-Hurwitz conditions (Murray 2002)

$$
A > 0, \quad C > 0, \quad AB - C > 0.
$$

As $H \geq Y \geq 0$, then the first condition holds. The second condition holds due to the existence condition (3.15). Therefore, the stability of the nontrivial steady state depends only on the third condition,

$$
a - aq - b \leq \frac{[(b + \alpha)\Gamma + u\beta\lambda(a - b)]\beta\lambda aq}{\Gamma^2} \tag{3.18}
$$

where

$$
\Gamma := \beta\lambda(a - b) - v(a + \alpha)(a - aq - b). \tag{3.19}
$$

If inequality (3.18) holds, then any initial conditions that start near the steady state value will be attracted towards it.

To gain a better understanding of the system, we can set $v = 0$ because parameter estimates indicate that this parameter is very small. Hence (3.18) reduces to

$$(a - b)(a - aq - b) \leq (a + \alpha + u)aq. \tag{3.20}$$

Therefore, the disease induced death, α, or proportion infected immediately after birth, q, needs to be sufficiently high to keep the population at a steady level. Furthermore, we see that as q increases from zero, the behaviour changes from oscillatory population cycles to a stable nontrivial solution. A further increase causes the nontrivial steady state to lose stability and existence, leaving the population to crash to a stable trivial steady state solution.
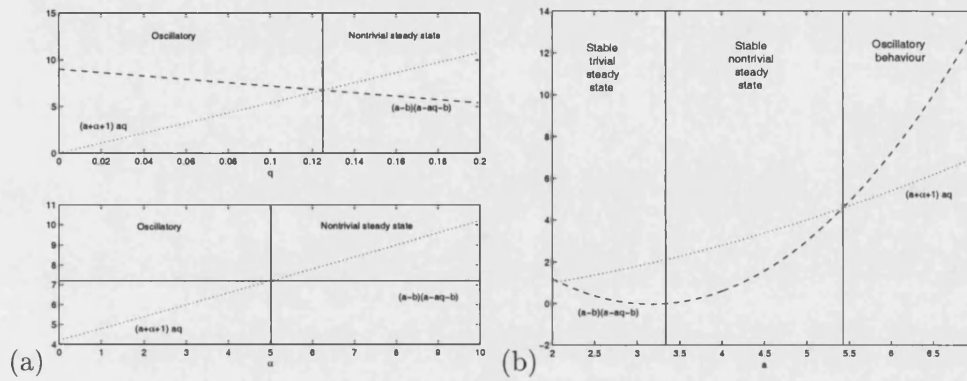
Figure 3-7: Plots show the population behaviour of the system for varying several key parameters. Figure (a) [top] varies the egg mass contamination proportion q, Figure (a) [bottom] varies disease induced mortality α, and Figure (b) varies the birth rate a.

Figure 3-7(a) [top] shows the change in behaviour as the proportion of infected egg masses due to overwinter contamination, q, increases. We see for small values of q oscillatory population cycles occur, but as q increases the behaviour changes to a stable nontrivial steady state solution as (3.20) is satisfied. Hence increasing q stabilises fluctuating gypsy moth populations. Similarly, Figure 3-7(a) [bottom] shows how the behaviour changes as the disease induced mortality rate, α increases. As α increases the gypsy moth populations become stabilised. In Figure 3-7(b), the birth rate, a, is increased. We see that for a low birth rate the population is unable to sustain itself and decays to a stable trivial steady state. As the birth rate increases we pass into a region where the nontrivial steady state exists and is stable, thus the populations remain at a constant level. For even larger values of a, the nontrivial steady state loses its stability and oscillating population cycles occur.

36

Case (ii): Tannin as a dynamic variable

We now analyse the model allowing tannin to vary. The steady states are given from the solution of the following simultaneous equations

$$0 = a(H - Y) - bH - \alpha Y \tag{3.21a}$$

$$0 = aq(H - Y) - (b + \alpha)Y + \frac{\beta}{1 + cT}W(H - Y) \tag{3.21b}$$

$$0 = \lambda Y - (u + vH)W \tag{3.21c}$$

$$0 = rH - sT \tag{3.21d}$$

Solving equations (3.21) gives three steady state solutions

$$(H^*, Y^*, W^*, T^*) = (0, 0, 0, 0);$$

$$\left(H_+^*, \frac{(a - b)}{a + \alpha}H_+^*, \frac{\lambda(a - b)}{(a + \alpha)(u + vH_+^*)}H_+^*, \frac{rH_+^*}{s} \right);$$

$$\left(H_-^*, \frac{(a - b)}{a + \alpha}H_-^*, \frac{\lambda(a - b)}{(a + \alpha)(u + vH_-^*)}H_-^*, \frac{rH_-^*}{s} \right);$$

where

$$H_\pm^* = \tfrac{1}{2} \left\{ \left(\frac{\beta\lambda(a - b)s}{(a + \alpha)(a - aq - b)vrc} - \frac{urc + vs}{vrc} \right) \right.$$
$$\left. \pm \sqrt{\left(\frac{\beta\lambda(a - b)s}{(a + \alpha)(a - aq - b)vrc} - \frac{urc + vs}{vrc} \right)^2 - 4\frac{us}{vrc}} \right\}$$

As in Case (i), the trivial steady state solution exists for all parameter values, yet both nontrivial steady states only exist if the following conditions hold

$$\frac{\beta\lambda(a - b)s}{(a + \alpha)(a - aq - b)} \geq urc + vs, \tag{3.22a}$$

$$\left(\frac{\beta\lambda(a - b)s}{(a + \alpha)(a - aq - b)} - urc - vs \right)^2 \geq 4usvrc. \tag{3.22b}$$

As discussed for (3.18), v is small in comparison to the parameters in the model. Consequently, for inequalities to hold parameters r and c need to be sufficiently small compared with s. Parameter c influences the amount tannin reduces the transmission rate of the virus to gypsy moths. If c were to be large, very little transmission would occur and the gypsy moth population would fail to be regulated by the virus. We therefore require this parameter to be small. Assuming r and s are of similar orders of magnitude to the remaining parameters then the existence conditions (3.22) will hold.

For stability analysis, the Jacobian matrix is given by

$$
J = \begin{pmatrix}
a - b & -a - \alpha & 0 & 0 \\
aq + \frac{\beta W}{1+cT} & -aq - b - \alpha - \frac{\beta W}{1+cT} & \frac{(H-Y)\beta}{1+cT} & -\frac{(H-Y)c\beta W}{(1+cT)^2} \\
-vW & \lambda & -(u + vH) & 0 \\
r & 0 & 0 & -s
\end{pmatrix}
$$

at $(H, Y, W) = (H^*, Y^*, W^*)$. The trivial steady state again depends on only one condition

$$
a - aq < b.
$$

As in Case (i), the rate of gypsy moths dying is greater than the number born. The conditions for stability for the nontrivial steady states are found from the characteristic polynomial

$$
\chi^4 + A\chi^3 + B\chi^2 + C\chi + D = 0
$$

where

$$
\begin{aligned}
A &= b + \alpha + s + u + vH_\pm \\
B &= s(b + \alpha + u + vH_\pm) + aq\frac{(b+\alpha)(u+vH_\pm)}{a-b} \\
C &= (b + \alpha)\left[u(a - aq - b) + aqs\frac{(u + vH_\pm)}{a-b} - rscH_\pm\frac{(a - aq - b)}{s + rcH_\pm}\right] \\
D &= (a - aq - b)(b + \alpha)s\left[\frac{(us + rcvH_\pm^2)}{s + rcH_\pm}\right]
\end{aligned}
$$

The Routh-Hurwitz conditions reduce to the three conditions

$$
0 < 2us - \left(\frac{\beta\lambda(a - b)s}{(a + \alpha)(a - aq - b)} - ucr - vs\right)H_\pm \tag{3.23a}
$$

$$
0 < (b + \alpha + s + u + vH_\pm)B - C \tag{3.23b}
$$

$$
0 < [(b + \alpha + s + u + vH_\pm)B - C]C \tag{3.23c}
$$

$$
-(b + \alpha + s + u + vH_\pm)^2(a - aq - b)(b + \alpha)s\left[u - rcH_\pm\frac{(u + vH_\pm)}{s + rcH_\pm}\right]
$$

where B and C are given above. From extensive numerical runs, it is seen that the stability conditions (3.23) for the steady state H_- often hold. Therefore, a stable nontrivial steady state may exist. However, the conditions for the steady state H_+ always fail to hold thus resulting in an unstable steady state.

38

3.3.3 Comparisons of constant and dynamic tannin levels

In the reduced system (3.12), we considered the effect of tannin on the gypsy moth-NPV interaction in only one way i.e. to reduce the susceptibility of gypsy moths to NPV infection. This is believed to have a destabilising effect on the gypsy moth-NPV system as NPV is the only regulator of the gypsy moth population. Thus, the reduced model has a positive feedback mechanism, (see Figure 1-2, Chapter 1). Case (i) shows the behaviour of the model (3.12) where levels of tannin remain constant. From the analysis, the model produces three types of behaviour dependent on parameter conditions. Table 3.1 summarises these behaviours.

Case	Behaviour	Conditions
A	Stable Trivial Steady State	$a - aq - b < 0$
B	Stable Nontrivial Steady State	$0 < a - aq - b$ $a - aq - b < \frac{[(b+\alpha)\Gamma + u\beta\lambda(a-b)]\beta\lambda aq}{\Gamma^2}$
C	Oscillations	$0 < a - aq - b$ & $\frac{[(b+\alpha)\Gamma + u\beta\lambda(a-b)]\beta\lambda aq}{\Gamma^2} < a - aq - b$

Table 3.1: Table of model behaviours for Case (i) with stability conditions, Γ is given in (3.19).

We turn our attention to the more interesting model behaviours in Case B & Case C in Table 3.1, and ask what impact does variable (dynamic) tannin levels (Case (ii)) have on these two cases? For Case B, we have a stable nontrivial steady state when tannin is constant. By allowing tannin to be dynamic, Case (ii), we look at varying parameters r and s ($r - s$ space) to see how the model behaviour changes. We predict

39

that tannin may destabilise the nontrivial steady state. Figure 3-8 show the behaviour for interesting parameter sets in $r - s$ space.
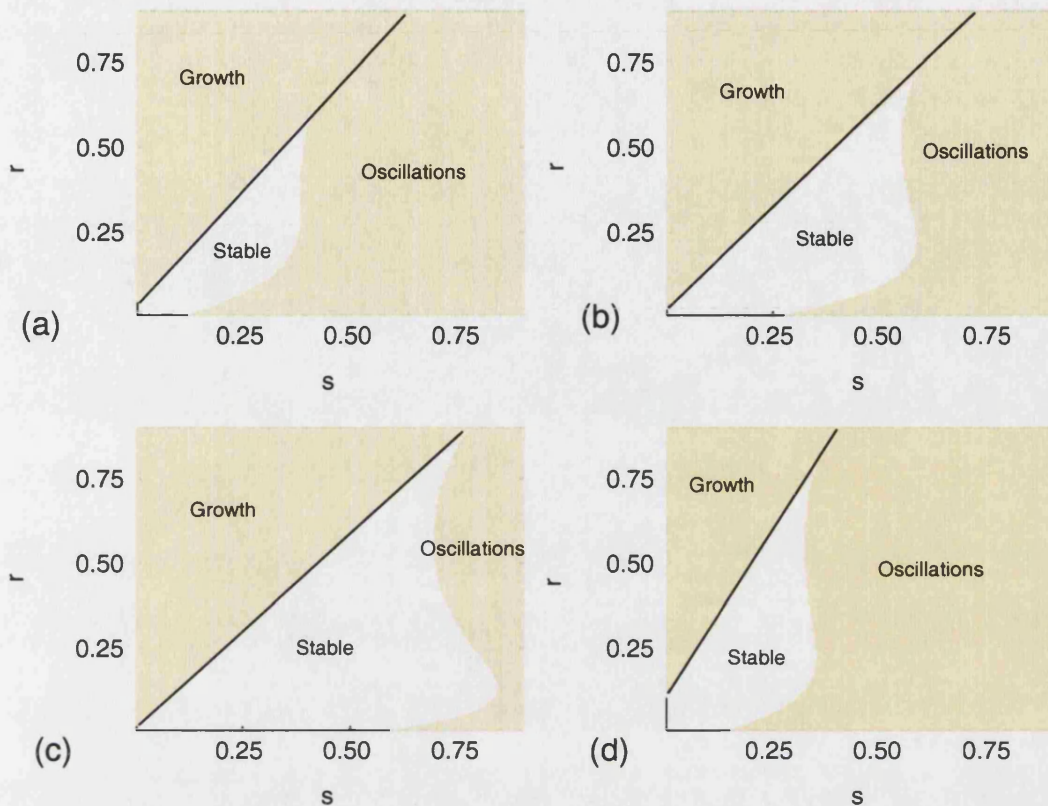
Figure 3-8: Plots show the regions of a stable nontrivial steady state in $r - s$ space. For Figure (a) $\alpha = 15$ $q = 0.25$, Figure (b) $\alpha = 15$ $q = 0.30$ and Figure (c) $\alpha = 15$ $q = 0.35$. Other parameters are $a = 6$, $b = 3$, $u = 1$, $c = 0.1$, $v = 0.001$, $\lambda = 3$ and $\beta = 0.1$. For Figure (d) $\alpha = 15$, $q = 0.30$, $v = 0.005$, $\lambda = 2$

From Figures 3-8, we do indeed see that tannin has destabilised the nontrivial steady state for particular r and s parameter values. Figures (3-8) all show the loss of stability for the nontrivial steady state as r and s increase. In each figure, stability is lost for a large production rate of tannin, r, and a small decay rate of tannin, s. In this case, the virus population is unable to regulate the gypsy moth population and the gypsy moths grow unbounded. For large s, the steady state is lost and bounded oscillatory population cycles appear. Figure 3-8(a) shows a small area of $r - s$ space where the nontrivial steady state remains stable. As parameter q increases, Figures 3-8(b) & 3-8(c) show this stability area growing. Figure 3-8(d) shows the behaviour for an alternative parameter set.

40

For Case C, we have oscillatory behaviour for constant tannin levels (Case (i)). Again, by making tannin a dynamic variable (Case (ii)), we look at $r - s$ space. This time the behaviour is already unstable, so we would expect that there will be no change in the stability of the nontrivial steady state. Figure 3-9 shows the model behaviour for particular parameter sets in $r - s$ space.

(a)   (b)
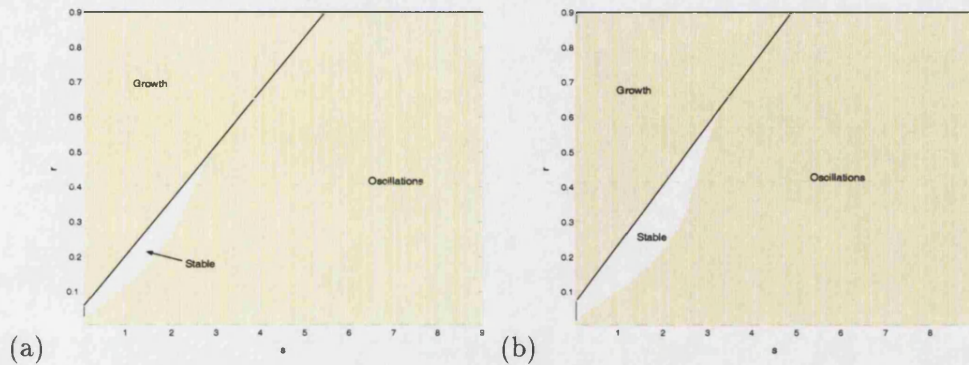
Figure 3-9: Plots showing the " pocket of stability". Parameters are $a = 6$, $b = 3$, $u = 1$, $c = 0.1$, $\alpha = 15$ and $\beta = 0.1$.

We find that a small region of parameter space appears where the addition of tannin has stabilised the oscillatory behaviour to a stable nontrivial steady state. In other words, for this parameter space we see that dynamic tannin has caused stabilisation, not destabilisation as expected. Additionally, we again see that for a large production rate of tannin, r, and small decay rate of tannin, s, unbounded growth for the gypsy moth population occurs. Also for large s, population cycles which are regulated by the virus arise. More interestingly, Figure 3-9 shows the existence of a "pocket of stability" when $r \approx s$ and r and s are small.

3.4   Summary and Discussion

Previous to this chapter, only Foster et al. (1992) had modelled the interference of plant food quality on the gypsy moth interaction with the NPV. Foster et al. (1992) however, only allowed tannin to exist at a constant level, although the authors acknowledged that tannin levels do change and their model may not be complete as a result. In this chapter, we extended the model by Foster et al. (1992) for modelling gypsy moth, NPV, tannin interactions by including tannin as a dynamic variable. Comparisons could then be drawn between the extended model with dynamic tannin and the Foster et al. (1992) model with constant tannin levels.

We began the chapter by making a modification to the overwinter contamination of egg masses function, $Q(W)$. By replacing the square root function, used by Foster et al. (1992), with a bounded function (3.2) the behaviour of the model generally remained the same. This includes the observation of realistic population fluctuations for a large range of parameter k values when the upper bound q was small. Yet, for larger values of q, the range of values for k, where realistic oscillations occur, decreased. Instead, either small oscillations or very large oscillations of the steady state were observed.

In the second section, a model was proposed to include tannin as a dynamic variable. Numerical simulations were presented to demonstrate the different behaviours observed for the model. We found that the behaviour of the model fell into 4 categories; a stable steady state, oscillatory population cycles, extinction, and persistence of gypsy moths with extinction of NPV. This compared well with the simulations of Foster et al. (1992) with the exception that our studies found gypsy moth persistence with NPV extinction whereas Foster et al. (1992) observed exponential growth of gypsy moth populations. Thus, the inclusion of tannin as a dynamic variable prevents the gypsy moth population from growing unbounded. Moreover, oscillatory population cycles were observed, which compared well with field data.

In the last section, a simplified model was analysed. In the simplified model we only include the plant's effect on the susceptibility of gypsy moths to infection. Without tannin, we would expect the virus to regulate the moth population. Therefore, when we include tannin, there should be less regulation on the system. This is because the tannin decreases the susceptibility of gypsy moths to viral infection. Here, we first find the expected result that the addition of tannin destabilises a model experiencing stable nontrivial behaviour. We see that the nontrivial steady state loses its stability more easily (see Figure 3-8) when the condition (3.18) is close to failing.

We would also expect that the addition of dynamic tannin to the model, when the behaviour was unstable, to also have a negative effect on the stability. However, there are cases where the addition of tannin has caused the regulation of gypsy moths by the virus to become more stable. Figure 3-9 shows the "pocket of stability" occurring in $r - s$ space. This is counter intuitive and is a surprising result from the analysis. It is not clear why there is a stabilising effect on the populations in the cases shown in Figure 3-9.

In summary, we have shown that the effect of adding tannin into the system may act as a destabilising or stabilising effect dependent on particular parameter sets. The addition of tannin as a more realistic, dynamic variable can also demonstrate cyclic population levels of gypsy moths similarly to the work of Foster et al. (1992) and field data.

Chapter 4

A new approach to modelling Gypsy Moth populations

In the previous chapter, we explored the gypsy moth NPV tannin interactions using a continuous time modelling approach, which was based on modelling attempts by Foster et al. (1992) and Dwyer & Elkinton (1993). Gypsy moths have fixed annual life cycles that form non-overlapping generations and they reproduce only once per generation. This life cycle is consistent with several other hosts whose populations are regulated by parasitoids. These host-parasitoid interactions have widely been modelled by discrete time systems as this method is believed to better reflect the discrete generations of the host. Therefore, we will take a new approach to modelling gypsy moth populations using a discrete time system.

In this chapter, we build on the continuous time modelling in the Chapter 3, by developing a discrete time model structure to reflect the discrete generations of the gypsy moth. We compare the behaviour from the newly-formed, discrete time model to the outcomes of the previous continuous time approach.

We begin the chapter by building a general framework to model the interactions between gypsy moths, virus and tannins. From the general framework, we choose specific functions to demonstrate particular model behaviours. We will then analyse the system by first simplifying the model in order to take a more detailed look at the effects of the inclusion of tannin. We then compare the results from the simplified model to the numerics from the complete system. Finally, we compare the behaviour of the discrete time model to that of the extended model in Chapter 3. The goal of this chapter is to confirm that the behaviour from the discrete time model gives the same realistic behaviour as the continuous time model.

4.1 Building up a model

We begin by building a general discrete time model to describe the population dynamics of gypsy moths. First, we model the gypsy moth population without any effects from the virus or tree tannins to determine the underlying moth dynamics. This is to get a good understanding of the dynamics and its behaviour at different biological parameter regions. We then introduce virus into the model creating a host-parasitoid system similar to the Nicholson & Bailey model (Nicholson & Bailey 1935). This model is analysed and steady states and stability conditions are given. Lastly, we incorporate the experimental results that tree tannins influence the gypsy moth-virus system. This model will represent the complete gypsy moth-virus-tree tannin dynamical system and from its analysis, comparisons can be drawn with the host-parasitoid model.

Whilst modelling the system, we only consider the main characteristics that influence the population levels in order to keep the model as simple as possible. General functions are chosen in this section, however specific forms are taken in following sections to demonstrate particular model behaviours.

4.1.1 Modelling gypsy moths

We begin with the simplest structure for modelling gypsy moth population levels. We let M_n be the number of gypsy moths in year (or generation), n, and a represents the average number of offspring per gypsy moth. To prevent exponential growth of the population, we introduce a carrying capacity. This leads to the Ricker model system (Ricker 1954):

$$
\begin{aligned}
M_{n+1} &= F(M_n) \\
&= a \exp(-rM_n)M_n
\end{aligned}
\tag{4.1}
$$

where parameter r represents a self-limit in the gypsy moth population.

The system (4.1) admits two steady state solutions, $M^* = M_{n+1} = M_n$. Substituting into (4.1) and solving gives us two solutions. The first is a trivial solution

$$
M^* = 0,
\tag{4.2}
$$

and the second is a nontrivial solution

$$
M^* = \frac{1}{r}\ln(a), \quad a > 1.
\tag{4.3}
$$

We can determine the stability of the two steady state solutions. A steady state is

linearly stable if and only if $|F'(M_n)| < 1$, i.e. if

$$-1 < (1 - rM^*)a \exp(-rM^*) < 1. \tag{4.4}$$

Therefore the trivial solution, (4.2), becomes

$$-1 < a < 1. \tag{4.5}$$

Yet parameter a is positive so the trivial steady state is only unstable if $a > 1$. This means that if the birth rate, a, of the gypsy moth is greater than 1 then the population can exist. On the other hand, if the birth rate is less than 1 then the population decreases each year and hence will become extinct.

Now we turn our attention to the nontrivial steady state. For this steady state to exist, we must have $a > 1$. The stability condition (4.4) then becomes

$$1 < a < \exp(2). \tag{4.6}$$

We see that the parameter, r, plays no role in the stability of either of the steady states. In contrast, the birth rate, a, plays a critical role. When $a < 1$, only the trivial steady state exists and this state is stable so the population will die out. However, when a is in the interval (4.6), a second steady state appears. Here the state is stable so the population of gypsy moths survive and tend to a constant population level (4.3). But what happens when a exceeds $\exp(2)$? A bifurcation occurs. Figure 4-1 shows the bifurcation diagram when the birth rate is varied. As a passes through the value $\exp(2)$, a -1 type bifurcation occurs resulting in the occurrence of a two cycle. A stable two cycle means that the number of gypsy moths will oscillate between two different population levels in successive years. As a continues to increase, further period doubling of the branches occurs. Note that Figure 4-1 also shows that we have a $+1$ bifurcation at $a = 1$. This bifurcation is transcritical; stability switches between the trivial and the nontrivial steady states.

Gypsy moth populations do oscillate between low and high levels, so a birth rate in excess of $\exp(2)$ may cause this behaviour. But estimates of gypsy moth birth rate are typically no higher than 6 gypsy moths per year. Hence, it is unlikely that the fecundity is solely a cause of the periodic levels in gypsy moth numbers as seen in the field.
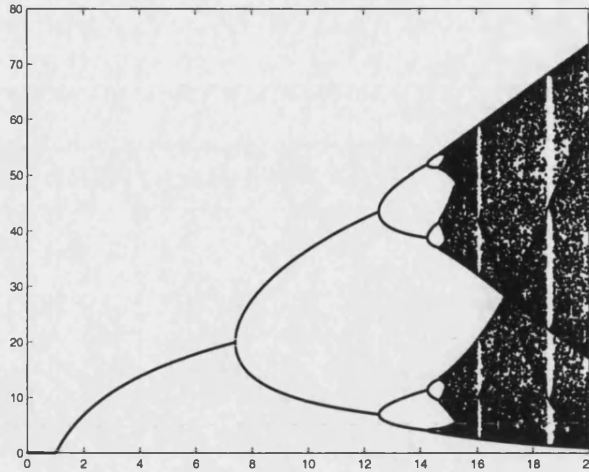
Figure 4-1: Bifurcation diagram for birth rate of gypsy moths a, and self-limit parameter $r = 0.1$.

4.1.2 Gypsy moth NPV interactions

Now, we explore the effects of introducing virus on the gypsy moth population dynamics. The model is changed by adding another difference equation to represent the free living virus in the environment. We begin to form the model by making the following assumptions:

- The virus lives freely in the environment and decreases at a constant rate σ_v.

- Gypsy moths contract the disease by ingesting the virus. The proportion of gypsy moths that ingest virus and become infected, in year n, is given by the probability function $1 - \sigma_m(V_n)$ where V_n is the number of free living virus particles.

- The time taken for infected gypsy moths to die is typically 14 days. Thus, the generation time is long enough to allow all the diseased gypsy moths to die during a single generation.

- When gypsy moths die due to infection their bodies decompose and release on average λ free living propagules, per gypsy moth, into the environment.

- Overwinter egg masses may become contaminated with virus before hatching (transovum vertical transmission). We let $Q(V_n)$ be the proportion of gypsy moths affected by transovum vertical transmission.

- No production of NPV from overwinter contamination of egg masses as this amount is negliable. This is in contrast to the continuous time model.

46

- No virus release in season

These assumptions lead to the pair of difference equations:

$$M_{n+1} = a[1 - Q(V_n)] \exp(-rM_n) \sigma_m(V_n) M_n \qquad \text{(4.7a)}$$

$$V_{n+1} = \sigma_v V_n + \lambda(1 - \sigma_m(V_n)) M_n \qquad \text{(4.7b)}$$

We can make some restrictions on the general functions $Q(V_n)$ and $\sigma_m(V_n)$. We assume that the probability function $Q(V_n)$ is an increasing function that is zero when $V_n = 0$

$$0 < Q(V_n) < 1, \quad V_n > 0$$
$$Q(V_n) = 0, \quad V_n = 0$$
$$\frac{dQ(V_n)}{dV_n} > 0.$$

Also, we assume that the probability of gypsy moths not becoming infected is a decreasing function and takes the value one when $V_n = 0$

$$0 < \sigma_m(V_n) < 1, \quad V_n > 0$$
$$\sigma_m(V_n) = 1, \quad V_n = 0$$
$$\frac{d\sigma_m(V_n)}{dV_n} < 0.$$

Model Analysis

Following the method described in section 4.1.1, we set

$$M^* = M_{n+1} = M_n, \qquad \text{(4.8a)}$$

$$V^* = V_{n+1} = V_n, \qquad \text{(4.8b)}$$

to find the steady states of the model (4.7). Substituting (4.8a) and (4.8b) into (4.7a) and (4.7b), we find that there are possibly three steady state solution pairs

$$(M^*, V^*) = (0, 0); \qquad \text{(4.9a)}$$

$$\left(\frac{1}{r} \ln(a), 0 \right); \qquad \text{(4.9b)}$$

$$\left(\frac{V^*(1 - \sigma_v)}{\lambda(1 - \sigma_m(V^*))}, V^* \right); \qquad \text{(4.9c)}$$

47

where V^* is given by any solutions to the equation

$$V^*(1 - \sigma_v) = \frac{1}{r} \ln[a(1 - Q(V^*))\sigma_m(V^*)]\lambda(1 - \sigma_m(V^*)). \qquad (4.10)$$

For the first two steady states, the virus population level is zero (extinct). Therefore, we call these states the trivial solutions. These steady state solution are exactly the same as those found in the previous subsection. The third steady state is a coexistence state. However, it is not clear if there are any solutions to (4.10) and therefore if a steady state does exist at all. In fact, there may be several solutions to (4.10) resulting in several steady states. This will depend on the specific functions chosen for $Q(V_n)$ and $\sigma_m(V_n)$. We explore this condition further when specific functions are explored in the next section.

We can find conditions for stability of the steady states from the Jacobian of the system

$$J = \begin{pmatrix} J_{11} & J_{12} \\ \lambda[1 - \sigma_m(V^*)] & \sigma_v - \lambda M^* \frac{d\sigma_m}{dV} \end{pmatrix} \qquad (4.11)$$

where

$$\begin{aligned} J_{11} &= (1 - rM^*)a(1 - Q(V^*))\sigma_m(V^*)e^{-rM^*} \\ J_{12} &= \left[(1 - Q(V^*))\frac{d\sigma_m}{dV} - \sigma_m(V^*)\frac{dQ}{dV}\right] aM^* e^{-rM^*} \end{aligned}$$

Evaluating (4.11) at the first trivial steady state, we have

$$J = \begin{pmatrix} a & 0 \\ 0 & \sigma_v \end{pmatrix} \qquad (4.12)$$

The eigenvalues of (4.12) determine the stability of the steady state. As σ_v is a proportion, we have the same stability condition as in (4.5). Therefore the addition of NPV in the model system has not changed this steady state or its stability conditions. For the other trivial steady state,

$$J = \begin{pmatrix} 1 - \ln(a) & \frac{\lambda}{r} \ln(a) \left[\frac{d\sigma_m}{dV} - \frac{dQ}{dV}\right] \\ 0 & \sigma_v - \frac{\lambda}{r} \ln(a)\frac{d\sigma_m}{dV} \end{pmatrix} \qquad (4.13)$$

the eigenvalues χ_i of (4.13) are

$$\chi_1 = 1 - \ln(a) \tag{4.14a}$$

$$\chi_2 = \sigma_v - \frac{\lambda}{r}\ln(a)\frac{d\sigma_m(0)}{dV} \tag{4.14b}$$

The first condition (4.14a) remains the same as (4.6). Therefore when $a = 1$, condition (4.14b) holds and we again have a transcritical bifurcation resulting in a change in stability from the trivial steady state (4.9a) to the steady state (4.9b). This steady state (4.9b) can lose stability in one of two ways. As parameter a increases from $a = 1$, stability is lost if $a > \exp 2$, as in (4.6), or if

$$-1 > \sigma_v - \frac{\lambda}{r}\ln(a)\frac{d\sigma_m(0)}{dV}$$

that is if σ_m is a sufficiently steep function of V. This will occur when either eigenvalue $\chi_1 = -1$ or $\chi_2 = -1$, whichever occurs first and a -1 bifurcation may occur (Figure 4-1).

For the nontrivial steady state, we use the Jury conditions (Murray 2002) to determine stability.

$$
\begin{aligned}
0 &< 1 - tr(J) + det(J) \\
&= rM^*\left(1 - \sigma_v + \lambda M^*\frac{d\sigma_m}{dV}\right) + \eta \tag{4.16a}
\end{aligned}
$$

$$
\begin{aligned}
0 &< 1 + tr(J) + det(J) \\
&= 2 - rM^*\left(1 + \sigma_v - \lambda M^*\frac{d\sigma_m}{dV}\right) + \eta \tag{4.16b}
\end{aligned}
$$

$$
\begin{aligned}
0 &< 1 - det(J) \\
&= 1 - (1 - rM^*)\left(\sigma_v - \lambda M^*\frac{d\sigma_m}{dV}\right) - \eta \tag{4.16c}
\end{aligned}
$$

where

$$
\begin{aligned}
tr(J) &= 1 - rM^* + \sigma_v - \lambda M^*\frac{d\sigma_m}{dV} \\
det(J) &= (1 - rM^*)\left(\sigma_v - \lambda M^*\frac{d\sigma_m}{dV}\right) + \eta
\end{aligned}
$$

and

$$\eta = V^*(1 - \sigma_v)\left[\frac{1}{1 - Q(V^*)}\frac{dQ(V^*)}{dV} - \frac{1}{\sigma_m(V^*)}\frac{d\sigma_m(V^*)}{dV}\right]$$

If all three conditions (4.16) hold, then the nontrivial steady state will be stable and gypsy moth and virus populations will tend to constant levels. Yet if the trivial steady

49

states and the nontrivial states are unstable then the model may display oscillatory population cycles. This is the behaviour seen in the field for gypsy moth populations. In further sections, we will refer back to these conditions when we choose specific functions for $\sigma_m(V_n)$ and $Q(V_n)$.

4.1.3 Gypsy moth NPV and plant food quality interactions

The model (4.7) shows the host pathogen interactions of gypsy moths and NPV. In this section, we are interested in the effects that plant food quality has on this dynamical system. Schultz's experimental results discovered that tannin has a major effect on the system. We therefore include tannin as a dynamic variable in our model to create a tritrophic system. Using Schultz's results, we make the following assumptions:

- An increase in tannin levels causes a decrease in gypsy moth fecundity, $a(T)$ (Rossiter, Schultz & Baldwin 1988).

- An increase in tannin levels decreases gypsy moth susceptibility to virus infection, $\sigma_m(V, T)$ (Keating et al. 1988, Keating et al. 1990).

- Tannin levels decay naturally with a constant rate, σ_t.

- An increase in gypsy moth numbers causes an increase in the plants' production of tannin, $\rho(M)$. Plants produce tannin as a defence mechanism against defoliation.

Incorporating these assumptions into the previous model (4.7), we obtain

$$
\begin{aligned}
M_{n+1} &= a(T_n)[1 - Q(V_n)]\exp(-rM_n)\sigma_m(V_n, T_n)M_n & \text{(4.17a)} \\
V_{n+1} &= \sigma_v V_n + \lambda(1 - \sigma_m(V_n, T_n))M_n & \text{(4.17b)} \\
T_{n+1} &= \sigma_t T_n + \rho(M_n) & \text{(4.17c)}
\end{aligned}
$$

where $a(T_n)$ is a decreasing function of tannin, $\sigma_m(V_n, T_n)$ is an increasing function with respect to tannin but a decreasing function with respect to virus and $\rho(M_n)$ is an increasing function with respect to gypsy moths.

Model Analysis

We look for steady state solutions of the system (4.17). As in the previous model (4.7), we have one trivial steady state solutions, namely

$$
(M^*, V^*, T^*) = (0, 0, 0) \tag{4.18}
$$

where $a = a(0)$. There may also exist nontrivial steady state solutions that arise from the solution of the equations

$$1 \quad = \quad a(T_n)[1 - Q(V_n)]\exp(-rM_n)\sigma_m(V_n, T_n) \qquad (4.19a)$$

$$(1 - \sigma_v)V_n \quad = \quad \lambda(1 - \sigma_m(V_n, T_n))M_n \qquad (4.19b)$$

$$(1 - \sigma_t)T_n \quad = \quad \rho(M_n) \qquad (4.19c)$$

The solutions to the equations (4.19) will depend on the specific functions used. In further sections, we will refer back to these equations. For the stability of the steady states, we look at the Jacobian

$$J = \begin{pmatrix} J_{11} & J_{12} & J_{13} \\ \lambda(1 - \sigma_m(V^*, T^*)) & \sigma_v - \lambda M^* \frac{\partial \sigma_m}{\partial V} & -\lambda M^* \frac{\partial \sigma_m}{\partial T} \\ \frac{\partial \rho}{\partial M} & 0 & \sigma_t \end{pmatrix} \qquad (4.20)$$

where

$$J_{11} \quad = \quad (1 - rM^*)a(T^*)(1 - Q(V^*))\sigma_m(V^*, T^*)e^{-rM^*}$$

$$J_{12} \quad = \quad \left[(1 - Q(V^*))\frac{\partial \sigma_m}{\partial V} - \sigma_m(V^*, T^*)\frac{\partial q}{\partial V}\right]a(T^*)M^*e^{-rM^*}$$

$$J_{13} \quad = \quad \left[\sigma_m(V^*, T^*)\frac{\partial a}{\partial T} + a(T^*)\frac{\partial \sigma_m}{\partial T}\right][1 - Q(V^*)]\exp(-rM^*)M^*$$

For the trivial steady state $(0, 0, 0)$, the Jacobian reduces to

$$J = \begin{pmatrix} a(0) & 0 & 0 \\ 0 & \sigma_v & 0 \\ \frac{\partial \rho(0)}{\partial M} & 0 & \sigma_t \end{pmatrix}. \qquad (4.21)$$

This yields the eigenvalues: σ_t, σ_v and $a(0)$. As σ_t and σ_v are both probabilities then this reduces to one condition which is that the fecundity is greater than one ($a(0) > 1$). Again if the birth rate of gypsy moths is below 1, then the population will die out. The stability condition for the trivial steady state still remains the same condition as found in models (4.1) and (4.7).

For the nontrivial steady states, the eigenvalues, χ, of the Jacobian matrix (4.20)

51

are given by the following cubic equation

$$
\begin{aligned}
0 \;=\; & \chi^3 - (1 - rM + \beta)\chi^2 + \left[(1 - rM)(\sigma_t + \beta) + \sigma_t\beta - \gamma + \frac{d\rho}{dM}\delta \right]\chi \\
& + \frac{d\rho}{dM}\left[\sigma_v\delta - \lambda e^{-rM} M^2 \sigma_m \left(a(T)\frac{\partial\sigma_m}{\partial T}\frac{dQ}{dV} + (1 - Q(V))\frac{\partial\sigma_m}{\partial V}\frac{da}{dT} \right) \right] \\
& + \sigma_t\gamma - \sigma_t(1 - rM)\beta
\end{aligned}
$$

where

$$
\begin{aligned}
\beta \;=\;& \sigma_v - \lambda M\frac{\partial\sigma_m}{\partial V} \\
\gamma \;=\;& a(T)e^{-rM}V(1 - \sigma_v)\left((1 - Q(V))\frac{\partial\sigma_m}{\partial V} - \sigma_v\frac{dQ}{dV} \right) \\
\delta \;=\;& (1 - Q(V))e^{-rM}M\left(a(T)\frac{\partial\sigma_m}{\partial T} - \sigma_m\frac{da}{dT} \right)
\end{aligned}
$$

So from the cubic equation, we get the Jury conditions

$$
\begin{aligned}
1 + A + B + C &> 0 & \text{(4.22a)} \\
-1 + A - B + C &> 0 & \text{(4.22b)} \\
1 &> |C| & \text{(4.22c)} \\
|1 - C^2| &> |B - A| & \text{(4.22d)}
\end{aligned}
$$

where

$$
\begin{aligned}
A \;=\;& -(1 - rM + \beta) \\
B \;=\;& \left[(1 - rM)(\sigma_t + \beta) + \sigma_t\beta - \gamma + \frac{d\rho}{dM}\delta \right] \\
C \;=\;& \frac{d\rho}{dM}\left[\sigma_v\delta - \lambda e^{-rM} M^2 \sigma_m \left(a(T)\frac{\partial\sigma_m}{\partial T}\frac{dQ}{dV} + (1 - Q(V))\frac{\partial\sigma_m}{\partial V}\frac{da}{dT} \right) \right] \\
& + \sigma_t\gamma - \sigma_t(1 - rM)\beta
\end{aligned}
$$

4.2 The model with specific functional forms

In this section, we suggest specific functional forms for the models (4.7) and (4.17). In order to obtain meaningful analysis, we choose the simplest functions that still display the main properties required, such as the function increasing or decreasing. The following subsection describes the functional forms chosen for the birth rate of gypsy moths, the susceptibility of gypsy moths to the virus, the overwinter contamination of gypsy moth egg masses and the production of tannin.

4.2.1 Birth rate of gypsy moths

Gypsy moth fecundity has been shown to vary depending on levels of tannin (Rossiter et al. 1988). Therefore, we choose a decreasing function in tannin for the birth rate

$$a(T) = \frac{a}{1 + dT} \tag{4.23}$$

where a is the birth rate of gypsy moths when no tannin is present in the plants and d is the coefficient representing the decrease in births due to tannin.
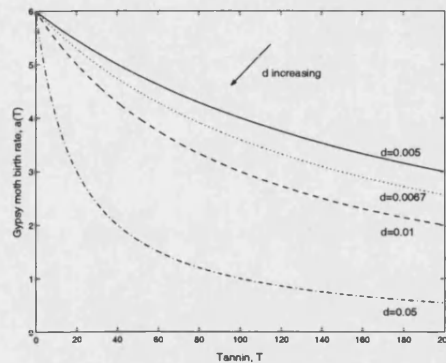
Figure 4-2: Plot of birth rate as a function of tannin $a(T)$ for various values of parameter d.

We see that as parameter d increases the birth rate drops quicker as tannin levels increase (Figure 4-2).

4.2.2 Overwinter contamination of egg masses

As discussed in Chapter 3, gypsy moth egg masses can become contaminated with the virus. This results in some proportion of the gypsy moths dying shortly after hatching, due to transovum vertical transmission of the virus which is dependent on the amount of free living virus in the environment. Death by transovum vertical transmission is an increasing function of the virus

$$Q(V) = \frac{qV}{k + V} \tag{4.24}$$

where V represents the free-living virus, q is an upper limit on the amount of eggs that get contaminated and k determines how quickly the function reaches that upper limit.
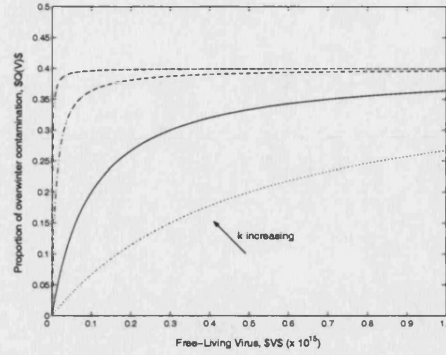
Figure 4-3: Plot of the proportion of overwinter contamination of egg masses against free-living virus $Q(V)$ for $q = 0.4$ and various values of parameter k.

4.2.3 Gypsy moth susceptibility to virus

Gypsy moths can become infected with the virus during the larval stage. We let the probability of gypsy moths not becoming infected with the virus be the zeroth term of the Poisson process. However, this probability also depends on the tannin levels, hence we form the probability function

$$\sigma_m(V_n, T_n) = \exp\left(\frac{-bV_n}{1 + cT_n}\right) \tag{4.25}$$

to represent the probability that a gypsy moth avoids infection. Figures 4-4 show two
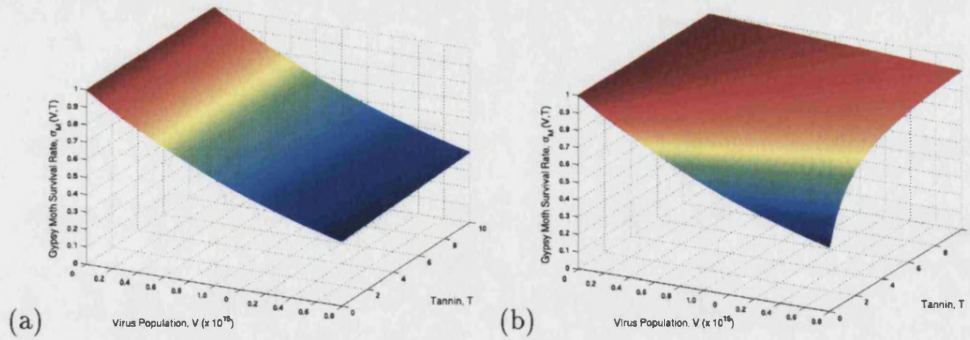
Figure 4-4: Plot shows survival of gypsy moth at different virus population and tannin levels. Figure (a) shows the effect when tannin has little impact on the gypsy moth interactions, $c = 0.01$. Figure (b) shows the effect when tannin has a significant impact on gypsy moth interactions, $c = 1.0$.

cases of tannin's impact on gypsy moth-NPV interactions. We see that when tannin

54

has a significant impact, the gypsy moths become more resistance to virus infection.

4.2.4 Production of tannin

Tannin levels increase due to the amount of attack that the plant is under by gypsy moth infestation. Thus, more of the plants resources are directed into defending itself and less into other things such as growth. For simplicity, we take this function as a linear increasing function.

$$\rho(M_n) = \rho M_n. \tag{4.26}$$

In Chapter 5 and Chapter 7, a more complicated functional form is used in order to carry out relevant analytic and numerical techniques.

4.2.5 The model and parameter estimates

Using the functions given in sections 4.2.1-4.2.4, the generalised model becomes

$$M_{n+1} = \frac{a}{1+dT_n}\frac{k+(1-q)V_n}{k+V_n}\exp\left(-rM_n - \frac{bV_n}{1+cT_n}\right)M_n \tag{4.27a}$$

$$V_{n+1} = \sigma_v V_n + \lambda\left[1 - \exp\left(\frac{-bV_n}{1+cT_n}\right)\right]M_n \tag{4.27b}$$

$$T_{n+1} = \sigma_t T_n + \rho M_n \tag{4.27c}$$

A list of the parameters in the model are given in Table 4.1, together with estimates of some of the parameters.

PARAMETER	SYMBOL	PARAMETER ESTIMATE	RESCALED VALUE	SOURCE
Gypsy Moth				
Birth rate	a	6.0	6.0	Schultz et al. (1990)
Susceptibility to virus	b	10^{-14}	0.1	Foster et al. (1992)
Resistance of virus due to tannin	c	-	-	-
Reduced fecundity due to tannin	d	0.0067	0.0067	Schultz et al. (1990)
Self-limit parameter	r	$10^{-6} - 10^{-7}$	$10^{-3} - 10^{-4}$	-
Overwinter contamination of egg masses	k	2×10^{14}	20.0	-
Maximum overwinter contamination	q	0.3	0.3	Foster et al. (1992)
NPV				
Survival rate	σ_v	0.37	0.37	Foster et al. (1992)
Average virus spores released per gypsy moth	λ	1.49×10^{10}	1.49	Shapiro, Presler & Robertson (1987)
Tannin				
Tannin production rate	ρ	-	-	-
Tannin decay rate	σ_t	-	-	-

Table 4.1: List of parameter estimates used of vital rates for gypsy moths, virus and tannin. Rescaled values are used for model analysis.

4.3 Model analysis

We analyse the model presented in section 4.1.3 (4.17) using the specific functions described in section 4.2 (4.23), (4.24), (4.25) & (4.26). We begin this section by analysing a simplified version of the model. We first look at the existence of steady states before going on to make a further simplification to analyse stability. Once a good understanding of the simplified model is achieved, we look at the complete model system numerically. Here we compare the understanding from the simplified model to the new numerics from the complete gypsy moth-virus-tannin model. Also, within this section, we refer to the cases where tannin has no influence in the gypsy moth virus system.

4.3.1 Simplified model

We make a simplification to the model by setting the overwinter virus contamination of egg masses, $Q(W)$, to remain as a constant proportion, q. Therefore, the model becomes

$$M_{n+1} = \frac{a}{1 + dT_n}(1 - q)\exp\left(-rM_n - \frac{bV_n}{1 + cT_n}\right)M_n \qquad (4.28a)$$

$$V_{n+1} = \sigma_v V_n + \lambda\left[1 - \exp\left(\frac{-bV_n}{1 + cT_n}\right)\right]M_n \qquad (4.28b)$$

$$T_{n+1} = \sigma_t T_n + \rho M_n \qquad (4.28c)$$

From steady state analysis, in section 4.1.3 we see that this model has two trivial steady state solutions. The first steady state is

$$(M^*, V^*, T^*) = (0, 0, 0) \qquad (4.29)$$

and the other steady state is

$$(M^*, V^*, T^*) = \left(\frac{(1 - \sigma_t)}{\rho}T^*, 0, T^*\right) \qquad (4.30)$$

where T^* is given from the solution of

$$1 + dT^* = a(1 - q)\exp\left(\frac{-r(1 - \sigma_t)}{\rho}T^*\right) \qquad (4.31)$$

We let $f(T)$ denote the right hand side of the equation (4.31) and $g(T)$ denote the left hand side of the equation (4.31),

$$f(T) := a(1-q) \exp\left(\frac{-r(1-\sigma_t)}{\rho}T\right),$$

$$g(T) := 1 + dT.$$

A solution to (4.31) exists if $a(1-q) > 1$, which is shown graphically in Figure 4-5.
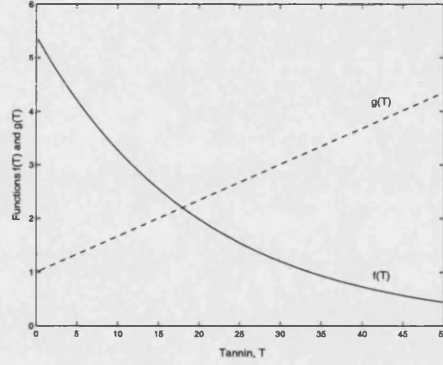
Figure 4-5: Plot showing the intersection of functions f(T) and g(T) for typical parameter set, $a = 6; q = 0.1; d = 0.0067; r = 0.01; \rho = 0.1; \sigma_t = 0.5$

From the figure, the functions intersect when $f(T) = g(T)$ so (4.31) holds at this point. $f(T)$ is an increasing function ($f(T) > 0$) and $g(T)$ is decreasing ($g(T) < 0$), therefore this is the only point of intersection for functions f and g.

Nontrivial steady state solutions exist whenever the following simultaneous equations have a real solution

$$1 = \frac{a}{1+dT}(1-q)\exp\left(-\frac{r}{\rho}(1-\sigma_t)T - \frac{bV}{1+cT}\right), \quad (4.33a)$$

$$V = \alpha T\left[1 - \exp\left(\frac{-bV}{1+cT}\right)\right], \quad (4.33b)$$

where

$$\alpha = \frac{(1-\sigma_t)\lambda}{(1-\sigma_v)\rho}.$$

Now from rearranging (4.33a) and then taking logs we get

$$F(T) := V$$

$$= \frac{1 + cT}{b} \left[\ln \frac{a(1-q)}{1+dT} - \frac{r}{\rho}(1 - \sigma_t)T \right] \tag{4.34a}$$

Also substituting (4.33a) into (4.33b) this becomes

$$
\begin{aligned}
G(T) &:= V \\
&= \alpha T \left[1 - \frac{1 + dT}{a(1-q)} \exp \left(\frac{r}{\rho}(1 - \sigma_t)T \right) \right]
\end{aligned}
\tag{4.34b}
$$

Differentiating the functions $F(T)$ and $G(T)$ gives

$$
\begin{aligned}
F'(T) &= \frac{c}{b} \left[\ln \left(\frac{a(1-q)}{1+dT} \right) - \frac{r}{\rho}(1 - \sigma_t)T \right] \\
&\quad - \frac{1 + cT}{b} \left[\frac{d}{1+dT} + \frac{r}{\rho}(1 - \sigma_t) \right]
\end{aligned}
\tag{4.35a}
$$

$$
\begin{aligned}
G'(T) &= \alpha \left[1 - \frac{1 + 2dT}{a(1-q)} \exp \left(\frac{r}{\rho}(1 - \sigma_t)T \right) \right] \\
&\quad - \alpha T \frac{1 + dT}{a(1-q)} \frac{r}{\rho}(1 - \sigma_t) \exp \left(\frac{r}{\rho}(1 - \sigma_t)T \right)
\end{aligned}
\tag{4.35b}
$$

At T^*, (4.35a) and (4.35b) reduce to

$$
\begin{aligned}
F'(T^*) &= -\frac{1 + cT}{b} \left[\frac{d}{1+dT} + \frac{r}{\rho}(1 - \sigma_t) \right] \\
G'(T^*) &= -\alpha \frac{dT}{1+dT} - \alpha T \frac{r}{\rho}(1 - \sigma_t)
\end{aligned}
$$

Then a sufficient condition for at least one nontrivial steady state to exist is

$$F'(T^*) > G'(T^*), \tag{4.36}$$

or more explicitly

$$\alpha T^* > \frac{1 + cT^*}{b}. \tag{4.37}$$

From realistic parameter estimates we plot the number of solutions to the nontrivial steady state in the interval $T \epsilon (0, T^*)$ for a range of ρ and σ_t values.
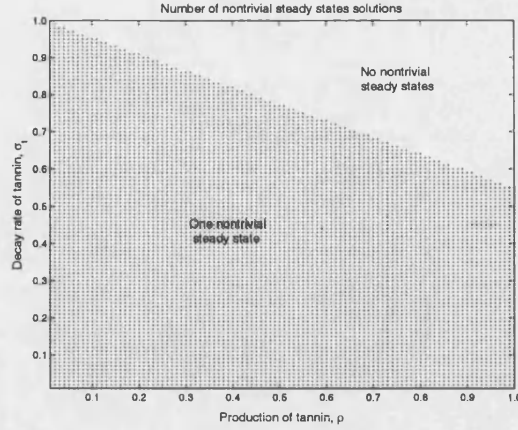
Figure 4-6: Plot displays the number of nontrivial steady state solutions in ρ-σ_t space. Parameters are $a = 6.0; b = 0.1; \lambda = 1.49; \sigma_v = 0.37; c = 0.1; q = 0.1; d = 0.0067; r = 0.001$.

We see from Figure 4-6 one steady state solution occurs for the majority of values of ρ and σ_t. However the existence of this nontrivial solution is lost at high ρ and σ_t values. At these points tannin decays slowly therefore tannin levels will remain high in trees that suffer defoliation for long periods of time. Coupled with this is the high production rate of tannin caused when trees begin to suffer defoliation. Thus high tannin levels sustained for long periods of time cause a large decrease in the susceptibility of gypsy moths to virus infection. Therefore it is likely that virus population levels will be unable to sustain themselves under these conditions. If this occurs then no nontrivial steady states would be found, as demonstrated in Figure 4-6.

Modelling without tannin

We compare this to a model where tannin is excluded and see what effect this on the steady state solutions. The model system reduces to become

$$M_{n+1} = a(1 - q)\exp(-rM_n)\exp(-bV_n)M_n$$
$$V_{n+1} = \sigma_v V_n + \lambda(1 - \exp(-bV_n))M_n$$

From (4.9), we have the trivial steady state solutions

$$(M^*, V^*) = (0, 0) \tag{4.38a}$$
$$= (\ln(a(1 - q)), 0) \tag{4.38b}$$

60

These are similar to the two trivial steady state solutions (4.29) and (4.30) found for dynamic tannin. The nontrivial steady states are given by

$$(M^*, V^*) = \left(\frac{V(1 - \sigma_v)}{\lambda(1 - \exp(-bV_n))}, V \right) \tag{4.39}$$

where V^* is a solution to

$$V(1 - \sigma_v) = \frac{1}{r}\lambda(1 - \exp(-bV_n))(\ln(a(1 - q)) - bV_n). \tag{4.40}$$

We investigate the number of nontrivial solutions by letting

$$
\begin{aligned}
f(V) &= V(1 - \sigma_v) \\
g(V) &= \frac{1}{r}\lambda(1 - \exp(-bV_n))(\ln(a(1 - q)) - bV_n)
\end{aligned}
$$

Figure 4-7 plots functions $f(V)$ and $g(V)$ to display the number of nontrivial solutions. The number of nontrivial solutions is given by the number of intersections of the two lines (solid and dashed) excluding the intersection at the origin. The intersection at the origin is the trivial steady state solution (4.38b).
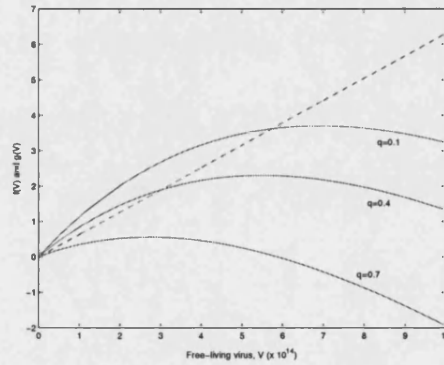
Figure 4-7: Plot shows the intersection of $f(V)$ (dashed line) and $g(V)$ (solid lines). Parameters are $a = 6.0; b = 0.1; \lambda = 1.49; \sigma_v = 0.37; r = 0.001$.

We see from Figure 4-7 that for high q no nontrivial steady state exists. For smaller, more realistic, values of q the nontrivial steady state does exists. As function f is a linear increasing function and function g is concave there can exist at most one nontrivial steady state solution as there will be at most one intersection for $V > 0$. Therefore, we have a similar situation to that of the model with tannin. There exists two trivial solutions: one in which the virus dies out and the gypsy moths persist at a

61

constant level and another in which both the virus and the gypsy moths die out. Yet in the case of the nontrivial steady state, we can only obtain at most one solution when tannin is constant. So the addition of tannin in the system has added the possibility of multiple nontrivial steady state solutions. However practically, for dynamic tannin, parameter estimates indicate that at most one nontrivial steady state solution exists.

4.3.2 Further simplification to the model

We simplify the model further to look at the stability of the system. The model is reduced by making the same simplifications as in Chapter 3, section 3.3, i.e. we only consider the impact of tannin on the susceptibility of gypsy moths to NPV infection. This is due to the observation by Schultz et al. (1990) that tannin reduces susceptibility to infection to a greater extent than reduction in fecundity. We also set the self-limit parameter $r = 0$, so that the only regulation on gypsy moth population is from virus infection. This is to be consistent with the model from Chapter 3. Our simplified model system becomes

$$M_{n+1} = a(1-q)\exp\left(\frac{-bV_n}{1+cT_n}\right)M_n \tag{4.41a}$$

$$V_{n+1} = \sigma_v V_n + \lambda\left[1 - \exp\left(\frac{-bV_n}{1+cT_n}\right)\right]M_n \tag{4.41b}$$

$$T_{n+1} = \sigma_t T_n + \rho M_n \tag{4.41c}$$

Performing steady state analysis, we find that there is now only one trivial steady state

$$(M^*, V^*, T^*) = (0,0,0) \tag{4.42}$$

The other trivial steady state in section 4.1.3 no longer exists as the self-limit parameter, r, has been set to zero.

For the nontrivial steady state, we find that there is one solution

$$(M^*, V^*, T^*) = \begin{pmatrix} \Omega(1-\sigma_t)(1-\sigma_v)a(1-q), \\ \Omega(1-\sigma_t)\lambda(a(1-q)-1), \\ \Omega\rho(1-\sigma_v)a(1-q) \end{pmatrix}$$

where

$$\Omega = \frac{\ln(a(1-q))}{b(1-\sigma_t)\lambda(a(1-q)-1) - c\rho a(1-q)(1-\sigma_v)\ln(a(1-q))}.$$

This solution exists if

$$b(1 - \sigma_t)\lambda(a(1 - q) - 1) > c\rho a(1 - q)(1 - \sigma_v)(\log a(1 - q)) \qquad (4.43a)$$

$$a(1 - q) > 1 \qquad (4.43b)$$

Stability for the trivial steady state is given by the Jacobian

$$J = \begin{pmatrix} a(0) & 0 & 0 \\ 0 & \sigma_v & 0 \\ \rho & 0 & \sigma_t \end{pmatrix}.$$

Therefore, we have one stability condition

$$a(1 - q) < 1$$

For the nontrivial steady state, the Jacobian is

$$J = \begin{pmatrix} 1 & -M^*\frac{b}{1+cT^*} & M^*cV^*\frac{b}{(1+cT^*)^2} \\ \lambda[1 - X] & \sigma_v + \lambda M^*\frac{b}{1+cT^*}X & -\lambda M^*cV^*\frac{b}{(1+cT^*)^2}X \\ \rho & 0 & \sigma_t \end{pmatrix}$$

where $X = \exp\left(\frac{-bV^*}{1+cT^*}\right)$. The eigenvalues are the solutions of the cubic expression

$$\chi^3 + A\chi^2 + B\chi + C = 0$$

where

$$A = -\left(1 + \sigma_v + \sigma_t + \frac{(1 - \sigma_v)\ln[a(1 - q)]}{a(1 - q) - 1}\right)$$

$$B = \sigma_v + \sigma_t + \sigma_v\sigma_t - \frac{\rho c(1 - \sigma_v)a(1 - q)(\ln[a(1 - q)])^2}{\lambda b(a(1 - q) - 1)}$$
$$+[a(1 - q) + \sigma_t]\frac{(1 - \sigma_v)\ln[a(1 - q)]}{a(1 - q) - 1}$$

$$C = \sigma_v\frac{\rho c(1 - \sigma_v)a(1 - q)(\ln[a(1 - q)])^2}{\lambda b(a(1 - q) - 1)}$$
$$-\sigma_t\left(\sigma_v + \frac{(1 - \sigma_v)a(1 - q)\ln[a(1 - q)]}{a(1 - q) - 1}\right)$$

The stability of the nontrivial steady state is determined by the Jury conditions (4.22).

63

For stability to occur only 3 of the conditions need to hold, (4.22b) (4.22c) (4.22d)

$$-1 + A - B + C \; > \; 0 \qquad (4.44a)$$
$$1 \; > \; |C| \qquad (4.44b)$$
$$|1 - C^2| \; > \; |B - A| \qquad (4.44c)$$

The remaining Jury condition (4.22a) is the same condition as the existence condition for the nontrivial condition (4.43a). Therefore this Jury condition holds whenever the nontrivial steady state exists.

Results of simplified model

Now we have analysed the simplified model we look at the behaviour of the model over realistic parameter estimates. We use estimates given in Table 4.1 over a range of values for ρ and σ_t. We fix parameter, c to $c = 1$. We investigate the impact tannin has on the gypsy moth virus system by allowing the production of tannin and the decay rate of tannin to vary. In Chapter 3 we found that for the continuous time model, oscillatory behaviour could become stabilised by the addition of tannin for particular parameter ranges of r and s (where r is a measure of the rate of production of tannin and s is a measure of the decay rate of tannin). We termed this $r - s$ parameter region where a stable steady state appeared the "pocket of stability". In Figure 4-8 we see
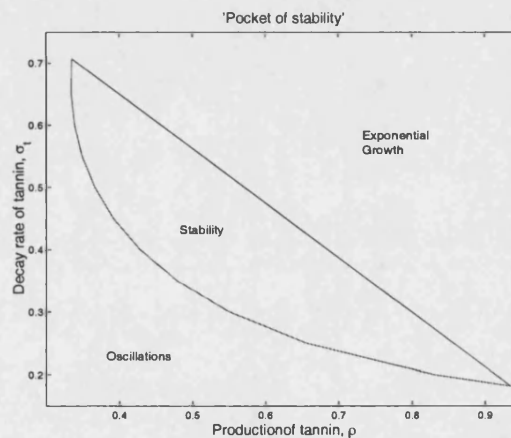
Figure 4-8: Plot shows the "pocket of stability" found from the addition of tannin to the gypsy moth NPV model. Parameters are $a = 6.0; b = 0.1; \lambda = 1.49; \sigma_v = 0.37; c = 0.1; q = 0.1$.

an analogous "pocket of stability" for the discrete time model. The figure also shows

ρ-σ_t parameter space where populations grow exponentially or oscillate. Figure 4-9(a) shows the population behaviour when exponential growth occurs. This is when ρ and σ_t are both large and here the existence condition (4.43a) (which is also the first Jury condition) fails. Figure 4-9(b) shows the oscillatory behaviour for low values of ρ and σ_t. The Jury condition (4.44c) fails to hold for these in this parameter region and a Naimark Sacker bifurcation occurs resulting in cyclic behaviour. Lastly Figure 4-9(c) shows populations when all the Jury conditions hold. Here the populations remain stable.

(a)   (b)   (c)
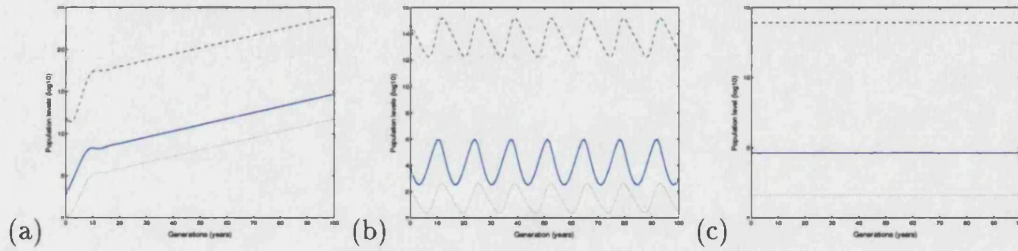
Figure 4-9: Plot shows model behaviour for the simplified model (gypsy moths - blue, NPV - green, tannin - red). Figure (a) shows exponential growth for $\rho = 0.7$ and $\sigma_t = 0.6$. Figure (b) shows oscillatory populations for $\rho = 0.4$ and $\sigma_t = 0.3$. Figure (c) shows stable nontrivial steady state for $\rho = 0.5$ and $\sigma_t = 0.5$. Parameters are $a = 6.0; b = 0.1; \lambda = 1.49; \sigma_v = 0.37; c = 0.1; q = 0.1$ with initial conditions $m(1) = 0.5; v(1) = 0.8; t(1) = 1$

Indeed from Figure 4-9(b), we observe for small ρ, σ_T the gypsy moth population is regulated by NPV as stable oscillations occur. As ρ and σ_T increase, these oscillations reduce until condition (4.44) holds and a stable steady state occurs, Figure 4-9(c). A further increase causes the existence condition for the nontrivial steady state to fail and the population becomes unregulated and grows exponentially (see Figure 4-9(a)).

Modelling without tannin

If we exclude tannin from the modelling process, model (4.41) reduces to a model similar to that of (Nicholson & Bailey 1935) discussed in Chapter 2. That is the model becomes

$$M_{n+1} = a(1-q)\exp(-bV_n)M_n \qquad (4.45a)$$

$$V_{n+1} = \sigma_V V_n + \lambda\left[1 - \exp(-bV_n)\right]M_n \qquad (4.45b)$$

This model has two steady state solutions, one trivial and one nontrivial. When the nontrivial steady state exists, both steady states will be unstable. Figure 4-10 shows the typical behaviour of growing oscillations for when both trivial and nontrivial steady states exist. This same unstable behaviour is commonly seen in the Nicholson-Bailey model (Nicholson & Bailey 1935), see (Hassell 1978). From the analysis of model (4.45)
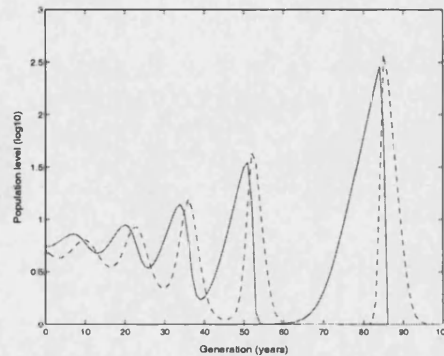
Figure 4-10: Plot shows the typical growing oscillations found in model (4.45) when the nontrivial steady state exists (prey - solid line, parasitoid - dashed line). Parameters are $a = 6.0; b = 0.1; \lambda = 1.49; \sigma_v = 0.37; q = 0.75$ with initial conditions $m(1) = 4.5; v(1) = 4.0$.

we see that the addition of the plants effect on the gypsy moth virus system has caused regulation for some $\rho - \sigma_t$ parameter space. We see that at low values of ρ and σ_t bounded oscillations occur. Therefore the addition of tannin has caused the growing oscillations from seen in Figure 4-10 to become regulated stable oscillations. Further to this, for larger ρ and σ_t growing oscillations are regulated to a stable steady state. Yet for larger ρ and σ_t exponential growth still remains.

Hence, adding tannin into the system has created a steady state solution, which is not present in the model without tannin. So the addition of tannin has had a stabilising effect on the system.

Including self-limit for gypsy moths

The simplified model (4.41) showed the model behaviour over a range of ρ and σ_t values. Amongst this behaviour was exponential growth where the virus alone was unable to regulate the gypsy moth population. We now include a self-limit for the gypsy moth growth by allowing $r \neq 0$. We let r be small ($r = 0.0001$) so that the self-limit only affects the unregulated gypsy moth populations. Figure 4-11 displays the behaviour of the model for both $r = 0$ and $r = 0.0001$. We see that the behaviour

remains unchanged from the inclusion of the self-limit parameter, r for oscillatory and stable steady state behaviour.
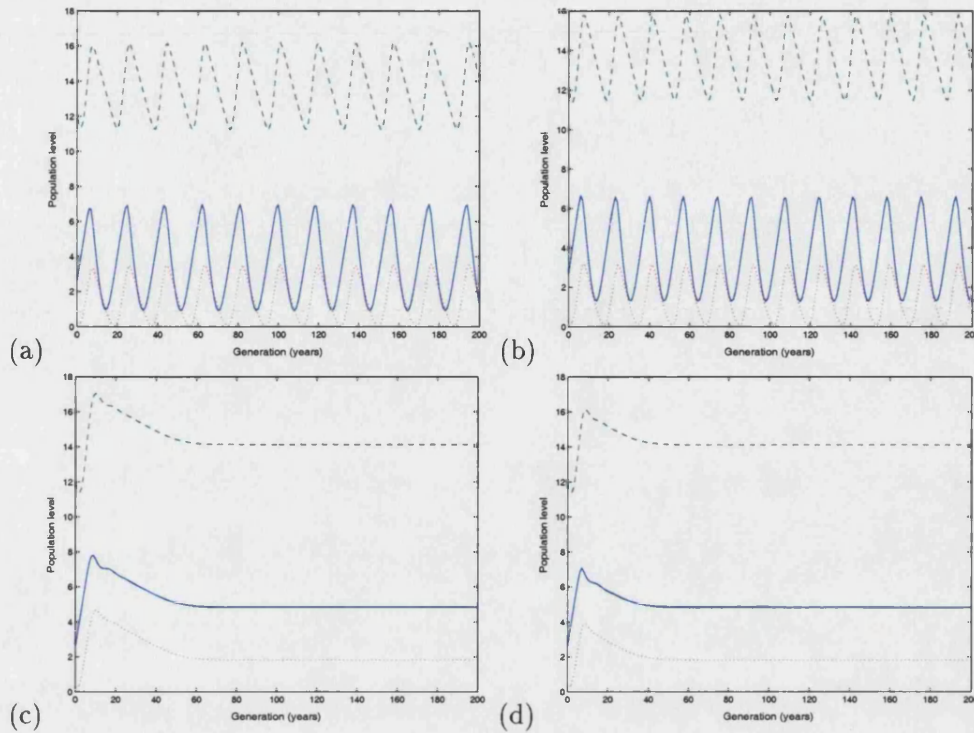
Figure 4-11: Plot shows the similar model behaviour from the inclusion of self-limit on gypsy moths (gypsy moths - blue, NPV - green, tannin - red). Figure (a) simplified model for $\rho = 0.1; \sigma_t = 0.8$. Figure (b) simplified model including self-limit for $\rho = 0.1; \sigma_t = 0.8 r = 0.0001;$. Figure (c) simplified model for $\rho = 0.4; \sigma_t = 0.8$. Figure (d) simplified model including self-limit for $\rho = 0.4; \sigma_t = 0.8 r = 0.0001;$. Parameters are $a = 6.0; b = 0.1; \lambda = 1.49; \sigma_v = 0.37; c = 0.1; q = 0.1$ with initial conditions $m(1) = 0.5; v(1) = 0.8; t(1) = 1$

We now look at the area of exponential growth. Figure 4-12 again shows the behaviour of the model for both $r = 0$ and $r = 0.0001$. Obviously the inclusion of $r \neq 0$ regulates the exponential growth. However three different behaviours are observed. In Figure 4-12(b) we see oscillatory behaviour. This occurs when ρ is small and σ_t is large. Much more commonly seen is a stable population at a nontrivial steady state. Figure 4-12(d) demonstrates this behaviour. Lastly we see a trivial steady state where gypsy moth and tannin levels persist but virus populations die out. This occurs at high ρ and σ_t values and is consistent with Figure 4-6 where existence of the nontrivial steady

67

state is lost.
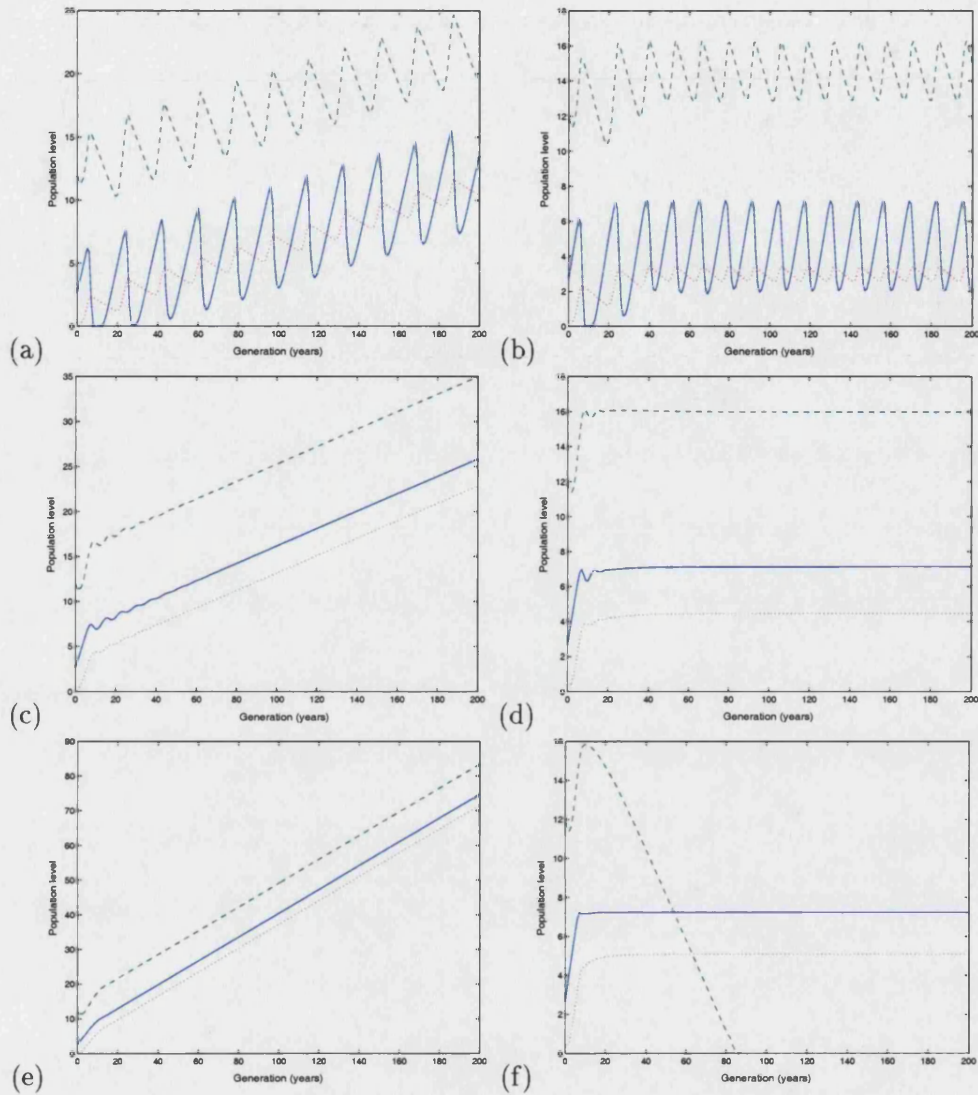
Figure 4-12: Plot shows the change in behaviour from the inclusion of self-limit on gypsy moths (gypsy moths - blue, NPV - green, tannin - red). Figure (a) simplified model for $\rho = 0.1; \sigma_t = 0.8$. Figure (b) simplified model including self-limit for $\rho = 0.1; \sigma_t = 0.8 r = 0.0001;$. Figure (c) simplified model for $\rho = 0.4; \sigma_t = 0.8$. Figure (d) simplified model including self-limit for $\rho = 0.4; \sigma_t = 0.8 r = 0.0001;$. Figure (e) simplified model for $\rho = 0.7; \sigma_t = 0.9$. Figure (f) simplified model including self-limit for $\rho = 0.7; \sigma_t = 0.9 r = 0.0001;$. Parameters are $a = 6.0; b = 0.1; \lambda = 1.49; \sigma_v = 0.37; c = 0.1; q = 0.1$ with initial conditions $m(1) = 0.5; v(1) = 0.8; t(1) = 1$

68

4.3.3 Complete model system

In the previous section we looked at simplified versions of the complete gypsy moth virus tannin model. We did this to gain an understanding of the system. We now compare our findings from the previous section with numerical simulations of the complete model system. From extensive numerical runs we find a few instances where the behaviours are different. This always occurs between the change in behaviour from oscillatory population cycles to stable steady state populations as ρ increases. We find that for the complete model this change occurs at slightly higher values of ρ. As ρ increases further we observe the same stable steady state behaviour as seen in the simplified model. Figure 4-13 shows the change in behaviour of the simplified model and the complete model.
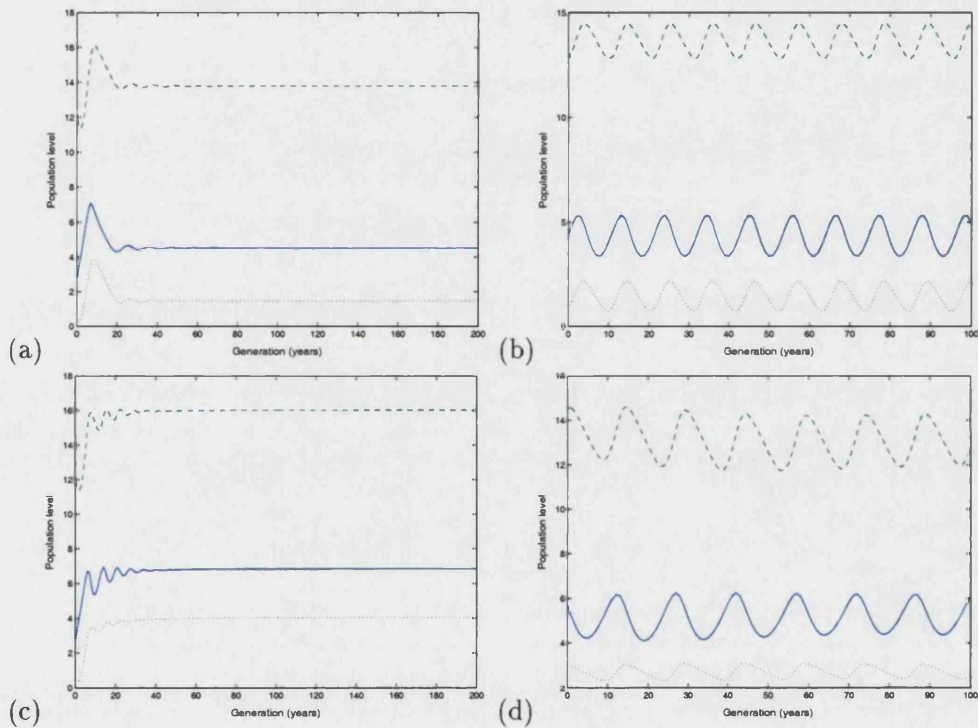
Figure 4-13: Plot shows the change in behaviour between the complete model system and the simplified version (gypsy moths - blue, NPV - green, tannin - red). Figure (a) simplified model for $\rho = 0.5; \sigma_t = 0.4$. Figure (b) complete model for $\rho = 0.5; \sigma_t = 0.4r = 0.0001;$. Figure (c) simplified model for $\rho = 0.3; \sigma_t = 0.8$. Figure (d) complete model for $\rho = 0.3; \sigma_t = 0.8r = 0.0001;$. Parameters are $a = 6.0; b = 0.1; \lambda = 1.49; \sigma_v = 0.37; c = 0.1; d = 0.0067; q = 0.4; k = 20$ with initial conditions $m(1) = 0.5; v(1) = 0.8; t(1) = 1$

69

More generally the behaviours observed from the complete model system are the same behaviours seen in the simplified model. This is demonstrated in Figure 4-14.
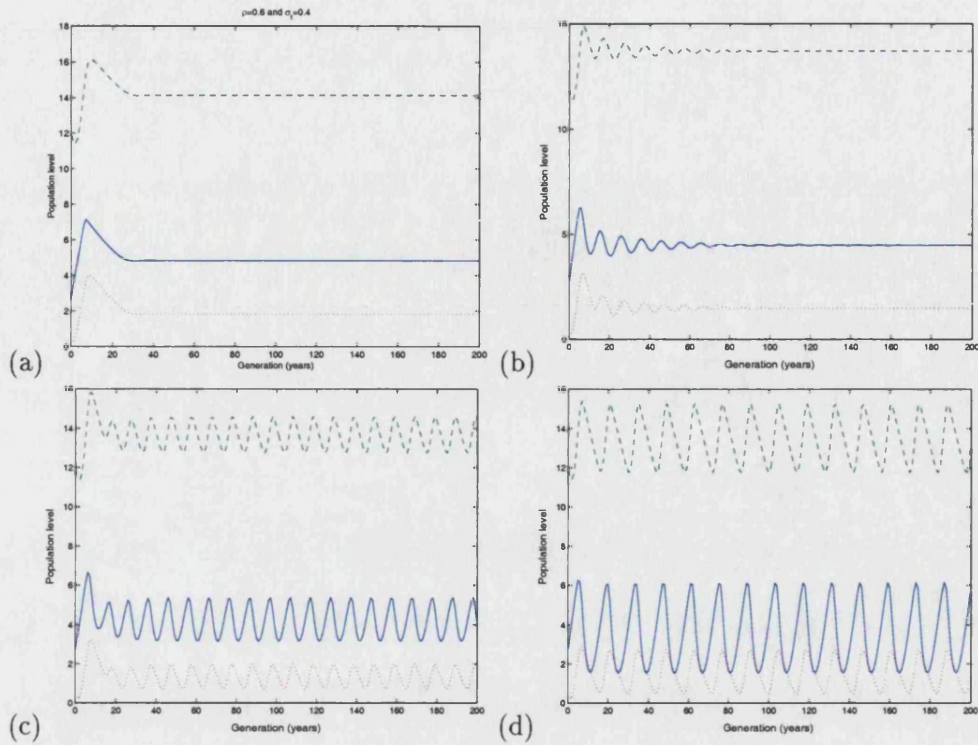
Figure 4-14: Plot shows the change in behaviour between the complete model system and the simplified version (gypsy moths - blue, NPV - green, tannin - red). Figure (a) simplified model for $\rho = 0.6; \sigma_t = 0.4$. Figure (b) complete model for $\rho = 0.6; \sigma_t = 0.4 r = 0.0001;$. Figure (c) simplified model for $\rho = 0.3; \sigma_t = 0.5$. Figure (d) complete model for $\rho = 0.3; \sigma_t = 0.5 r = 0.0001;$. Parameters are $a = 6.0; b = 0.1; \lambda = 1.49; \sigma_v = 0.37; c = 0.1; d = 0.0067; q = 0.4; k = 20$ with initial conditions $m(1) = 0.5; v(1) = 0.8; t(1) = 1$.

Therefore from the simulations we conclude that the type of behaviour found in the simplified model, described in the previous section, also gives a good account of the behaviour observed in the complete model system. However oscillatory behaviour is slightly more common in the complete model system. This may well be due to the fluctuations in the birth rate for the complete model.

4.4 Summary and Discussion

In this chapter, we have shown an alternative way to modelling the gypsy moth-NPV-tannin system. Instead of using continuous time equations to describe the system, we instead built up a discrete time relationship. This is believed to more appropriately model the system as the gypsy moth has annual reproduction and has no overlapping generations.

A generalised model was built first, in order to explain the interactions and combine the main processes involved in the interactions between the gypsy moth, the virus and tannin. Whilst building the model we discovered that period doubling and chaos exist in the system. This was popularised in discrete time models by May (1976) for the logistic map and we see the same behaviour when only gypsy moth populations are modelled. A two cycle occurs where populations oscillate between high and low levels. However two cycles and period doubling occur when the gypsy moth birth rate is high, yet birth rate estimates do not concur with this high value.

A model system was formed by adding NPV and later tannin based on known assumptions. The addition of NPV and subsequently tannin allows the model system to display a rich variety of behaviours. In order to explore these behaviours further it was required to define specific functions as shown in section 4.2. Functions were chosen to have the basic characteristics, yet to be as simple as possible for analysis to be tractable. Also several vital rates and other estimates are known which are summarised in Table 4.1. Using these functions in the models from section 4.1.3, the systems were analysed mathematically. From a simplified version of the model we found that when tannin was included many steady states may occur. This depends on the exact parameters, however using realistic estimates, at most one nontrivial steady state solution is found. Yet when tannin was excluded only one nontrivial steady state occurred. From a further simplification we analysed the stability of the nontrivial steady state.

As discussed in Chapter 3, we expect that the addition of tannin to the gypsy moth-NPV virus interactions will cause a destabilising effect. However in Chapter 3, we found that this is not always the case and on some occasions the opposite effect, stabilisation, appears. In the discrete time model we see that there also exists a parameter range (σ_t-ρ) where stabilisation occurs. Again stabilisation occurs in a small pocket from high decay rate of tannin with low production rate of tannin to small decay rate with high production rate of tannin. Furthermore high values of either production of tannin or decay of tannin causes a loss in regulation of gypsy moth populations by NPV and hence gypsy moths grow without bound. On the other hand, small values for the production

71

of tannin and decay rate results in oscillatory behaviour. All these behaviours are consistent with the behaviour found in the continuous time model. Hence the change from continuous time modelling to discrete has not caused a change in the observed behaviour. More importantly the cyclic population levels of gypsy moths seen in field observations is readily seen in both continuous and discrete models. However, the structure of the gypsy moth life cycle makes a discrete time model more appropriate to reflect the rigid annual life cycle of the gypsy moth.

Chapter 5

Optimal Control for the Gypsy Moth Model

The damage caused by gypsy moths is extensive. Whole areas of woodland have been defoliated resulting in the gypsy moth becoming one of Americas most devastating forest pest.

As gypsy moths are such a destructive forest pest with considerable economic impact, the US government is committed to controlling gypsy moth populations. Numerous control attempts have been made, but we will focus on one popular choice a biocontrol agent called Gypchek. Despite this method of control being very expensive it is still used regularly due to its effectiveness. Yet due to the costs of Gypchek it is restricted to use in only small quantities. However the widespread use of Gypchek, even in small quantities, results in a huge sum of money spent by the USDA on gypsy moth control.

In this chapter we aim to find a control strategy that is cost effective. We do this by first assigning a cost to account for the damage caused by gypsy moths. This cost can be reduced by lowering gypsy moth population size. This can be achieved by the use of the control Gypchek. However there is also a cost to produce and use Gypchek. Therefore by summing the two costs, the cost of damage and the cost of control, we obtain a total cost. We then seek a control strategy that minimises the total cost function.

In section 1 we describe the mathematical set up of the bioeconomic problem. Section 2 then shows the existence of an optimal solution. Section 3 gives a characterisation of an optimal control by finding the adjoint system. A uniqueness condition is proved in section 4 under certain criteria. The last section gives numerical results and interpretations of optimal solutions.

5.1   Mathematical model set up

We aim to optimise such that the sum of the costs of control and the cost of damage are minimised over a set, or fixed, period of time. We do this by forming a cost function which we will refer to as the objective functional. We then minimise the objective function subject to the set of constraints given by the state equations.

We represent the objective functional as cost of damage plus the cost of control for each year over a finite number N years

$$J(p) \;=\; \sum_{n=0}^{N} \left[A_n M_n + \frac{B_n}{2} p_n^2 \right]. \tag{5.1}$$

where p_n is the manufactured NPV sprayed into the environment at generation n. Here A_n is the cost of "damage" per gypsy moth. Therefore for simplicity we assume a linearly proportional increase in damage with increasing gypsy moth population levels. The constants B_n are the cost parameters for the control. Due to the labour intensive method of production of Gypchek we assume the costs of treatment are nonlinear and take the quadratic form given here.

The set of controls is bounded above as Gypchek can cause irritation at high levels to humans. Hence the controls belong to the bounded set

$$U \;=\; \{ 0 \le p_n \le P_{max} | n = 0, 1, ..N \} \tag{5.2}$$

with P_{max} being the maximum application for each generation. The objective function however is subject to constraints. These constraints are the set of equations of the gypsy moth model with the addition of the control term. This addition describes the effect of spraying the control agent on gypsy moth infested areas each year. Hence the constraints are

$$M_{n+1} \;=\; \frac{a}{1 + dT_n} \frac{k + (1-q)V_n}{k + V_n} \exp\left(-rM_n - \frac{bV_n}{1 + cT_n} \right) M_n \tag{5.3a}$$

$$V_{n+1} \;=\; \sigma_v V_n + \lambda \left(1 - \exp\left(\frac{-bV_n}{1 + cT_n} \right) \right) M_n + p_n \tag{5.3b}$$

$$T_{n+1} \;=\; \rho M_n + \sigma_t T_n \tag{5.3c}$$

The other variables and parameters remain the same as in the previous chapter. The

equations also have the initial conditions

$$M_0 = M_{int}, \tag{5.4a}$$

$$V_0 = V_{int}, \tag{5.4b}$$

$$T_0 = T_{int}. \tag{5.4c}$$

We note that by an iterative construction that given $p\epsilon U$ where $p = \{p_0, p_1 \ldots p_N\}$, there exists $(M, V, T) = (M(p), V(p), T(p))$ satisfying (5.3)-(5.4).

5.1.1 Existence of an Optimal Solution

First of all we show that a solution to the optimal control problem (5.1)-(5.4) exists. The objective functional J depends on the controls p and also the state variables. The set of all possible objective function values, $\{J(p)|p\epsilon U\}$, is clearly bounded below by zero. This boundedness along with the completeness property of the reals implies the infimum of the set $\{J(p)|p\epsilon U\}$ exists. Yet the existence of the infimum does not guarantee that a minimum is achieved by some control and its corresponding state variables. Thus we now prove that a minimum for the objective function J does exist for an optimal control $p^*\epsilon U$ (see Macki & Strauss (1982) for ideas in existence results).

Theorem 5.1.1. *There exists an optimal control $p^*\epsilon U$ that minimises the objective function $J(p)$.*

Proof. By the approximation property of infimum (Wade 2000) there exists a minimising sequence $\{p^K\}_{K=1}^{\infty}$ of controls for the objective functional J. Due to the fixed initial conditions (5.4a)-(5.4c) we have

$$
\begin{aligned}
M_1 &= \frac{a}{1 + dT_0} \frac{k + (1-q)V_0}{k + V_0} \exp\left(-rM_0 - \frac{bV_0}{1 + cT_0}\right) M_0 \\
V_1^K &= \left[\sigma_v V_0 + \lambda\left(1 - \exp\left(\frac{-bV_0}{1 + cT_0}\right)\right) M_0\right] + p_0^K \\
T_1 &= \rho M_0 + \sigma_t T_0
\end{aligned}
$$

Here M_1 and T_1 remain fixed however V_1^K is sequence dependent. By a further two iterations we see that M_3^K, V_3^K and T_3^K are all sequence dependent. So $\{M^K\}_{K=1}^{\infty}$, $\{V^K\}_{K=1}^{\infty}$ and $\{T^K\}_{K=1}^{\infty}$ are corresponding state sequences to the control sequence $\{p^K\}_{K=1}^{\infty}$. As each sequence consists of a finite set of numbers the sequences are bounded, thus by Bolzano-Weierstrass theorem there exists subsequences $\{p^k\}$, $\{M^k\}$,

$\{V^k\}$ and $\{T^k\}$ where

$$p_n^k \rightarrow p_n^*,$$
$$M_n^k \rightarrow M_n^*,$$
$$V_n^k \rightarrow V_n^*,$$
$$T_n^k \rightarrow T_n^*,$$

for all $n = 0, 1...N$. By the continuous structure of the state system we have $M^* = M(p^*)$, $V^* = V(p^*)$ and $T^* = T(p^*)$. This convergence implies

$$\min_{p \epsilon U} J(p) = \lim_{k \to \infty} \sum_{n=0}^{N} \left(A_n M_n^k + \frac{B_n}{2}(p_n^k)^2 \right)$$
$$= \sum_{n=0}^{N} A_n \left(\lim_{k \to \infty} M_n^k \right) + \sum_{n=0}^{N} \frac{B_n}{2} \left(\lim_{k \to \infty} (p_n^k)^2 \right)$$
$$= \sum_{n=0}^{N} \left(A_n M_n^* + \frac{B_n}{2}(p_n^*)^2 \right)$$

As the range of values for the control is a closed interval of the reals then $p^* \epsilon U$. Hence there exists a control p^* with corresponding states M^*, V^* and T^* that is optimum. $\square$

5.1.2 Optimality system

There are generalisations of Pontryagin's Maximum Principle for ordinary differential equations to discrete time systems (Clark 1990, Sethi & Thompson 2000). Such generalisations can be derived by differentiating the objective functional with respect to the control. Therefore we must differentiate the map

$$p \longrightarrow J(p)$$

which first requires the differentiation of the maps

$$p \rightarrow M = M(p)$$
$$p \rightarrow V = V(p)$$
$$p \rightarrow T = T(p)$$

We call the directional derivatives ψ^M, ψ^V, ψ^T of the solution maps the sensitivities of the states with respect to the control (see Lenhart & Bhat (1992) and Fister (1997) for examples of the use of sensitivities to characterise optimal controls).

Definition 5.1.1. *For ease we define the following: for $\varepsilon > 0$*

$$M^\varepsilon := M(p + \varepsilon l), \quad V^\varepsilon := V(p + \varepsilon l), \quad T^\varepsilon := T(p + \varepsilon l).$$
$$M := M(p), \qquad V := V(p), \qquad T := T(p).$$

Proposition 5.1.1. *Let $p \epsilon U$, then the mappings*

$$p \to M = M(p) \quad p \to V = V(p) \quad p \to T = T(p)$$

are differentiable in the sense

$$
\begin{aligned}
\psi_n^M &= \lim_{\varepsilon \to 0^+} \left(\frac{M_n^\varepsilon - M_n}{\varepsilon} \right) \\
\psi_n^V &= \lim_{\varepsilon \to 0^+} \left(\frac{V_n^\varepsilon - V_n}{\varepsilon} \right) \\
\psi_n^T &= \lim_{\varepsilon \to 0^+} \left(\frac{T_n^\varepsilon - T_n}{\varepsilon} \right)
\end{aligned}
$$

such that $(p + \varepsilon l) \epsilon U$ for small ε and l a directional vector.

Proof. Consider the control maps

$$
\begin{aligned}
p \to M = M(p), \quad p + \varepsilon l \to M^\varepsilon = M(p + \varepsilon l), \\
p \to V = V(p), \quad p + \varepsilon l \to V^\varepsilon = V(p + \varepsilon l), \\
p \to T = T(p), \quad p + \varepsilon l \to T^\varepsilon = T(p + \varepsilon l).
\end{aligned}
$$

From the state equations (5.3a)-(5.3c)

$$
\begin{aligned}
M_{n+1}^\varepsilon - M_{n+1} &= \frac{a}{1 + dT_n^\varepsilon} \frac{k + (1-q)V_n^\varepsilon}{k + V_n^\varepsilon} \exp\left(-rM_n^\varepsilon - \frac{bV_n^\varepsilon}{1 + cT_n^\varepsilon} \right) M_n^\varepsilon \\
&\quad - \frac{a}{1 + dT_n} \frac{k + (1-q)V_n}{k + V_n} \exp\left(-rM_n - \frac{bV_n}{1 + cT_n} \right) M_n \\
V_{n+1}^\varepsilon - V_{n+1} &= \sigma_v V_n^\varepsilon + \lambda \left(1 - \exp\left(\frac{-bV_n^\varepsilon}{1 + cT_n^\varepsilon} \right) \right) M_n^\varepsilon + \varepsilon l_n \\
&\quad - \sigma_v V_n - \lambda \left(1 - \exp\left(\frac{-bV_n}{1 + cT_n} \right) \right) M_n \\
T_{n+1}^\varepsilon - T_{n+1} &= \rho M_n^\varepsilon + \sigma_t T_n^\varepsilon - \rho M_n - \sigma_t T_n
\end{aligned}
$$

Then from above equations the initial conditions (5.4) we have

$$M_1^\varepsilon - M_1 = 0, \tag{5.5a}$$

$$V_1^\varepsilon - V_1 = \varepsilon l_0, \tag{5.5b}$$

$$T_1^\varepsilon - T_1 = 0. \tag{5.5c}$$

Therefore the first sensitivities are bounded

$$\psi_1^M = 0,$$
$$|\psi_1^V| \leq C_1^V,$$
$$\psi_1^T = 0.$$

Similarly for the second sensitivities we have

$$M_2^\varepsilon - M_2 = \left[\frac{a}{1+dT_1^\varepsilon} \frac{k+(1-q)V_1^\varepsilon}{k+V_1^\varepsilon} \exp\left(-rM_1^\varepsilon - \frac{bV_1^\varepsilon}{1+cT_1^\varepsilon} \right) M_1^\varepsilon \right.$$
$$\left. - \frac{a}{1+dT_1} \frac{k+(1-q)V_1}{k+V_1} \exp\left(-rM_1 - \frac{bV_1}{1+cT_1} \right) M_1 \right] \tag{5.6a}$$

$$V_2^\varepsilon - V_2 = \left[\sigma_v V_1^\varepsilon + \lambda \left(1 - \exp\left(\frac{-bV_1^\varepsilon}{1+cT_1^\varepsilon} \right) \right) M_1^\varepsilon \right. \tag{5.6b}$$
$$\left. - \sigma_v V_1 - \lambda \left(1 - \exp\left(\frac{-bV_1}{1+cT_1} \right) \right) M_1 \right] + \varepsilon l_1$$

$$T_2^\varepsilon - T_2 = \rho M_1^\varepsilon + \sigma_t T_1^\varepsilon - \rho M_1 - \sigma_t T_1 \tag{5.6c}$$

From the first sensitivities $M_1^\varepsilon = M_1$, (5.5a), and $T_1^\varepsilon = T_1$, (5.5c), therefore (5.6a) is rewritten

$$M_2^\varepsilon - M_2 = \left[\frac{a}{1+dT_1} \frac{k+(1-q)V_1^\varepsilon}{k+V_1^\varepsilon} \exp\left(-rM_1 - \frac{bV_1^\varepsilon}{1+cT_1} \right) M_1 \right.$$
$$\left. - \frac{a}{1+dT_1} \frac{k+(1-q)V_1}{k+V_1} \exp\left(-rM_1 - \frac{bV_1}{1+cT_1} \right) M_1 \right] \tag{5.7}$$

Dividing through by ε (> 0) and adding and subtracting the term

$$\frac{k+(1-q)V_1^\varepsilon}{k+V_1^\varepsilon} \exp\left(-rM_1 - \frac{bV_1}{1+cT_1} \right) \tag{5.8}$$

78

(5.7) then this becomes,

$$
\frac{M_2^\varepsilon - M_2}{\varepsilon} = \frac{1}{\varepsilon} \left[\frac{k + (1-q)V_1^\varepsilon}{k + V_1^\varepsilon} \exp\left(-rM_1 - \frac{bV_1^\varepsilon}{1 + cT_1}\right) \right.
$$
$$
- \frac{k + (1-q)V_1^\varepsilon}{k + V_1^\varepsilon} \exp\left(-rM_1 - \frac{bV_1}{1 + cT_1}\right)
$$
$$
+ \frac{k + (1-q)V_1^\varepsilon}{k + V_1^\varepsilon} \exp\left(-rM_1 - \frac{bV_1}{1 + cT_1}\right)
$$
$$
\left. - \frac{k + (1-q)V_1}{k + V_1} \exp\left(-rM_1 - \frac{bV_1}{1 + cT_1}\right) \right] M_1 \frac{a}{1 + dT_1}
$$
$$
= \frac{1}{\varepsilon} \left[\left(\frac{k + (1-q)V_1^\varepsilon}{k + V_1^\varepsilon} - \frac{k + (1-q)V_1}{k + V_1} \right) \exp\left(-rM_1 - \frac{bV_1}{1 + cT_1}\right) \right.
$$
$$
+ \frac{k + (1-q)V_1^\varepsilon}{k + V_1^\varepsilon} \left(\exp\left(-rM_1 - \frac{bV_1^\varepsilon}{1 + cT_1}\right) \right.
$$
$$
\left. \left. - \exp\left(-rM_1 - \frac{bV_1}{1 + cT_1}\right) \right) \right] M_1 \frac{a}{1 + dT_1}
$$

Taking the limit

$$
\psi_2^M = \lim_{\varepsilon \to 0^+} \left(\frac{M_2^\varepsilon - M_2}{\varepsilon} \right)
$$
$$
= \left(\frac{qk}{(k + V_1)^2} - \frac{b}{1 + cT_1} \frac{k + (1-q)V_1}{k + V_1} \right) M_1 \frac{a}{1 + dT_1}
$$
$$
\exp\left(-rM_1 - \frac{bV_1}{1 + cT_1}\right) \psi_1^V
$$
$$
=: D_1 \psi_1^V
$$

Then as ψ_1^V is bounded it follows that ψ_2^M is bounded

$$
|\psi_2^M| \leq D_1 C_1^V
$$
$$
=: C_2^M.
$$

Following the same process for (5.6c) and (5.6c) we find ψ_2^V, ψ_2^T are bounded

$$
\psi_2^V = \lim_{\varepsilon \to 0} \left(\frac{V_2^\varepsilon - V_2}{\varepsilon} \right)
$$
$$
= \left(\sigma_v + \frac{\lambda b}{1 + cT_1} \exp\left(\frac{-bV_1}{1 + cT_1} \right) \right) M_1 \psi_1^V + l_n
$$
$$
= D_2 \psi_1^V + D_3
$$
$$
|\psi_2^V| \leq D_2 C_1^V + D_3
$$
$$
=: C_2^V
$$

79

and

$$\psi_2^T = \lim_{\varepsilon \to 0} \left(\frac{T_2^\varepsilon - T_2}{\varepsilon} \right)$$
$$= 0$$

from (5.5a), (5.5c) and (5.6c). We can continue iteratively to show

$$|\psi_n^M| \leq C_n^M$$
$$|\psi_n^V| \leq C_n^V$$
$$|\psi_n^T| \leq C_n^T$$

So the sensitivities are bounded. $\square$

Proposition 5.1.2. *The sensitivities ψ satisfy the following system*

$$
\begin{aligned}
\psi_{n+1}^M &= (1 - rM_n)\frac{a}{1+dT_n}\frac{k+(1-q)V_n}{k+V_n}\exp\left(-rM_n - \frac{bV_n}{1+cT_n}\right)\psi_n^M \\
&\quad + \left(\frac{qk}{(k+V_n)^2} - \frac{b}{1+cT_n}\frac{k+(1-q)V_n}{k+V_n}\right)\exp\left(-rM_n - \frac{bV_n}{1+cT_n}\right) \\
&\quad M_n\frac{a}{1+dT_n}\psi_n^V - \left(\frac{cbV_n}{(1+cT_n)^2}\frac{a}{1+dT_n} + \frac{ad}{1+dT_n}\right)M_n \\
&\quad \frac{k+(1-q)V_n}{k+V_n}\exp\left(-rM_n - \frac{bV_n}{1+cT_n}\right)\psi_n^T \quad (5.9a) \\
\psi_{n+1}^V &= \lambda\left(1 - \exp\left(\frac{-bV_n}{1+cT_n}\right)\right)\psi_n^M + \left(\sigma_v + \frac{\lambda bM_n}{1+cT_n}\exp\left(\frac{-bV_n}{1+cT_n}\right)\right)\psi_n^V \\
&\quad - \frac{\lambda cbM_nV_n}{(1+cT_n)^2}\exp\left(\frac{-bV_n}{1+cT_n}\right)\psi_n^T + l_n \quad (5.9b) \\
\psi_{n+1}^T &= \rho\psi_n^M + \sigma_t\psi_n^T \quad (5.9c)
\end{aligned}
$$

Proof. It follows from the proof of Proposition 5.1.1. $\square$

Theorem 5.1.2. *Given an optimal control p^* and corresponding state solutions M^*, V^*, T^* then there exists adjoint variables q^M, q^V, q^T such that the adjoint variables satisfy the system*

$$
\begin{aligned}
q_{n-1}^M &= (1 - rM_n^*)\frac{a}{1+dT_n^*}\frac{k+(1-q)V_n^*}{k+V_n^*}\exp\left(-rM_n^* - \frac{bV_n^*}{1+cT_n^*}\right)q_n^M \\
&\quad + \lambda\left(1 - \exp\left(\frac{-bV_n^*}{1+cT_n^*}\right)\right)q_n^V + \rho q_n^T + A_n \quad (5.10a) \\
q_{n-1}^V &= \left(\frac{qk}{(k+V_n^*)^2} - \frac{b}{1+cT_n^*}\frac{k+(1-q)V_n^*}{k+V_n^*}\right)\exp\left(-rM_n^* - \frac{bV_n^*}{1+cT_n^*}\right)
\end{aligned}
$$

80

$$M_n^* \frac{a}{1 + dT_n^*} q_n^M + \left(\sigma_v + \frac{\lambda b M_n^*}{1 + cT_n^*} \exp\left(\frac{-bV_n^*}{1 + cT_n^*} \right) \right) q_n^V \tag{5.10b}$$

$$
\begin{aligned}
q_{n-1}^T = & -\left(\frac{cbV_n^*}{(1 + cT_n^*)^2} \frac{a}{1 + dT_n^*} + \frac{ad}{1 + dT_n^*} \right) M_n^* \exp\left(-rM_n^* - \frac{bV_n^*}{1 + cT_n^*} \right) \\
& \frac{k + (1 - q)V_n^*}{k + V_n^*} q_n^M - \frac{\lambda cb M_n^* V_n^*}{(1 + cT_n^*)^2} \exp\left(\frac{-bV_n^*}{1 + cT_n^*} \right) q_n^V + \sigma_t q_n^T
\end{aligned}
\tag{5.10c}
$$

with the transversality conditions

$$q_N^M = 0 \tag{5.11a}$$

$$q_N^V = 0 \tag{5.11b}$$

$$q_N^T = 0 \tag{5.11c}$$

Furthermore the optimal control is given by

$$p_n^* = \max\left(0, \min\left(-\frac{q_n^V}{B_n}, P_{max} \right) \right) \tag{5.12}$$

Proof. We start by taking the directional derivative of the objective functional. Then for $\varepsilon > 0$ and directional vector l,

$$
\begin{aligned}
0 \leq\ & \frac{\partial(J(p^*))}{\partial p} \\
=\ & \lim_{\varepsilon \to 0^+} \frac{1}{\varepsilon} [J(p^* + \varepsilon l) - J(p^*)] \\
=\ & \lim_{\varepsilon \to 0^+} \frac{1}{\varepsilon} \left[\sum_{n=0}^{N} \left(A_n M_n^{*\varepsilon} + \frac{B_n}{2}(p_n^{*\varepsilon})^2 \right) - \sum_{n=0}^{N} \left(A_n M_n^* - \frac{B_n}{2}(p_n^*)^2 \right) \right] \\
=\ & \sum_{n=0}^{N} \left[A_n \lim_{\varepsilon \to 0^+} \left(\frac{M_n^{*\varepsilon} - M_n^*}{\varepsilon} \right) + \frac{B_n}{2} \lim_{\varepsilon \to 0^+} \left(\frac{(p_n^{*\varepsilon})^2 - (p_n^*)^2}{\varepsilon} \right) \right] \\
=\ & \sum_{n=0}^{N} \left[A_n \psi_n^M + B_n p_n^* l_n \right]
\end{aligned}
\tag{5.13}
$$

$$\tag{5.14}$$

where

$$
\begin{aligned}
p^\varepsilon &= p + \varepsilon l \\
M^\varepsilon &= M(p + \varepsilon l)
\end{aligned}
$$

and from Proposition 5.1.1

$$\psi^M = \lim_{\varepsilon \to 0^+} \left(\frac{M^\varepsilon - M}{\varepsilon} \right)$$

Note also from Proposition 5.1.1

$$\psi^V = \lim_{\varepsilon \to 0^+} \left(\frac{V^\varepsilon - V}{\varepsilon} \right)$$

$$\psi^T = \lim_{\varepsilon \to 0^+} \left(\frac{T^\varepsilon - T}{\varepsilon} \right)$$

ψ_n^M in (5.14), can be replaced with parameters from the original problem by finding the costate variables of the adjoint equations. From Proposition 2 we re-write this system of coupled linear equations in matrix form

$$\begin{pmatrix} \psi_{n+1}^M \\ \psi_{n+1}^V \\ \psi_{n+1}^T \end{pmatrix} - A \begin{pmatrix} \psi_n^M \\ \psi_n^V \\ \psi_n^T \end{pmatrix} = \begin{pmatrix} 0 \\ l_n \\ 0 \end{pmatrix} \tag{5.15}$$

where

$$A = \begin{pmatrix} a_{11} & a_{12} & a_{13} \\ \lambda \left(1 - \exp\left(\frac{-bV_n}{1+cT_n} \right) \right) & \sigma_v + \frac{\lambda b M_n}{1+cT_n} \exp\left(\frac{-bV_n}{1+cT_n} \right) & \frac{\lambda cb M_n V_n}{(1+cT_n)^2} \exp\left(\frac{-bV_n}{1+cT_n} \right) \\ \rho & 0 & \sigma_t \end{pmatrix}$$

and

$$a_{11} = \frac{a}{1+dT_n} \frac{k + (1-q)V_n}{k + V_n} (1 - rM_n) \exp\left(-rM_n - \frac{bV_n}{1+cT_n} \right)$$

$$a_{12} = \left(\frac{qk}{(k+V_n)^2} - \frac{b}{1+cT_n} \frac{k+(1-q)V_n}{k+V_n} \right) \frac{a}{1+dT_n} \exp\left(-rM_n - \frac{bV_n}{1+cT_n} \right) M_n$$

$$a_{13} = -\left(\frac{cbV_n}{(1+cT_n)^2} \frac{a}{1+dT_n} + \frac{ad}{1+dT_n} \right) \frac{k+(1-q)V_n}{k+V_n} \exp\left(-rM_n - \frac{bV_n}{1+cT_n} \right) M_n$$

(for convenience we omit the *'s). Let q_n denote the costate variables then the adjoint

equations are found in the following way. Consider

$$S = \sum_{n=0}^{N-1} \begin{pmatrix} q_n^M & q_n^V & q_n^T \end{pmatrix} \left[\begin{pmatrix} \psi_{n+1}^M \\ \psi_{n+1}^V \\ \psi_{n+1}^T \end{pmatrix} - A \begin{pmatrix} \psi_n^M \\ \psi_n^V \\ \psi_n^T \end{pmatrix} \right] \tag{5.16}$$

$$= \sum_{n=0}^{N-1} \begin{pmatrix} q_n^M & q_n^V & q_n^T \end{pmatrix} \begin{pmatrix} \psi_{n+1}^M \\ \psi_{n+1}^V \\ \psi_{n+1}^T \end{pmatrix} - \sum_{n=0}^{N-1} \begin{pmatrix} q_n^M & q_n^V & q_n^T \end{pmatrix} A \begin{pmatrix} \psi_n^M \\ \psi_n^V \\ \psi_n^T \end{pmatrix}$$

$$= \sum_{n=0}^{N-1} \begin{pmatrix} \psi_{n+1}^M & \psi_{n+1}^V & \psi_{n+1}^T \end{pmatrix} \begin{pmatrix} q_n^M \\ q_n^V \\ q_n^T \end{pmatrix} - \sum_{n=0}^{N-1} \begin{pmatrix} \psi_n^M & \psi_n^V & \psi_n^T \end{pmatrix} A^T \begin{pmatrix} q_n^M \\ q_n^V \\ q_n^T \end{pmatrix}$$

We remove a term in the second summation using the fact that the initial conditions for the sensitivities $\begin{pmatrix} \psi_0^M & \psi_0^V & \psi_0^T \end{pmatrix}$ are all zero (as $M_0^\varepsilon = M_0$ etc). Also we force the terminal conditions for the costate variables $\begin{pmatrix} q_N^M & q_N^V & q_N^T \end{pmatrix}$ to be zero and include this term in to the second summation. Then renumbering the indices of the first sum in order to match that of the second this gives

$$S = \sum_{n=1}^{N} \begin{pmatrix} \psi_n^M & \psi_n^V & \psi_n^T \end{pmatrix} \begin{pmatrix} q_{n-1}^M \\ q_{n-1}^V \\ q_{n-1}^T \end{pmatrix} - \sum_{n=1}^{N} \begin{pmatrix} \psi_n^M & \psi_n^V & \psi_n^T \end{pmatrix} A^T \begin{pmatrix} q_n^M \\ q_n^V \\ q_n^T \end{pmatrix}$$

$$= \sum_{n=1}^{N} \begin{pmatrix} \psi_n^M & \psi_n^V & \psi_n^T \end{pmatrix} \left[\begin{pmatrix} q_{n-1}^M \\ q_{n-1}^V \\ q_{n-1}^T \end{pmatrix} - A^T \begin{pmatrix} q_n^M \\ q_n^V \\ q_n^T \end{pmatrix} \right] \tag{5.17}$$

Now as the only sensitivity that appears in the derivative of the objective function (5.14) is ψ_n^M then for each n

$$\psi_n^M A_n = \begin{pmatrix} \psi_n^M & \psi_n^V & \psi_n^T \end{pmatrix} \begin{pmatrix} A_n \\ 0 \\ 0 \end{pmatrix} \tag{5.18}$$

Hence combining (5.17) and (5.18) the adjoint equations are given by

$$\begin{pmatrix} q_{n-1}^M \\ q_{n-1}^V \\ q_{n-1}^T \end{pmatrix} - A^T \begin{pmatrix} q_n^M \\ q_n^V \\ q_n^T \end{pmatrix} = \begin{pmatrix} A_n \\ 0 \\ 0 \end{pmatrix},$$

or more explicitly

$$q^M_{n-1} = (1 - rM_n)\frac{a}{1 + dT_n}\frac{k + (1-q)V_n}{k + V_n}\exp\left(-rM_n - \frac{bV_n}{1 + cT_n}\right)q^M_n$$
$$+ \lambda\left(1 - \exp\left(\frac{-bV_n}{1 + cT_n}\right)\right)q^V_n + \rho q^T_n + A_n$$

$$q^V_{n-1} = \left(\frac{qk}{(k + V_n)^2} - \frac{b}{1 + cT_n}\frac{k + (1-q)V_n}{k + V_n}\right)\exp\left(-rM_n - \frac{bV_n}{1 + cT_n}\right)$$
$$M_n\frac{a}{1 + dT_n}q^M_n + \left(\sigma_v + \frac{\lambda bM_n}{1 + cT_n}\exp\left(\frac{-bV_n}{1 + cT_n}\right)\right)q^V_n$$

$$q^T_{n-1} = -\left(\frac{cbV_n}{(1 + cT_n)^2}\frac{a}{1 + dT_n} + \frac{ad}{1 + dT_n}\right)M_n\exp\left(-rM_n - \frac{bV_n}{1 + cT_n}\right)$$
$$\frac{k + (1-q)V_n}{k + V_n}q^M_n - \frac{\lambda cbM_nV_n}{(1 + cT_n)^2}\exp\left(\frac{-bV_n}{1 + cT_n}\right)q^V_n + \sigma_t q^T_n.$$

Also from (5.15) and (5.16), for each n

$$q^V_n l_n = \begin{pmatrix} q^M_n & q^V_n & q^T_n \end{pmatrix}\begin{pmatrix} 0 \\ l_n \\ 0 \end{pmatrix}$$

So combining (5.15)-(5.18) gives, for each n

$$\sum_{n=1}^{N}\psi^M_n A_n = \sum_{n=0}^{N-1}q^V_n l_n \tag{5.19}$$

Therefore we can make a replacement in (5.14) with (5.19)

$$0 \leq \frac{\partial(J(p^*))}{\partial p} \tag{5.20}$$

$$= \sum_{n=0}^{N}[A_n\psi^M_n + B_np^*_n l_n]$$

$$= A_0\psi^M_0 + \sum_{n=1}^{N}A_n\psi^M_n + \sum_{n=0}^{N-1}B_np^*_n l_n + B_Np^*_N l_N$$

$$= \sum_{n=1}^{N}A_n\psi^M_n + \sum_{n=0}^{N-1}B_np^*_n l_n$$

$$= \sum_{n=0}^{N-1}[l_n(q^V_n + B_np^*_n)] \tag{5.21}$$

So using (5.21) and the boundary conditions (5.2) for a minimum to occur

$$
p_n^* = \begin{cases} 0 & \text{if} & 0 \le q_n^V \\ -\frac{q_n^V}{B_n} & \text{if} & -PB_n \le q_n^V \le 0 \\ P & \text{if} & q_n^V \le -PB_n \end{cases} \tag{5.22}
$$

Hence

$$
p_n^* = \max \left(0, \min \left(-\frac{q_n^V}{B_n}, P \right) \right)
$$

and we get the system as originally stated. $\square$

5.1.3 Uniqueness of the Optimal Control

We use a convexity argument to show the uniqueness of our optimal control (Lenhart & Liang 2000).

Theorem 5.1.3. *If B_n for $n=0,1...N$ are sufficiently large, then the optimal control is unique.*

Proof. We prove a uniqueness result by showing the objective functional J(p) is strictly convex (Rockafellar 1970). We begin by defining the function

$$
\begin{aligned}
g(\varepsilon) &= J((1-\varepsilon)p + \varepsilon l) \\
&= J(p + \varepsilon(l - p))
\end{aligned} \tag{5.23}
$$

For convexity we need to show that the second derivative of (5.23) is strictly positive

$$
g''(\varepsilon) > 0.
$$

The first derivative of (5.23) gives

$$
\begin{aligned}
g'(\varepsilon) &= \lim_{\tau \to 0} \left(\frac{J(p + (\tau + \varepsilon)(l-p)) - J(p + \varepsilon(l-p))}{\tau} \right) \\
&= \lim_{\tau \to 0} \sum_{n=0}^{N} A_n \left(\frac{M_n^{\tau+\varepsilon} - M_n^{\varepsilon}}{\tau} \right) \\
&\quad + \frac{B_n}{2} \left(\frac{[p_n + (\tau + \varepsilon)(l_n - p_n)]^2(x) - [p_n + \varepsilon(l_n - p_n)]^2}{\tau} \right) \\
&= \sum_{n=0}^{N} A_n \psi_n^{M,\varepsilon} + B_n(l_n - p_n)[p_n + \varepsilon(l_n - p_n)] \tag{5.24}
\end{aligned}
$$

We now define

$$\sigma_{n+1}^{M,\varepsilon} := \lim_{\tau \to 0} \left(\frac{\psi_{n+1}^{M,\tau+\varepsilon} - \psi_{n+1}^{M,\varepsilon}}{\tau} \right) \tag{5.25a}$$

$$\sigma_{n+1}^{V,\varepsilon} := \lim_{\tau \to 0} \left(\frac{\psi_{n+1}^{V,\tau+\varepsilon} - \psi_{n+1}^{V,\varepsilon}}{\tau} \right) \tag{5.25b}$$

$$\sigma_{n+1}^{T,\varepsilon} := \lim_{\tau \to 0} \left(\frac{\psi_{n+1}^{T,\tau+\varepsilon} - \psi_{n+1}^{T,\varepsilon}}{\tau} \right) \tag{5.25c}$$

Then by a similar result to Proposition 2 (5.9) we have

$$\psi_{n+1}^{M,\varepsilon} = \left[\frac{\partial F}{\partial M_n^\varepsilon} \psi_n^{M,\varepsilon} + \frac{\partial F}{\partial V_n^\varepsilon} \psi_n^{V,\varepsilon} + \frac{\partial F}{\partial T_n^\varepsilon} \psi_n^{T,\varepsilon} \right] \tag{5.26a}$$

$$\psi_{n+1}^{V,\varepsilon} = \left[\frac{\partial G}{\partial M_n^\varepsilon} \psi_n^{M,\varepsilon} + \frac{\partial G}{\partial V_n^\varepsilon} \psi_n^{V,\varepsilon} + \frac{\partial G}{\partial T_n^\varepsilon} \psi_n^{T,\varepsilon} \right] + (l_n - p_n) \tag{5.26b}$$

$$\psi_{n+1}^{T,\varepsilon} = \rho \psi_n^{M,\varepsilon} + \sigma_t \psi_n^{T,\varepsilon} \tag{5.26c}$$

where

$$F = \frac{a}{1 + dT_n^\varepsilon} \frac{k + (1-q)V_n^\varepsilon}{k + V_n^\varepsilon} \exp\left(-rM_n^\varepsilon - \frac{bV_n^\varepsilon}{1 + cT_n^\varepsilon} \right) M_n^\varepsilon \tag{5.27}$$

and

$$G = \sigma_v V_n^\varepsilon + \lambda \left(1 - \exp\left(\frac{-bV_n^\varepsilon}{1 + cT_n^\varepsilon} \right) \right) M_n^\varepsilon \tag{5.28}$$

Then (5.25) combined with (5.26) yields

$$\sigma_{n+1}^{M,\varepsilon} = \left[\frac{\partial F}{\partial M_n^\varepsilon} \sigma_n^{M,\varepsilon} + \frac{\partial^2 F}{\partial M_n^{\varepsilon 2}} (\psi_n^{M,\varepsilon})^2 \right] + \left[\frac{\partial F}{\partial V_n^\varepsilon} \sigma_n^{V,\varepsilon} + \frac{\partial^2 F}{\partial V_n^{\varepsilon 2}} (\psi_n^{V,\varepsilon})^2 \right]$$
$$+ \left[\frac{\partial F}{\partial T_n^\varepsilon} \sigma_n^{T,\varepsilon} + \frac{\partial^2 F}{\partial T_n^{\varepsilon 2}} (\psi_n^{T,\varepsilon})^2 \right] \tag{5.29a}$$

$$\sigma_{n+1}^{V,\varepsilon} = \left[\frac{\partial G}{\partial M_n^\varepsilon} \sigma_n^{M,\varepsilon} + \frac{\partial^2 G}{\partial M_n^{\varepsilon 2}} (\psi_n^{M,\varepsilon})^2 \right] + \left[\frac{\partial G}{\partial V_n^\varepsilon} \sigma_n^{V,\varepsilon} + \frac{\partial^2 G}{\partial V_n^{\varepsilon 2}} (\psi_n^{V,\varepsilon})^2 \right]$$
$$+ \left[\frac{\partial G}{\partial T_n^\varepsilon} \sigma_n^{T,\varepsilon} + \frac{\partial^2 G}{\partial T_n^{\varepsilon 2}} (\psi_n^{T,\varepsilon})^2 \right] \tag{5.29b}$$

$$\sigma_{n+1}^{T,\varepsilon} = \rho \sigma_n^{M,\varepsilon} + \sigma_t \sigma_n^{T,\varepsilon} \tag{5.29c}$$

Now the initial sensitivities are all zero, $\psi_0^{M,\varepsilon} = 0$, $\psi_0^{V,\varepsilon} = 0$ and $\psi_0^{T,\varepsilon} = 0$. Then using

(5.26) we calculate the next sensitivities. Thus the next sensitivities are

$$
\begin{aligned}
\psi_1^{M,\varepsilon} &= 0 \\
\psi_1^{V,\varepsilon} &= (l_o - p_o) \\
\psi_1^{T,\varepsilon} &= 0
\end{aligned}
$$

Continuing this process iteratively we find the following expression

$$
|\psi_{n+1}^{M,\varepsilon}| \le \sum_{j=0}^{n} \alpha_j (l_{n-j} - p_{n-j})
$$

$$
|\psi_{n+1}^{V,\varepsilon}| \le \sum_{j=0}^{n} \beta_j (l_{n-j} - p_{n-j})
$$

$$
|\psi_{n+1}^{T,\varepsilon}| \le \sum_{j=0}^{n} \gamma_j (l_{n-j} - p_{n-j})
$$

where

$$
\alpha_0 = 0 \quad \beta_0 = 1 \quad \gamma_0 = 0
$$
$$
\alpha_1 = \frac{\partial F}{\partial V_n^\varepsilon} \quad \beta_1 = \frac{\partial G}{\partial V_n^\varepsilon} \quad \gamma_1 = 0
$$

and for $i = 1, 2 \ldots n - 1$,

$$
\alpha_{j+1} = \left(\frac{\partial F}{\partial M_n^\varepsilon}, \frac{\partial F}{\partial V_n^\varepsilon}, \frac{\partial F}{\partial T_n^\varepsilon} \right) \cdot (\alpha_j, \beta_j, \gamma_j) \tag{5.30}
$$

$$
\beta_{j+1} = \left(\frac{\partial G}{\partial M_n^\varepsilon}, \frac{\partial G}{\partial V_n^\varepsilon}, \frac{\partial G}{\partial T_n^\varepsilon} \right) \cdot (\alpha_j, \beta_j, \gamma_j) \tag{5.31}
$$

$$
\gamma_{j+1} = (\rho, 0, \sigma_t) \cdot (\alpha_j, \beta_j, \gamma_j) \tag{5.32}
$$

Also note that $\sigma_0^{M,\varepsilon} = 0$, $\sigma_0^{V,\varepsilon} = 0$ and $\sigma_0^{T,\varepsilon} = 0$. Then similarly from (5.29) we can compute the successive values using $ab \ge \frac{-1}{2}(a^2 + b^2)$ (see Appendix B1)

$$
|\sigma_{n+1}^{M,\varepsilon}| \le \sum_{j=0}^{n} C_j^M (l_{n-j} - p_{n-j})^2,
$$

$$
|\sigma_{n+1}^{V,\varepsilon}| \le \sum_{j=0}^{n} C_j^V (l_{n-j} - p_{n-j})^2,
$$

$$
|\sigma_{n+1}^{T,\varepsilon}| \le \sum_{j=0}^{n} C_j^T (l_{n-j} - p_{n-j})^2.
$$

Hence we easily obtain the following

$$\sum_{i=0}^{n} |\sigma_{i+1}^{M,\varepsilon}| \le \sum_{i=0}^{n} D_i^M (l_{n-i} - p_{n-j})^2,$$

$$\sum_{i=0}^{n} |\sigma_{i+1}^{V,\varepsilon}| \le \sum_{i=0}^{n} D_i^V (l_{n-j} - p_{n-j})^2,$$

$$\sum_{i=0}^{n} |\sigma_{i+1}^{T,\varepsilon}| \le \sum_{i=0}^{n} D_i^T (l_{n-j} - p_{n-j})^2.$$

We can now take the second derivative of the function g. Hence differentiating (5.24) and using the bound (5.33a)

$$
\begin{aligned}
g''(\varepsilon) &= \sum_{n=0}^{N} A_n \lim_{\tau \to 0} \left(\frac{\psi_n^{M,\varepsilon+\tau} - \psi_n^{M,\varepsilon}}{\tau} \right) + B_n(l_n - p_n) \\
&\quad \lim_{\tau \to 0} \left(\frac{[p_n + (\varepsilon + \tau)(l_n - p_n)] - [p_n + \varepsilon(l_n - p_n)]}{\tau} \right) \\
&= \sum_{n=0}^{N} A_n \sigma_n^{M,\varepsilon} + B_n(l_n - p_n)^2 \\
&\ge \sum_{n=0}^{N} (B_n - \hat{C})(l_n - p_n)^2 \\
&> 0
\end{aligned}
$$

So for sufficiently large B_n's the function is convex. Hence the optimal control is unique. $\square$

5.2 Numerical Results

In this section we look numerically at an optimal control strategy for the model. This uses an iterative method consisting of 6 difference equations from the state and adjoint equations. The iterative process begins by solving the state system forward in time with specific initial conditions and with an initial guess for the adjoint variables qV_n, for $n = 0, 1...N - 1$. Then using the transversality conditions and the values calculated for the state variables, the adjoint equations are solved backwards in time. Thus a new set of adjoint variables qV_n are calculated. These new adjoint values are compared with the initial guess. If the absolute difference between them is greater then a specified tolerance for any n then the new values are used as the initial guess for the adjoint variables. The process of calculate state variables forward in time and adjoint variables

backwards in time continues until the absolute difference between successive qV_n sets is less than the tolerance level. Once this has occurred the system is solved and we have an optimal control set p_n. For more information on such iterative methods see Hackbusch (1978).

This method may not necessarily converge. Difficulties in the convergence of the optimality system for the model leads us to make an adaption to the model. This involves the replacement of the linear term for the production of tannin given in the previous chapter (4.26). In its replacement we use a bounded function $\rho(M) = \frac{\rho M}{1+\tau M}$. In this case we find the method to converge. Other updating methods for control, such as convex combinations of old and new adjoint variables as used in Jung, Lenhart & Feng (2002) had little effect on the ability to converge yet it did have an effect on the speed of convergence.

The parameters used in the numerics are taken from Chapter 4 with the exception of σ_t and ρ. Due to the change in the production of tannin term new values for σ_t, ρ and τ were chosen to give qualitatively the same behaviour as discussed in the previous chapter.

5.2.1 Optimal spray strategies

For Figures 5-1 and 5-3 optimal control strategies are give over a 50 year time period. Population levels and control levels have been scaled to appear on the same graph. Population levels of gypsy moths are scaled by 10^{-3} and virus levels scaled by 10^{-13}.

Figure 5-1 shows 6 plots of the optimal control solution for varying costs of control, B_n. Figure 5-1(a) shows an optimal control solution where the cost of control is extremely high. Here it is not beneficial in terms of cost, to try to control the population at all. Therefore we see that the figure displays the oscillatory cycles as seen in Chapter 4.

Figures 5-1(b-d) show how, as the cost of control reduces, the use of control plays a greater role in the optimal solution. Figure 5-1(b) has a high cost and hence there is little use of control and subsequently little effect on the population cycles. More control is seen in Figure 5-1(c) which reduces the fluctuations and has a slight dampening on the fluctuations towards the end of the time period. A further reduction in cost of the control has a much greater effect on the dampening of the fluctuations, Figure 5-1(d). Also we observe that the control is used in a greater quantity at times when the virus populations are at their lowest levels. This is the stage of the cycle when gypsy moth populations begin to outbreak.

Reducing the cost of control further we see in Figure 5-1(e) that the amount of control used in some years reaches the maximum quantity. Control is used less in years

where virus populations are at there highest and gypsy moths are in decline. Further dampening of the oscillations has occurred. Finally Figure 5-1(f) shows that at very low costs of control the optimal solution is to use the maximum amount of control each year. An interesting observation in this case is that although the oscillations are dampened they have slightly increased in comparison to Figure 5-1(e). This suggests that when the control is oscillatory this helps dampen the population cycle. However, the application of a constant control inhibits the fluctuation to a lesser degree.
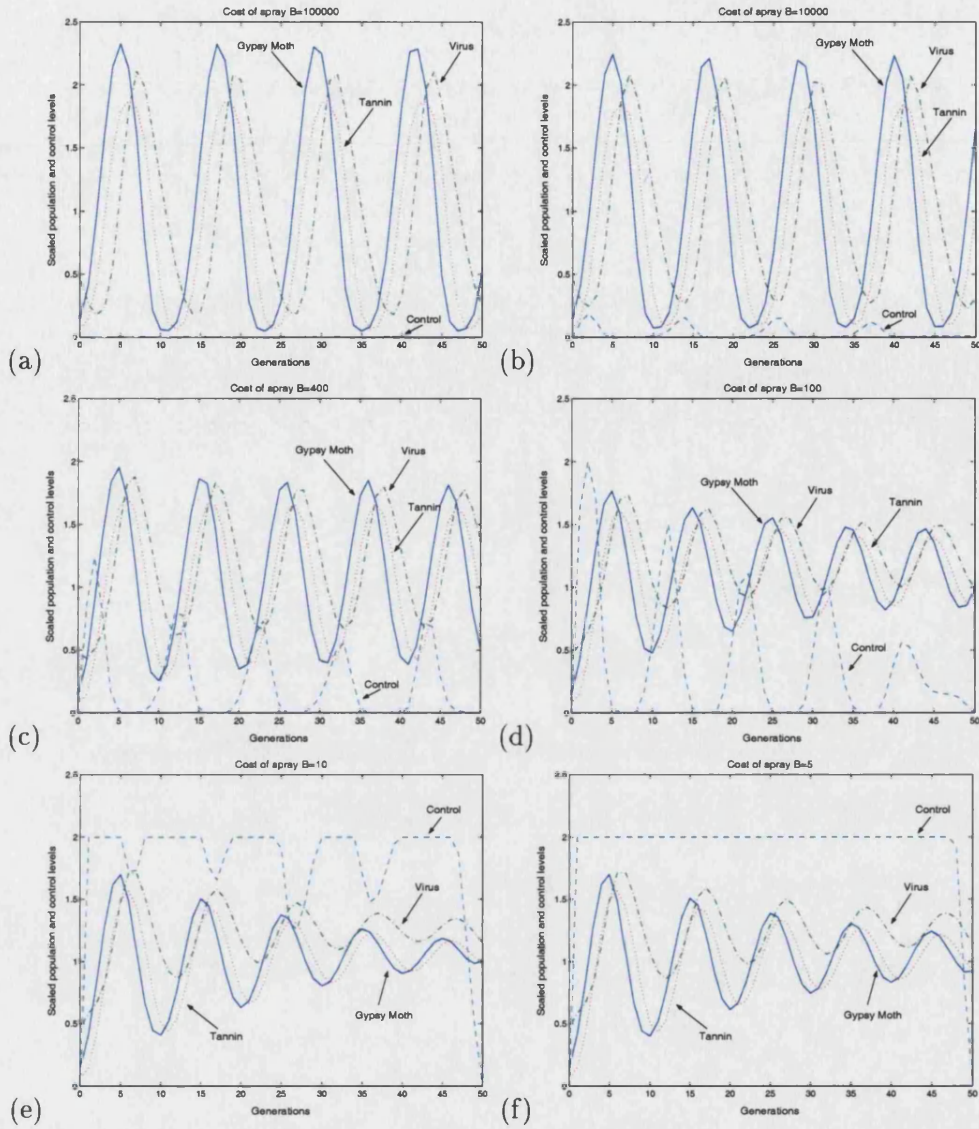
Figure 5-1: Plots show optimal cost solution applied to oscillatory population dynamics. Figure (a) for cost of spray, B=10000, Figure (b) for B=1000, Figure (c) for B=400, Figure (d) for B=100, Figure (e) for B=10, Figure (f) for B=5. Other parameters are $a = 6.0$, $b = 0.1$, $c = 0.1$, $d = 0.067$, $q = 0.4$, $k = 3.0$, $r = 0.001$, $\lambda = 1.49$, $\sigma_v = 0.37$, $\sigma_t = 0.1$, $\rho = 1.0$, $\tau = 0.01$ and $A = 10$.
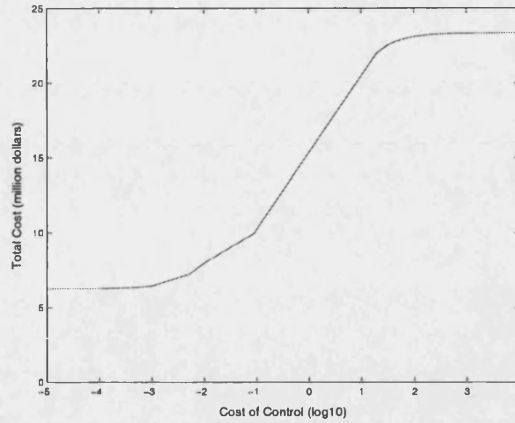
Figure 5-2: Plot shows the Total cost of the minimised objective function against cost of control. Parameters are $a = 6.0$, $b = 0.1$, $c = 0.1$, $d = 0.067$, $q = 0.4$, $k = 3.0$, $r = 0.001$, $\lambda = 1.49$, $\sigma_v = 0.37$, $\sigma_t = 0.1$, $\rho = 1.0$, $\tau = 0.01$ and $A = 10$.

Figure 5-2 shows that when the cost of control is very high then slight changes in the cost of control makes little difference to the total cost calculated by the objective function. Similarly the same is true at very low costs of control. Yet in between these cases even a relatively small change in the cost of the control can have considerable effect on the total cost. This region is in the interval [-3,2] in Figure 5-2 which corresponds to the interval for the cost of control [1,10000]. A decrease in cost of control from 100 (Figure 5-1(d)) to 50 (Figure 5-1(e)) results in a 2.2 million dollar reduction in the total cost. Hence money spent on the advancement of cutting the cost of control may well be money well spent. But in the case where the cost of control is high reducing the cost of control may not be beneficial. For low cost of control this would certainly not be of benefit. From another point of view an organisation providing the control (and hence benefitting from the cost of the control) may take advantage at low costs of control. That is they could price there products higher and have little effect on the total cost of control.

92
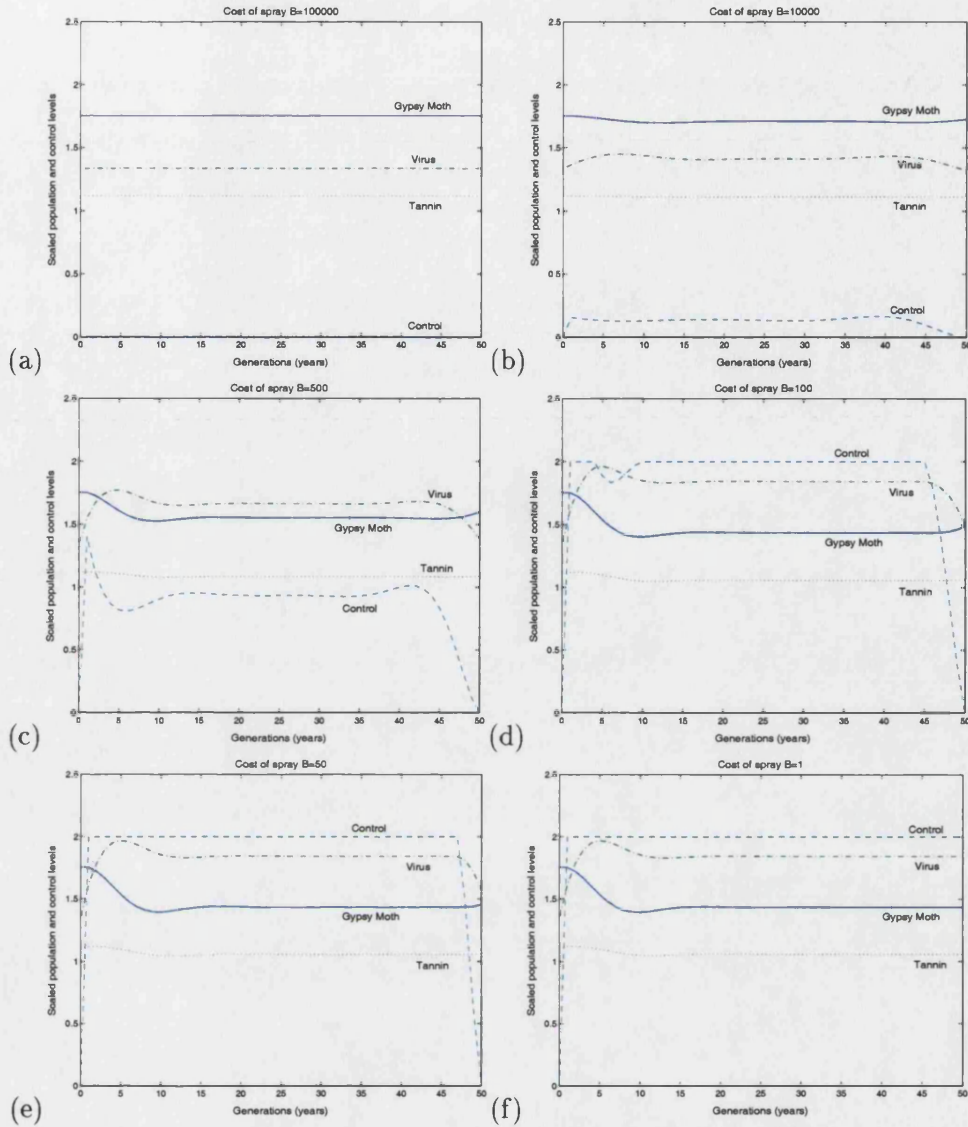
Figure 5-3: Plots show optimal cost solution applied to stable steady state populations. Figure (a) for cost of spray, B=10000, Figure (b) for B=1000, Figure (c) for B=500, Figure (d) for B=100, Figure (e) for B=50, Figure (f) for B=1. Other parameters are $a = 6.0$, $b = 0.1$, $c = 0.1$, $d = 0.067$, $q = 0.4$, $k = 3.0$, $r = 0.001$, $\lambda = 1.49$, $\sigma_v = 0.37$, $\sigma_t = 0.3$, $\rho = 5.0$, $\tau = 0.1$ and $A = 10$.

Figure 5-3 shows 6 plots of optimal control solutions for a system for which population levels are at a steady state. Figure 5-3(a) has a very high cost of control and hence the optimal solution is not to use control leaving the populations at a steady state. Figures 5-3(b) and 5-3(c) show the control lowering the gypsy moth population.

93

In particular Figure 5-3(c) shows that the optimal solution reduces the gypsy moth population early in the control sequence. However immediately after the initial high input of control there is a dip in the amount of control used. This is demonstrated again in Figure 5-3(d) where the control is at the maximum level except at the point where the gypsy moth population have been reduced. Figures 5-3(e) and 5-3(f) show controls at maximum levels. In each of the optimal solutions the population levels remain relatively constant even though they have been reduced by different degrees. It is suggested that the reason for the drop in control after the initial high input is to dampen any fluctuations in the populations that may occur as a result of the sudden input of control.
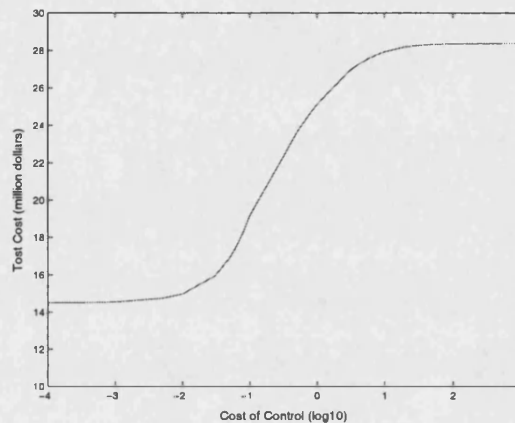
Figure 5-4: Plot shows the Total cost of the minimised objective function against cost of control. Parameters are $a = 6.0$, $b = 0.1$, $c = 0.1$, $d = 0.067$, $q = 0.4$, $k = 3.0$, $r = 0.001$, $\lambda = 1.49$, $\sigma_v = 0.37$, $\sigma_t = 0.3$, $\rho = 5.0$, $\tau = 0.1$ and $A = 10$.

Figure 5-4 shows the same behaviour as Figure 5-2. This time the critical cost region is in the interval [-2,1] corresponding to the cost of control [10,10000]. We again see that in this region a reduction in the cost of spray can have a big impact on reducing the total cost. Yet outside this interval a small reduction in the cost of control has little if any affect on the total cost.

5.2.2 Other spray strategies

An optimal control strategy, although most cost effective , may not be the most practical solution. Instead a strategy where an application of control only occurs if a set criterion is met, may prove to be more pragmatic. This for example could be to spray when virus populations are at a certain level. Indeed from Figure 5-1(d) we see that

the optimal control strategy applies control when virus levels are at their lowest. Similarly the least control (in fact no control) is applied when the virus population is at its highest values. We therefore construct a spraying strategy in which the control is only used when the virus population is low. However virus levels are hard to determine in the field but instead we can monitor the gypsy moth populations. From Figure 5-1 the fluctuations of virus levels match the fluctuations of the gypsy moth population except with a time delay of either 2 to 3 generations. We can use this information on gypsy moth numbers as an indicator for when to apply control.

We will now look at several different spray strategies and compare these with the optimum control solutions. We will compare the total costs and the behaviours of the populations. For each case we set the cost of damage A to be \$10 and the the cost of spray B to be \$100. In this case the optimal solution gives a total cost of \$10.201m and without any control the cost is \$46.812m.

Case 1

In the first case we use control for one generation at the maximum level. This is applied two years after gypsy moth population levels begin to increase. Figure 5-5(a) shows the solution to this control strategy.
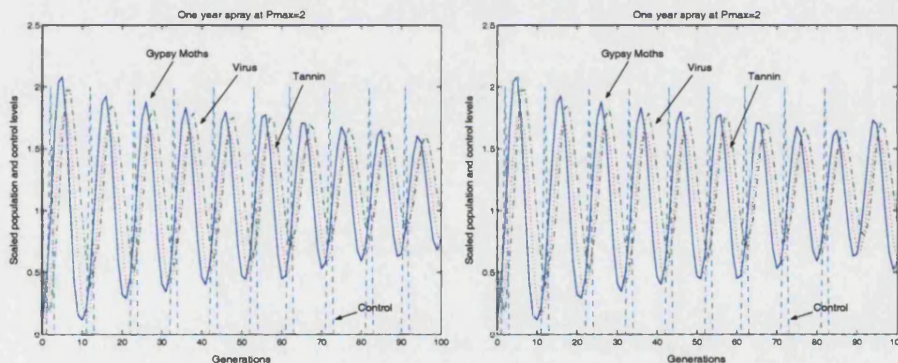
Figure 5-5: Plots show the population levels under control form applying control method in Case 1. Parameters are $a = 6.0$, $b = 0.1$, $c = 0.1$, $d = 0.067$, $q = 0.4$, $k = 3.0$, $r = 0.001$, $\lambda = 1.49$, $\sigma_v = 0.37$, $\sigma_t = 0.1$, $\rho = 1.0$, $\tau = 0.01$ and $A = 10$.

We see that the control reduces the fluctuations similar to the optimal control. Yet the total cost for the strategy is \$25.445m, more than double the cost of the optimum strategy. However a slight reduction in cost can be achieved by excluding the last year of spray, see Figure 5-5(b). Here the cost reduces to \$25.369m.

95

Case 2

In the second case we spray for two generations at the maximum quantity. This time we apply the control one year after an increase in gypsy moth populations.
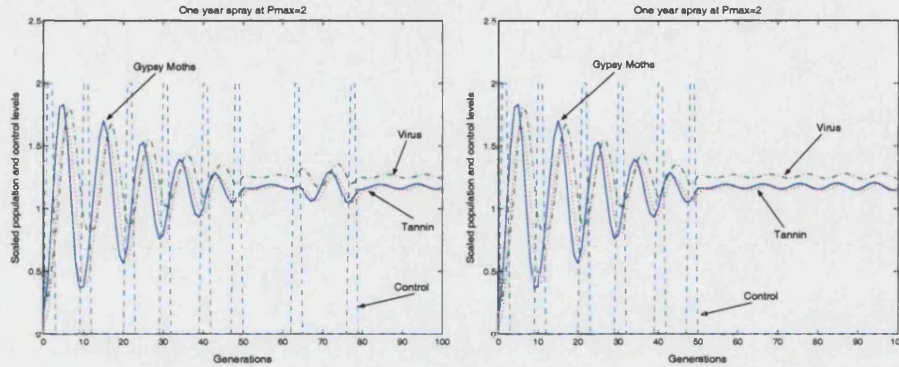
Figure 5-6: Plots show the population levels under control form applying control method in Case 2. Parameters are $a = 6.0$, $b = 0.1$, $c = 0.1$, $d = 0.067$, $q = 0.4$, $k = 3.0$, $r = 0.001$, $\lambda = 1.49$, $\sigma_v = 0.37$, $\sigma_t = 0.1$, $\rho = 1.0$, $\tau = 0.01$ and $A = 10$.

Figure 5-6(a) shows the solution. We see that the control has dampened the oscillations over the first 50 years. The next 50 years the control is used less frequently and the population fluctuations are small. The total cost has reduced to $21.581m. In Figure 5-6(b) control is only used in the first 50 years. We see that the population levels remain fluctuating only slightly over the next fifty years even without control. The cost in this scenario is decreased to $20.103m.

Case 3 and 4

In case 3 we spray for an extra year. Figure 5-7(a) shows control used for three generations at the maximum quantity. This time the fluctuations are reduced much more quickly. After 3 applications of control we see that the total cost has reduced to $19.119m. Further use of control decreases fluctuations but increases the total cost.
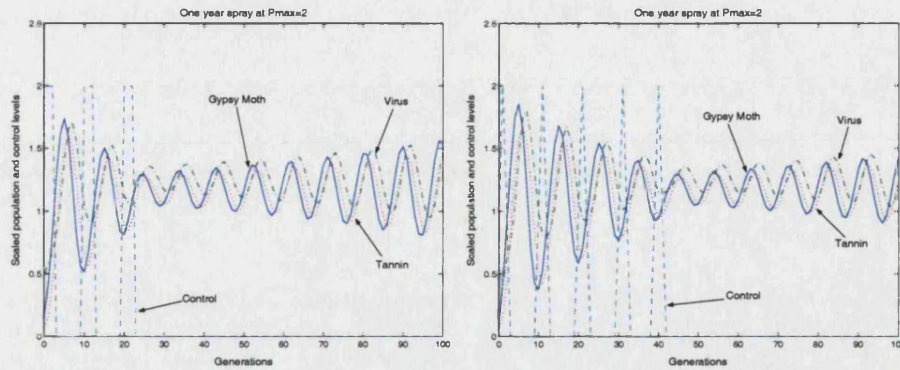
Figure 5-7: Plots show the population levels under control form applying control method in Case 3 (Figure (a)) and Case 4 (Figure (b)). Parameters are $a = 6.0$, $b = 0.1$, $c = 0.1$, $d = 0.067$, $q = 0.4$, $k = 3.0$, $r = 0.001$, $\lambda = 1.49$, $\sigma_v = 0.37$, $\sigma_t = 0.1$, $\rho = 1.0$, $\tau = 0.01$ and $A = 10$.

For case 4 we apply the same strategy as case 3 except we use a different amount of control in the three generations. We spray only half the amount in the first and the last year of each 3 year spraying process. From Figure 5-7(b) we see that this slowed down the reduction in fluctuations compared with Figure 5-7(a). The total cost for case 4 is \$19.255m more than the case before. Again as with case 3 further applications of control could be used than shown in Figure 7(b) but this results in a higher total cost.

Case 5

For the final scenario we again apply the control for only one generation, as in case 1. This time we let the maximum quantity of control be half the amount in other cases. Here we see that this restriction has had a big effect on the population outcome. By limiting the maximum amount of control we see in Figure 5-8 that the control has had only a slight impact on the reduction of fluctuations in comparison with case 1-4. The total cost has also had less of an effect as the other cases, \$29.142m.

97
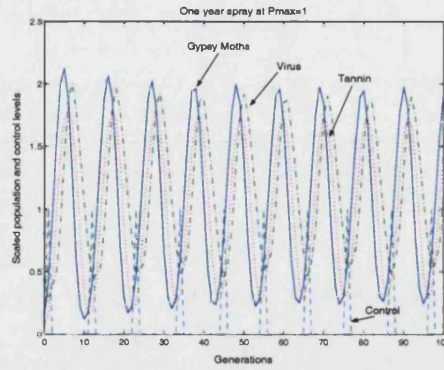
Figure 5-8: Plot shows the population levels under control form applying control method in Case 5. Parameters are $a = 6.0$, $b = 0.1$, $c = 0.1$, $d = 0.067$, $q = 0.4$, $k = 3.0$, $r = 0.001$, $\lambda = 1.49$, $\sigma_v = 0.37$, $\sigma_t = 0.1$, $\rho = 1.0$, $\tau = 0.01$ and $A = 10$.

## 5.3   Summary and Discussion

In this chapter we have presented a bioeconomic model for the control of gypsy moth populations. We have also proved existence and uniqueness conditions for the optimal solution. A numerical method to determine the optimal solution has been discussed and results given.

From the numerical results several points arise. Figures 5-1 show a control being added to populations with cyclic behaviour. Here we see that when the control is economically viable, the application occurs when virus populations are at their lowest and hence when gypsy moth populations are in outbreak phase. Also the population fluctuations are heavily reduced when large inputs of control are used at these instances. Hence the optimal control appears to try to remove fluctuating populations in favour of steady population behaviour.

Figures 5-3 show the populations at constant steady state values. Here, adding the control appears not to destabilise the population level, yet the control does reduce the amount of gypsy moths. The optimal solution however is not to apply the control constantly over the time period. Instead a large application appears at the beginning of the control sequence followed by a significant reduction in the amount used shortly after, then a higher amount of control is used constantly over the remaining time period. The dip that occurs shortly after the initial input may be in order to stabilise the population levels. Hence from this and the effect of the optimal control in Figures 5-1 it suggests that it is more beneficial in terms of cost not to have fluctuating populations.

Further to this, we discover that there is a critical area for the cost of control where

a small change in cost may have a significant effect on the total cost. This could be of critical use in deciding if efforts to reduce the cost of control will be worthwhile. Also, particularly at low costs of control, this information could be useful for organisations on pricing their product, in order to increase product price with negligible effect demand.

A more practical approach has also been considered. Several different control strategies were proposed. Some of these control strategies worked well in reducing gypsy moth fluctuations but none of them were as cost effective as the optimum control. We saw that in case 3 the fluctuations were reduced quickly however, after the control had finished the oscillations began to grow fairly rapidly. In case 2 it took longer for the fluctuations to reduce but once this had occurred they remained low. Therefore a combination of these two strategies could be effective.

Chapter 6

Integrodifference model for Gypsy Moth populations

In the previous chapters, models have considered changes in population levels over time. Those models did not take into account the effect of space. It has been shown that spatially implicit models can display very different behaviour to their spatially explicit counterparts. For example, Turing (1952) showed how stable steady state behaviour from an ordinary differential equation (ODE) system can become unstable when diffusion is added, forming a partial differential (PDE) system, commonly known as reaction diffusion equations. This was later transferred to ecology by Segel & Jackson (1972), Segel & Levin (1976) and Levin & Segel (1976). These instabilities caused by diffusion may well result in spatial patterning forming in homogeneous environments (Mackas & Boyd 1979, Levin 1992). This has led to a growing literature on pattern formation by diffusive instabilities in ecology (Okubo 1980).

However, reaction diffusion systems assume Fickian diffusion, that is, a species moves randomly and subsequently has Gaussian distribution. Recently integrodifference and integrodifferential population models have been used to model species (Kot & Schaffer 1986, Hardin, Takáč & Webb 1988b, Hardin, Takáč & Webb 1988a, Hardin, Takáč & Webb 1990, Kot 1992, Andersen 1991). Integrodifference models are now well used for populations with discrete non-overlapping generations and well-defined growth and dispersal stages (Neubert et al. 1995). These models have an advantage over reaction diffusion models as the assumption of Fickian diffusion is not required. This allows for different dispersal distributions to be used that more accurately reflect the true dispersal of the species.

Not only has the addition of space allowed for the investigation of patterning but also spread rates can be determined. The spread or invasion of a species has originally

100

been modelled by reaction diffusion equations (Fisher 1937, Skellam 1951) which readily give rise to constant speed travelling waves (Fisher 1937). The speed of these waves, commonly referred to as Fishers speed, have often accurately predicted real speeds of invasion (Van Den Bosch, Hengeveld & Metz 1992). However sometimes reaction diffusion equations have underestimated true invasion rates. The most notorious example is Reid's paradox (Skellam 1951, Clark 1998). A more recent alternative to modelling spread is either integrodifference or integrodifferential equations. The advantage of losing the constraint of Fickian diffusion allows for different constant speed travelling waves depending on the chosen dispersal kernel. Indeed some dispersal kernels (fat-tailed kernels) produce accelerating invasions with asymptotically infinite speeds (Kot et al. 1996, Lewis 1997).

In this chapter we introduce space to our discrete time gypsy moth model. We do this in the form of integrodifference equations as these are ideal for populations with discrete non-overlapping generations. We begin by introducing the integrodifference model and the dispersal kernels to look at spatial variation. First, a simplified version of the model is analysed to discover when an originally stable steady state can be destabilised by dispersal. We then compare this with the numerics for this simplified model with the inclusion of gypsy moth self limit. We then look numerically at how dispersal affects the complete model system. Section 2 concerns itself with a general predator-prey travelling wave system. Here we investigate the effect on the prey travelling wave when a predator is introduced to the system behind the wave front. We look at a simple model to compare how reaction diffusion and integrodifference models describe spatial spread. In section 3 we use the results of section 2 to investigate the spread rate of gypsy moths and NPV. We then consider using NPV in the form of Gypchek as a barrier control to reduce gypsy moth spread.

6.1 Spatial variability in gypsy moth populations

In this section we describe the incorporation of space into the complete gypsy moth model system presented in Chapter 4. We first discuss appropriate dispersal kernels for the movement of both the gypsy moths and NPV. We then use the chosen dispersal kernels to form a set of integrodifference equations to describe the spatial representation of the model system.

Previous analysis on a predator prey system by Neubert et al. (1995) showed how a stable steady state in a spatially homogeneous model can be driven unstable in a spatial model. We use this analysis on a simplified version of the gypsy moth system and then compare this with numerics of the complete model system for varying dispersal

101

parameters.

6.1.1 Dispersal and the Integrodifference model

Reaction diffusion systems inherently assume dispersal is Gaussian or Fickian. In integrodifference models and similar integrodifferential models dispersal kernels can be chosen appropriately to approximate the dispersal distribution, thus overcoming Reid's paradox. For gypsy moths, one study considered only the short range dispersal (Dwyer & Elkinton 1995), which accounts only for the movement by crawling or ballooning (wind dispersal) at the caterpillar stage of their life cycle. No distribution is assumed during the adult stage, as the female gypsy moth (which has an extra larval or feeding stage) is too heavy to fly. Therefore the study assumed the dispersal as Fickian diffusion. However, one of the main causes for the large spread of gypsy moths across Northeastern United States is due to long range dispersal. This is often caused by accidental human intervention which is well documented and usually is a result of the insects attaching themselves on items that are moved long distances. A more accurate description of dispersal would take into account both the short range and long range mechanisms. These distributions are known as leptokurtic and the Laplace distribution is a well known example (Neubert et al. 1995, Kot 2002)

$$K(x) = \frac{1}{2}\alpha \exp\left(-\alpha|x|\right) \tag{6.1}$$

where α is the dispersal coefficient. This distribution has exponentially bounded tails and gives rise to a constant speed travelling wave. We will use distribution (6.1) as the dispersal kernel for the gypsy moths.

There is little known about the distribution of NPV. It may be assumed that it diffuses randomly and therefore is appropriate for a Gaussian distribution

$$K(x) = \frac{1}{4\pi D} \exp\left(\frac{-x^2}{4D}\right). \tag{6.2}$$

D is a diffusion coefficient. However, gypsy moths may act as a vector for NPV and this would cause NPV's distribution to also be leptokurtic. In this chapter we will consider both the Gaussian and the Laplace distribution as dispersal kernels for NPV.

Using these dispersal kernels, the spatial gypsy moth model is given by the set of

integrodifference equations

$$M_{n+1}(x) = \int K_1(x-y)f[M_n(y), V_n(y), T_n(y)]dy \tag{6.3a}$$

$$V_{n+1}(x) = \int K_2(x-y)g[M_n(y), V_n(y), T_n(y)]dy \tag{6.3b}$$

$$T_{n+1}(x) = \sigma_t T_n(x) + \rho M_n(x) \tag{6.3c}$$

where f and g are the growth dynamics

$$f[M_n, V_n, T_n] = \frac{a}{1+dT_n} \frac{k+(1-q)V_n}{k+V_n} \exp\left(-rM_n - \frac{bV_n}{1+cT_n}\right)M_n$$

$$g[M_n, V_n, T_n] = \left(\sigma_v V_n + \lambda\left[1 - \exp\left(\frac{-bV_n}{1+cT_n}\right)\right]M_n\right)$$

and K_1 is the Laplace kernel (6.1) and K_2 is either Laplace or Gaussian kernel (6.2). The model parameters are as given in Chapter 4.

6.1.2 Simplified integrodifference model for gypsy moths

We reduce the complete model system (6.3) by making the same simplifications as in Chapter 4. That is, we allow tannin to only affect the susceptibility of gypsy moth infection to NPV, the overwinter contamination remains constant and we set the self limit parameter, r, to be zero. Consequently, the simplified integrodifference model is given by

$$M_{n+1}(x) = \int K_1(x-y)a(1-q)\exp\left(-\frac{bV_n}{1+cT_n}\right)M_n dy,$$

$$V_{n+1}(x) = \int K_2(x-y)\left(\sigma_V V_n + \lambda\left[1 - \exp\left(\frac{-bV_n}{1+cT_n}\right)\right]M_n\right)dy,$$

$$T_{n+1}(x) = \sigma_t T_n + \rho M_n.$$

K_1 and K_2 are the dispersal kernels for gypsy moths and NPV. We consider dispersal driven instability where the addition of diffusion can destabilise a stable spatially explicit steady state solution. We suppose (M^*, V^*, T^*) is a nontrivial steady state solution of the nonspatial discrete time model

$$M_{n+1} = h_1[M_n(y), V_n(y), T_n(y)], \tag{6.4a}$$

$$V_{n+1} = h_2[M_n(y), V_n(y), T_n(y)], \tag{6.4b}$$

$$T_{n+1} = h_3[M_n(y), T_n(y)], \tag{6.4c}$$

where

$$h_1 = a(1-q)\exp\left(-\frac{bV_n}{1+cT_n}\right)M_n,$$

$$h_2 = \sigma_v V_n + \lambda\left[1 - \exp\left(\frac{-bV_n}{1+cT_n}\right)\right]M_n,$$

$$h_3 = \sigma_t T_n + \rho M_n.$$

The stability of the steady state (6.4) is determined from the Jury conditions. We find the Jury conditions from the characteristic polynomial of the Jacobian matrix

$$J = \begin{pmatrix} \frac{\partial h_1}{\partial M_n} & \frac{\partial h_1}{\partial V_n} & \frac{\partial h_1}{\partial T_n} \\ \frac{\partial h_2}{\partial M_n} & \frac{\partial h_2}{\partial V_n} & \frac{\partial h_2}{\partial T_n} \\ \frac{\partial h_3}{\partial M_n} & 0 & \frac{\partial h_3}{\partial T_n} \end{pmatrix}. \tag{6.5}$$

The corresponding characteristic polynomial of the Jacobian matrix (6.5) is,

$$\chi^3 + A\chi^2 + B\chi + C = 0. \tag{6.6}$$

The details of finding the characteristic polynomial (6.6) are given in Chapter 4. Thus the steady state is stable if the Jury conditions are satisfied

$$1 + A + B + C > 0$$
$$-1 + A - B + C > 0$$
$$1 > |C|$$
$$|1 - C^2| > |B - AC|$$

Now to determine the stability of a steady state solution for the integrodifference model, we look at the Jury conditions of the matrix KJ where

$$K = \begin{pmatrix} \hat{k}_1(w) & 0 & 0 \\ 0 & \hat{k}_2(w) & 0 \\ 0 & 0 & 1 \end{pmatrix}.$$

The functions $\hat{k}_1(w)$, $\hat{k}_2(w)$ are Fourier transforms of dispersal kernels K_1, K_2 respectively. Furthermore, the characteristic polynomial for the matrix KJ is

$$\chi^3 + \hat{A}\chi^2 + \hat{B}\chi + \hat{k}_1\hat{k}_2 C = 0$$

where

$$\hat{A} = \hat{k}_1 \frac{\partial h_1}{\partial M_n} + \hat{k}_2 \frac{\partial h_2}{\partial V_n} + \frac{\partial h_3}{\partial T_n}$$

$$\hat{B} = \hat{k}_1 \left(\frac{\partial h_1}{\partial T_n} \frac{\partial h_3}{\partial M_n} - \frac{\partial h_1}{\partial M_n} \frac{\partial h_3}{\partial T_n} \right) - \hat{k}_2 \left(\frac{\partial h_2}{\partial V_n} \frac{\partial h_3}{\partial T_n} \right)$$
$$+ \hat{k}_1 \hat{k}_2 \left(\frac{\partial h_1}{\partial T_n} \frac{\partial h_3}{\partial M_n} - \frac{\partial h_1}{\partial M_n} \frac{\partial h_2}{\partial V_n} \right)$$

Likewise, if the Jury conditions hold then a steady state solution is stable if

$$1 + \hat{A} + \hat{B} + \hat{k}_1 \hat{k}_2 C > 0 \tag{6.7a}$$

$$-1 + \hat{A} - \hat{B} + \hat{k}_1 \hat{k}_2 C > 0 \tag{6.7b}$$

$$1 > |\hat{k}_1 \hat{k}_2 C| \tag{6.7c}$$

$$|1 - (\hat{k}_1 \hat{k}_2 C)^2| > |\hat{B} - \hat{A} \hat{k}_1 \hat{k}_2 C| \tag{6.7d}$$

In this case, the Jury conditions (6.7) must hold for all $w \in \Re$. Now by using Laplace distributions for the dispersal kernels, the Fourier transforms of K_1 and K_2 are

$$\hat{k}_1(w) = \frac{\alpha^2}{\alpha^2 + w^2}$$
$$\hat{k}_2(w) = \frac{\beta^2}{\beta^2 + w^2}$$

where α and β are dispersal coefficients for gypsy moths and NPV respectively. Using parameter estimates from Chapter 4, which produce a spatially homogeneous stable steady state and by fixing α, we vary β to demonstrate any dispersal driven instability. Figure 6-1 shows the spatially explicit solution when the dispersal rate for the gypsy moth and NPV are similar, $\alpha = 100$ and $\beta = 160$. Here the steady state solution of the spatially explicit model remains stable after the addition of dispersal.

(a)   (b)
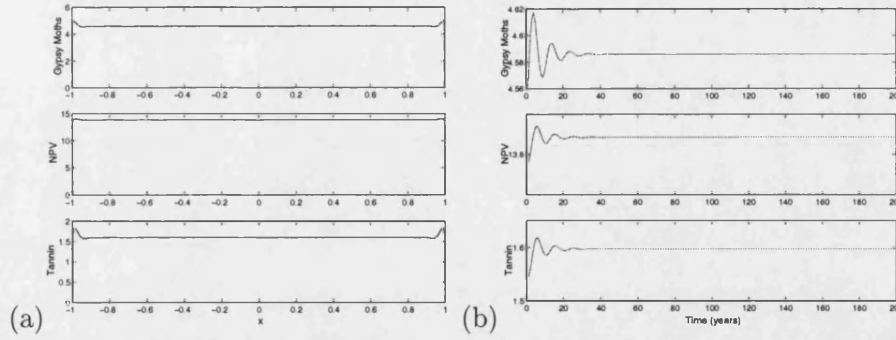
Figure 6-1: Plots show a spatially uniform stable steady state solution. Figure (a) shows population levels over the spatial domain. Figure (b) shows population levels over time at a fixed location. Parameters are $a = 6.0; c = 0.1; q = 0.35; b = 0.1; \lambda = 1.49; \sigma_v = 0.37; \sigma_t = 0.5; \rho = 0.5$ with Laplace dispersal kernels with coefficients $\alpha = 100$ and $\beta = 160$. Initial conditions are $M = 34; V = 60; T = 34$.

However for smaller NPV dispersal a Hopf bifurcation appears. This occurs when β is sufficiently large that inequality (6.7d) is reversed which results in oscillatory population dynamics. Figure 6-2(a) shows a snapshot of the spatial solution of the population levels in one generation and Figure 6-2(b) shows the population levels at one particular location over time. We see that population levels remain constant in space and fluctuate in time.

(a)   (b)
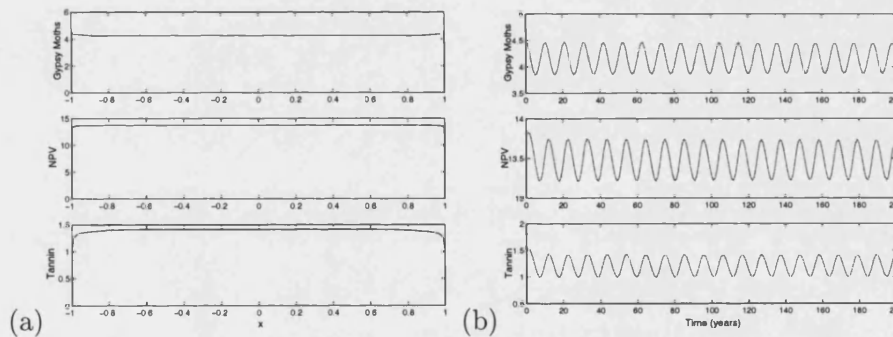
Figure 6-2: Plots show a spatially uniform oscillatory solution. Figure (a) shows population levels over the spatial domain. Figure (b) shows population levels over time at a fixed location. Parameters are $a = 6.0; c = 0.1; q = 0.35; b = 0.1; \lambda = 1.49; \sigma_v = 0.37; \sigma_t = 0.5; \rho = 0.5$ with Laplace dispersal kernels with coefficients $\alpha = 100$ and $\beta = 1000$. Initial conditions are $M = 34; V = 60; T = 34$.

On the other hand, if we suppose NPV diffuses much faster than the gypsy moths,

106

a plus-one bifurcation occurs where the uniform steady state is lost to a spatially structured solution. This occurs when inequality (6.7a) is reversed. Figure 6-3 shows the solution for $\alpha = 100$ and $\beta = 80$. As seen in Figure 6-3(a), a problem arises due to the unboundness of the simplified system. At the boundary edges the gypsy moth population escapes regulation by the virus and grows unbounded, which in turn is followed by exponential tannin and NPV growth. To rectify this we allow $r \neq 0$ in the numerics. This bounds the solution and the spatial patterning of the plus-one bifurcation is then observed.
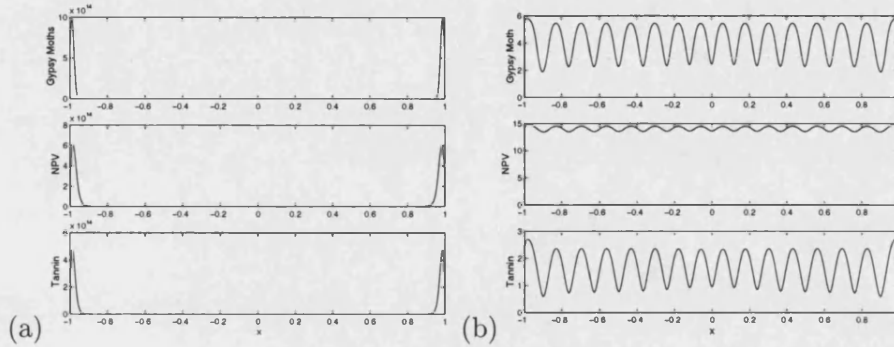
Figure 6-3: Plots show a stable spatial pattern fixed in time. Figure (a) shows unbounded growth at the edges of the domain when $r = 0$. Figure (b) shows the spatial pattern when $r = 0.001$. Parameters are $a = 6.0; c = 0.1; q = 0.35; b = 0.1; \lambda = 1.49; \sigma_v = 0.37; \sigma_t = 0.5; \rho = 0.5$ with Laplace dispersal kernels with coefficients $\alpha = 100$ and $\beta = 80$. Initial conditions are $M = 34; V = 60; T = 34$.

Hence dispersal driven instability can occur in the simplified model. Furthermore stability can be lost in two ways either by a plus-one bifurcation, when the model includes a self limit for gypsy moth growth, or by a Hopf bifurcation. Significantly a Hopf bifurcation produces cyclic population levels which are concurrent with field observations. Therefore, parameter sets which produced stable steady state behaviour in the spatially implicit model may produce cyclic population levels in the spatially explicit model.

6.1.3 Full integrodifference model for gypsy moths

We now look at dispersal instabilities for the complete model system. From numerical simulations we find that the same dispersal driven instability is observed. For a spatially implicit stable nontrivial steady state, we find that the addition of space results in either stable constant population levels, periodic population cycles or spatial patterning

depending on the virus dispersal rate.

(a)　　　　　　　　　　　　　　(b)
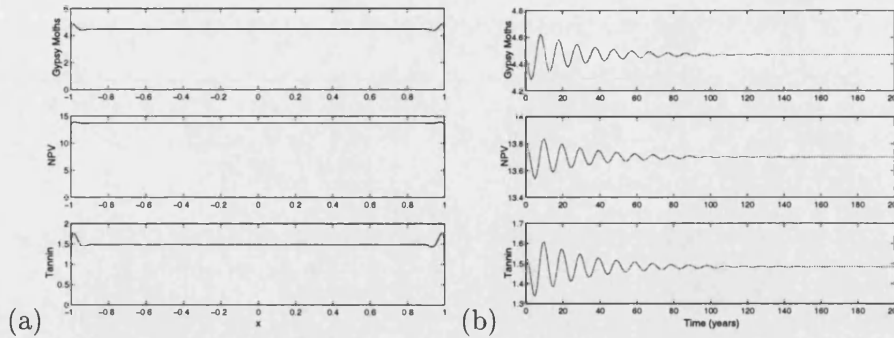
Figure 6-4: Plots show a spatially uniform stable steady state solution for the complete model. Figure (a) shows population levels over the spatial domain. Figure (b) shows population levels over time at a fixed location. Parameters are $a = 6.0; r = 0.0001; c = 0.1; d = 0.0067; q = 0.4; k = 20; b = 0.1; \lambda = 1.49; \sigma_v = 0.37; \sigma_t = 0.4; \rho = 0.6$ with Laplace dispersal kernels with coefficients $\alpha = 100$ and $\beta = 100$. Initial conditions are $M = 30; V = 60; T = 34$.

In Figure 6-4 we see the stability of the spatially explicit nontrivial steady state remains, when the dispersal rates of gypsy moths and NPV are similar.

(a)　　　　　　　　　　　　　　(b)
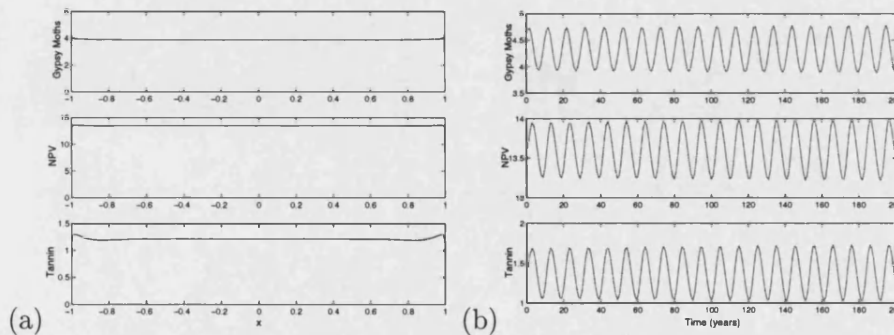
Figure 6-5: Plots show a spatially uniform oscillatory solution for the complete model. Figure (a) shows population levels over the spatial domain. Figure (b) shows population levels over time at a fixed location. Parameters are $a = 6.0; r = 0.0001; c = 0.1; d = 0.0067; q = 0.4; k = 20; b = 0.1; \lambda = 1.49; \sigma_v = 0.37; \sigma_t = 0.4; \rho = 0.6$ with Laplace dispersal kernels with coefficients $\alpha = 100$ and $\beta = 1000$. Initial conditions are $M = 13.6; V = 15.5; T = 9.0$.

We see in Figure 6-5, for slower dispersing NPV relative to gypsy moth dispersal,

108

periodic population cycles exist.
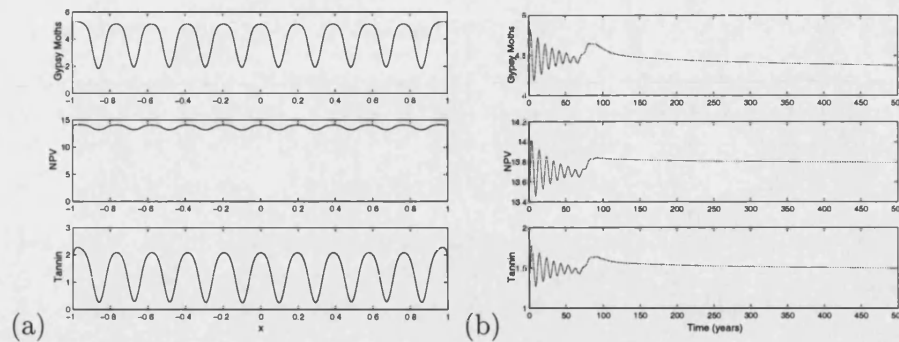
Figure 6-6: Plots show a stable spatial pattern fixed in time for the complete model. Figure (a) shows population levels over the spatial domain. Figure (b) shows population levels over time at a fixed location. Parameters are $a = 6.0; r = 0.0001; c = 0.1; d = 0.0067; q = 0.4; k = 20; b = 0.1; \lambda = 1.49; \sigma_v = 0.37; \sigma_t = 0.4; \rho = 0.6$ with Laplace dispersal kernels with coefficients $\alpha = 100$ and $\beta = 50$. Initial conditions are $M = 34; V = 60; T = 34$.

For faster dispersing NPV relative to gypsy moth dispersal, this results in spatial patterning of the population levels as seen in the simplified model and shown in Figure 6-4. Therefore, the complete model has the same qualitative behaviour as the simplified model. In summary for $\alpha \approx \beta$ a spatial uniform constant population level exists. Yet, as indicated in the simplified model, a decrease in β causes a Hopf bifurcation which generates fluctuating populations. Conversely an increase in β destabilises the spatially stable steady state solution giving rise to spatial patterning.

Furthermore the observed behaviours are also seen for the Gaussian distribution for NPV dispersal. Figures 6-7-6-9 demonstrate the same dispersal driven instabilities as the Laplace distribution for NPV.

109
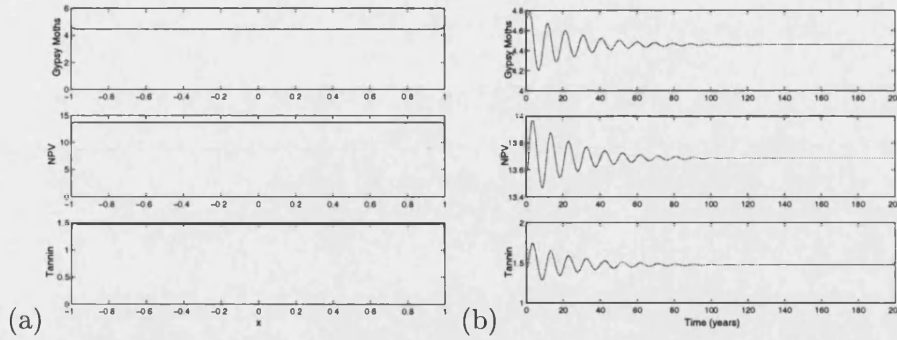
Figure 6-7: Plots show a spatially uniform stable steady state solution for the complete model. Figure (a) shows population levels over the spatial domain. Figure (b) shows population levels over time at a fixed location. Parameters are $a = 6.0; r = 0.0001; c = 0.1; d = 0.0067; q = 0.4; k = 20; b = 0.1; \lambda = 1.49; \sigma_v = 0.37; \sigma_t = 0.4; \rho = 0.6$ with Laplace dispersal kernel for gypsy moths and Gaussian distribution for NPV with coefficients $\alpha = 100$ and $D = 0.01$. Initial conditions are $M = 18.2; V = 16.6; T = 3.3$.
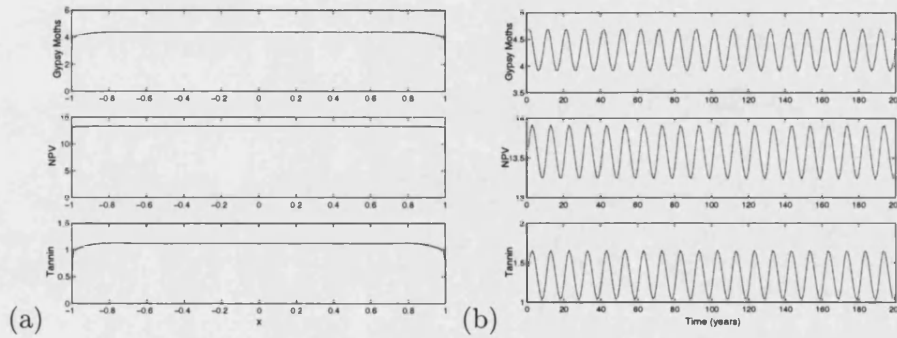
Figure 6-8: Plots show a spatially uniform oscillatory solution for the complete model. Figure (a) shows population levels over the spatial domain. Figure (b) shows population levels over time at a fixed location. Parameters are $a = 6.0; r = 0.0001; c = 0.1; d = 0.0067; q = 0.4; k = 20; b = 0.1; \lambda = 1.49; \sigma_v = 0.37; \sigma_t = 0.4; \rho = 0.6$ with Laplace dispersal kernel for gypsy moths and Gaussian distribution for NPV with coefficients $\alpha = 100$ and $D = 0.00075$. Initial conditions are $M = 18.2; V = 16.6; T = 3.3$.

110
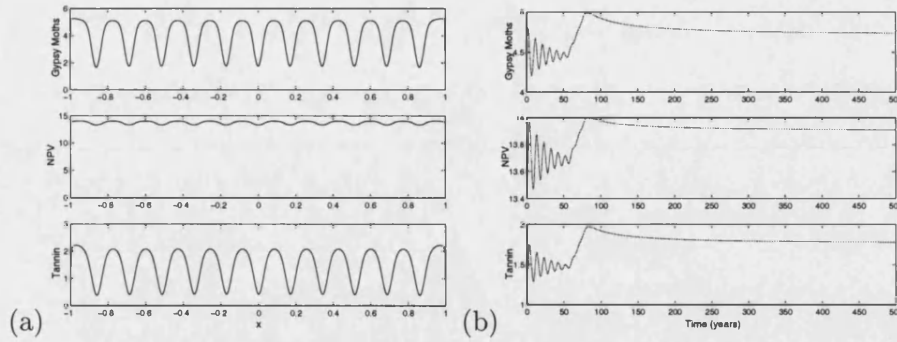
Figure 6-9: Plots show a stable spatial pattern fixed in time for the complete model. Figure (a) shows population levels over the spatial domain. Figure (b) shows population levels over time at a fixed location. Parameters are $a = 6.0; r = 0.0001; c = 0.1; d = 0.0067; q = 0.4; k = 20; b = 0.1; \lambda = 1.49; \sigma_v = 0.37; \sigma_t = 0.4; \rho = 0.6$ with Laplace dispersal kernel for gypsy moths and Gaussian distribution for NPV with coefficients $\alpha = 100$ and $D = 1.0$. Initial conditions are $M = 18.2; V = 16.6; T = 3.3$.

Therefore, dispersal driven instabilities are present in the gypsy moth model and low dispersal of NPV may be an explanation for the observed population cycles seen in the field.

6.2 Travelling waves in predator-prey models

In this section we explore the invasion of both predators and prey, in the form of travelling waves, into a virgin environment. We consider the travelling wave to be a hetroclinic connection between a nontrivial (nonzero) stable steady state solution and a trivial (zero) steady state solution that advances in time and does not change shape as it moves. We aim to calculate the speed of the advancing wave front.

In particular, we look at two different systems, one a reaction diffusion model and the other an integrodifference model. For each of these model systems we consider a prey species advancing in a virgin environment. We then introduce a predator species to the system at a specific location behind the advancing prey wave front. Then, if the prey species invades faster (or at the same rate) than the predator species, by which we mean that the prey diffusion rate is greater than (or equal to) the predator diffusion, then the predator will invade the prey yet never catch the prey wave front. Therefore it can be shown that the prey will continue to invade the virgin environment at the same speed as when the predator is not present.

However if we allow the predator species to invade faster than the prey species,

111

this presents an interesting scenario. As the predator is diffusing faster, it will catch the prey wave front in finite time. The question arises, what happens to the speed of the invasion of both the prey and the predators? We first look at a simple system of reaction diffusion equations studied by Conway (1984). We then compare the reaction diffusion system to a similar system (Neubert et al. 1995) of integrodifference equations.

6.2.1   A predator-prey reaction-diffusion model

We investigate a reaction diffusion model to ascertain what happens to a prey species travelling wave speed when a faster diffusing predator species catches the prey wave front. We use a standard reaction diffusion predator prey model

$$
\begin{aligned}
\frac{\partial N}{\partial t} &= f(N,P) + D_1 \frac{\partial^2 N}{\partial x^2} \\
\frac{\partial P}{\partial t} &= g(N,P) + D_2 \frac{\partial^2 P}{\partial x^2}
\end{aligned}
$$

where N, P represent the prey and predator population densities respectively, D_1, D_2 represent dispersal coefficients, t represents time and x the space variable. Functions f and g describe the growth dynamics of the prey and predator species. For the purpose of numerically demonstrating the impact when predators catch the wave front of the prey species, we look at the system with logistic prey growth rate, mass action predation and density independent mortality of predation,

$$
\begin{aligned}
f(N,P) &= rN\left(1 - \frac{N}{K}\right) - \beta NP, \\
g(N,P) &= \beta NP - \gamma P.
\end{aligned}
$$

where r is the intrinsic growth rate of prey, K is the carring capacity of the prey, β is the transmission (or predation) rate and γ is predator mortality rate. First, if the predator population cannot catch the wave front of the prey the travelling waves will continue separately at the same speed. Figure 6-10 demonstrates the travelling waves and their wave speed when the predator population is introduced behind the advancing wave front of the prey. In this case the predator and prey travelling waves have the same speed (Figures 6-10 (b) & (c)).

112
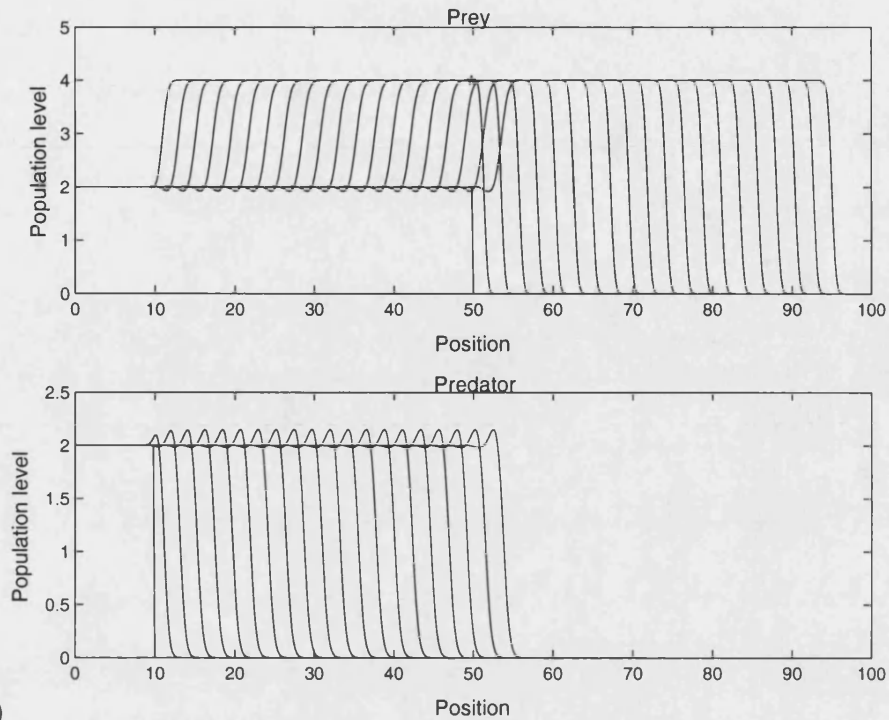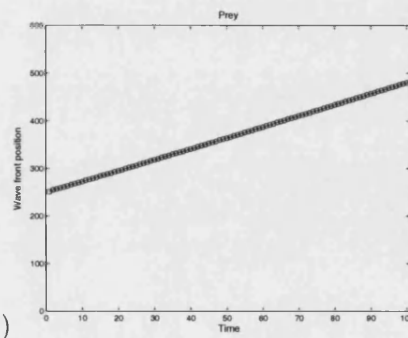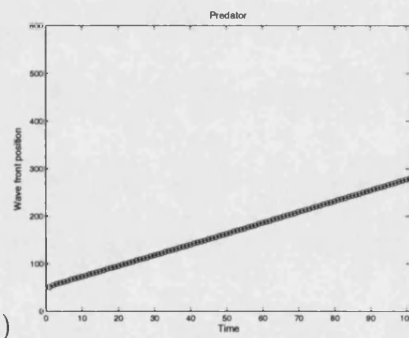
Figure 6-10: Plots show travelling waves and wave front location when an invading predator cannot catch an advancing prey wave front in a reaction diffusion model. Figure (a) shows the travelling wave at 5 year intervals. Figure (b) shows the prey wave front location over time. Figures (c) shows the predator wave front location over time. Parameters are $r = 1; K = 4; \gamma = 0.5; \beta = 0.25$; and diffusion rates $D_1 = 0.001; D_2 = 0.002$.

The spread of the prey wave can be calculated by $2\sqrt{rD}$ where r is the intrinsic growth, $r = f'(0)$ and D is the diffusibility, of the prey. This is commonly known as Fishers speed (Fisher 1937). For our example the prey travelling wave speed, c, is given

113

by

$$c = 2\sqrt{rD_1} \qquad (6.8)$$
$$= 0.0632.$$

For the predator wave, its speed can be calculated by $2\sqrt{(\beta K - \gamma)D_2}$. This speed is calculated in Dunbar (1983) although an approximation for the system also gives the same speed, derived in Murray (2003). Again, for our example, the predator travelling wave speed is given by

$$c = 2\sqrt{(\beta K - \gamma)D_2} \qquad (6.9)$$
$$= 0.0632.$$

These speeds are the same, so as the predator is introduced behind the prey wave front, it is unable to catch the advancing prey wave front.

Next we introduce the predator with a greater diffusion rate ($D_2 = 0.25$). Figure 6-11 shows the behaviour as the predator wave catches the prey front.

114
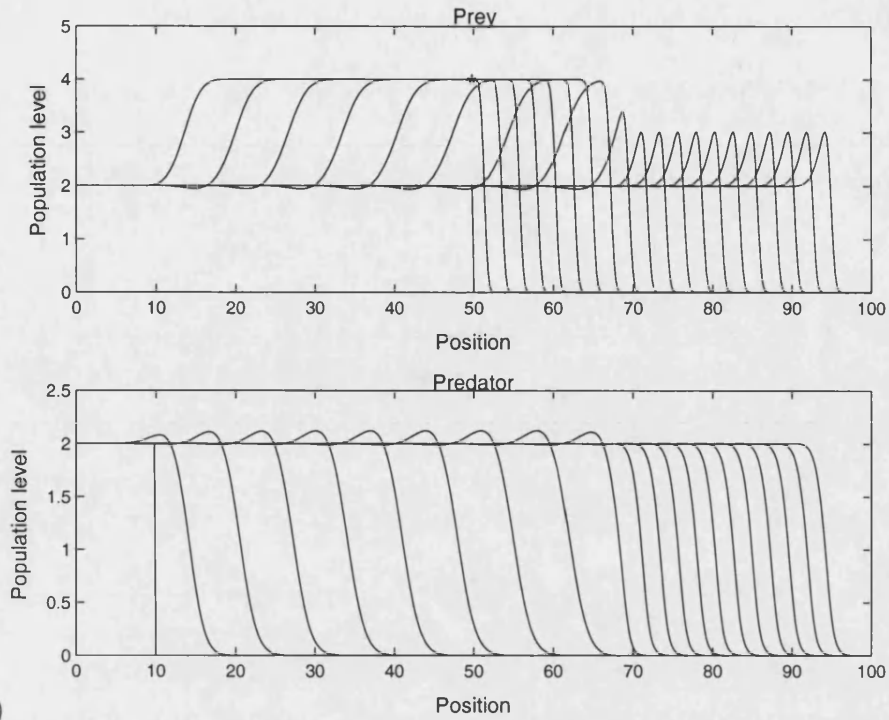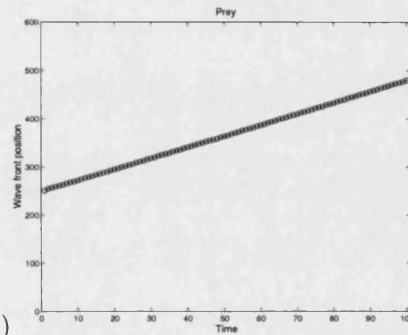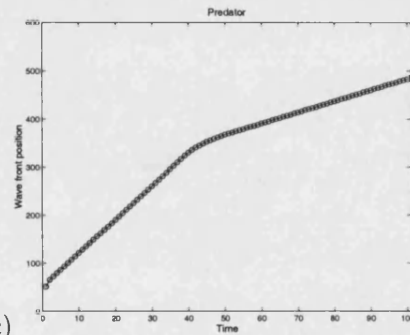
Figure 6-11: Plots show travelling waves and wave front location when an invading predator catches an advancing prey wave front in a reaction diffusion model. Figure (a) shows the travelling wave at 5 year intervals. Figure (b) shows the prey wave front location over time. Figures (c) shows the predator wave front location over time. Parameters are $r = 1; K = 4; \gamma = 0.5; \beta = 0.25$; and diffusion rates $D_1 = 0.001; D_2 = 0.25$.

Initially the predator forms a travelling wave that invades the prey population with a wave speed $c = 1.412$ as calculated in (6.9). The prey initially travels with wave speed $c = 0.0632$ as before (6.8). Yet when the predators catch up with the prey wave front the predators wave speed reduces and both waves continue to travel at the preys wave

115

speed. This is proved in Owen & Lewis (2001). Therefore the waves travel together with wave speed $c = 0.0632$, demonstrated in Figure 6-11.

We also note that a transient period occurs when the predators first catch the wave front of the prey. Here we see a slight reduction in the prey wave speed as the predator wave slows, Figure 6-12.
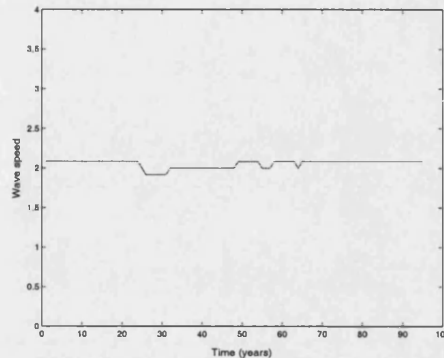
Figure 6-12: Plot shows the transient behaviour when a predator population catches a prey wave front. Parameters are $r = 1; K = 4; \gamma = 0.5; \beta = 0.25; D_1 = 0.001; D_2 = 0.25$.

After a short while the prey returns to its original wave speed where it continues to spread, along with the predator. We conclude that when the predator wave front catches the prey front only a slight decrease in wave speed momentarily occurs, otherwise the preys wave speed is unaffected.

6.2.2 A predator-prey Integrodifference model

We now investigate a similar situation for an integrodifference model system. We form a general integrodifference model, as described in section 1

$$
\begin{aligned}
N_{t+1}(x) &= \int K_1(x - y) f(N_t(y), P_t(y)) dy \\
P_{t+1}(x) &= \int K_2(x - y) g(N_t(y), P_t(y)) dy
\end{aligned}
$$

where N_t, P_t represent the prey and predator population densities respectively at generation t, K_1 and K_2 represents the dispersal kernels and x the space variable. Functions f and g describe the growth dynamics of the prey and predator species respectively.

116

For the purpose of numerics we use the following functions for f and g

$$
\begin{aligned}
f(N_t, P_t) &= N_t \exp\left[r\left(1 - N_t - P_t\right)\right], \\
g(N_t, P_t) &= \beta N_t P_t + \gamma P_t.
\end{aligned}
$$

where r is the intrisic growth rate of the prey, β is the transmission (or predation) rate and γ is the survival rate of the predator. In order to compare the similar reaction diffusion and integrodifference models we use Gaussian diffusion for both dispersal kernels K_1 and K_2.

We again introduce a predator species at a location behind the prey wave front. First we let the predators diffusion rate be slower than the prey. We calculate the prey wave speed by $c = \min_{s \epsilon S}\left[\frac{1}{s}\ln\left(R_0 M(s)\right)\right]$ where $R_0 = f'(0)$ and $M(s)$ is the moment generating function of the dispersal kernel, $M(s) = \int K(x)e^{sx}dx$, for some neighbourhood of s about zero (Weinberger 1978). S is the set of all $s > 0$ for which the moment generating function converges. For the Gaussian distribution the moment generating function is given by $M(s) = \exp\left(Ds^2\right)$. We calculate the prey travelling wave speed

$$
\begin{aligned}
c &= \min_{s \epsilon S}\left[\frac{1}{s}\ln\left(R_0 M(s)\right)\right] \\
&= \min_{s \epsilon S}\left[\frac{1}{s}\ln\left(R_0 \exp\left(Ds^2\right)\right)\right] \\
&= \min_{s \epsilon S}\left[Ds + \frac{\ln\left(R_0\right)}{s}\right] \\
&= D\sqrt{\frac{\ln\left(R_0\right)}{D}} + \frac{\ln\left(R_0\right)}{\frac{\ln\left(R_0\right)}{D}} \\
&= 2\sqrt{D\ln\left(R_0\right)}
\end{aligned}
$$

The speed for $D = 5\text{x}10^{-6}$ and $r = 0.9$ is then

$$
c = 0.0042. \tag{6.10}
$$

Figure 6-13 shows the behaviour of the travelling waves and their speeds for both the prey and the predator.
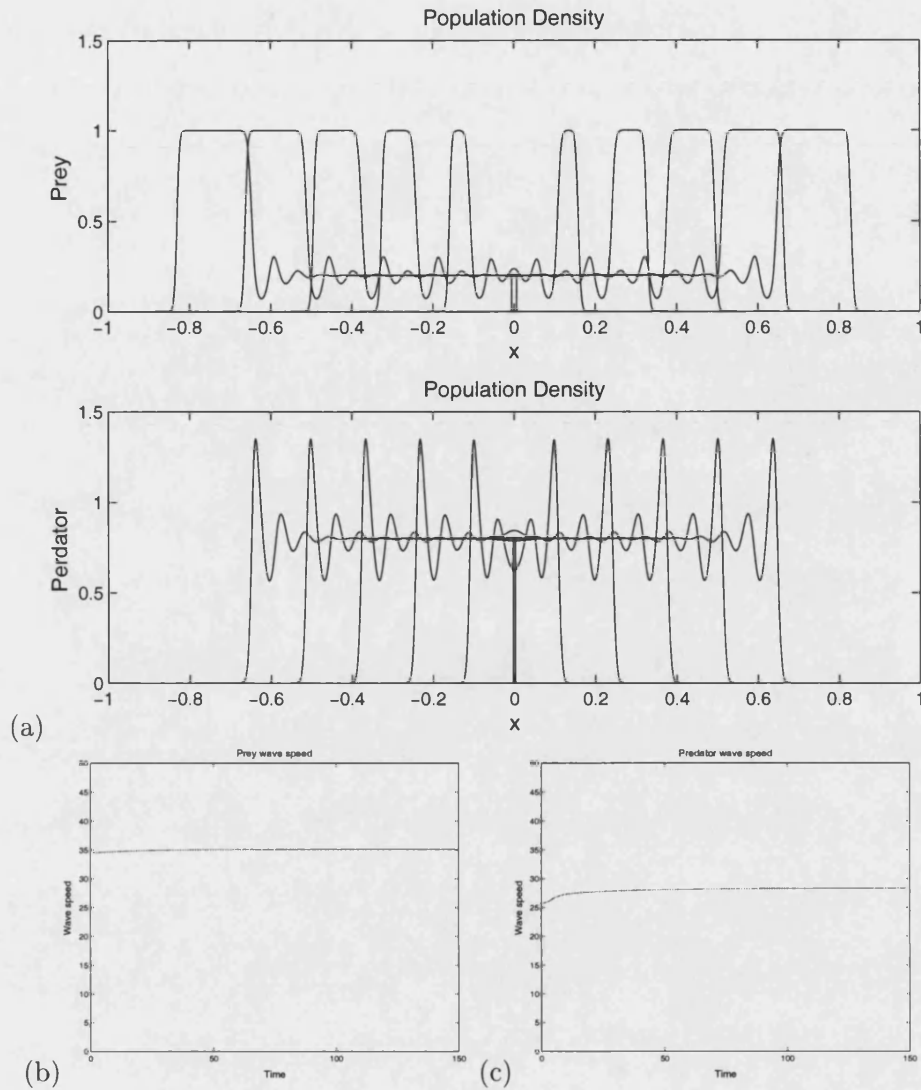
Figure 6-13: Plots show travelling waves and wave speeds when an invading predator cannot catch an advancing prey wave front in an integrodifference model. Figure (a) shows the travelling wave at 40 year intervals. Figure (b) shows the prey wave speed over time. Figures (c) shows the predator wave speed over time. Parameters are $r = 0.9; c = 1.0; \gamma = 0.8$; and dispersal coefficients $D_1 = 5\mathrm{x}10^{-6}; D_2 = 5\mathrm{x}10^{-6}$.

The figure is plotted on a grid size of 2^{14}. We see that the travelling wave of the prey does indeed travel with speed 0.0042, as calculated from (6.10). The predator wave travels at a calculated speed of 0.0034.

Next we introduce the predator with a greater diffusion rate. Figure 6-14 shows the

118

behaviour as the predator wave catches the prey.
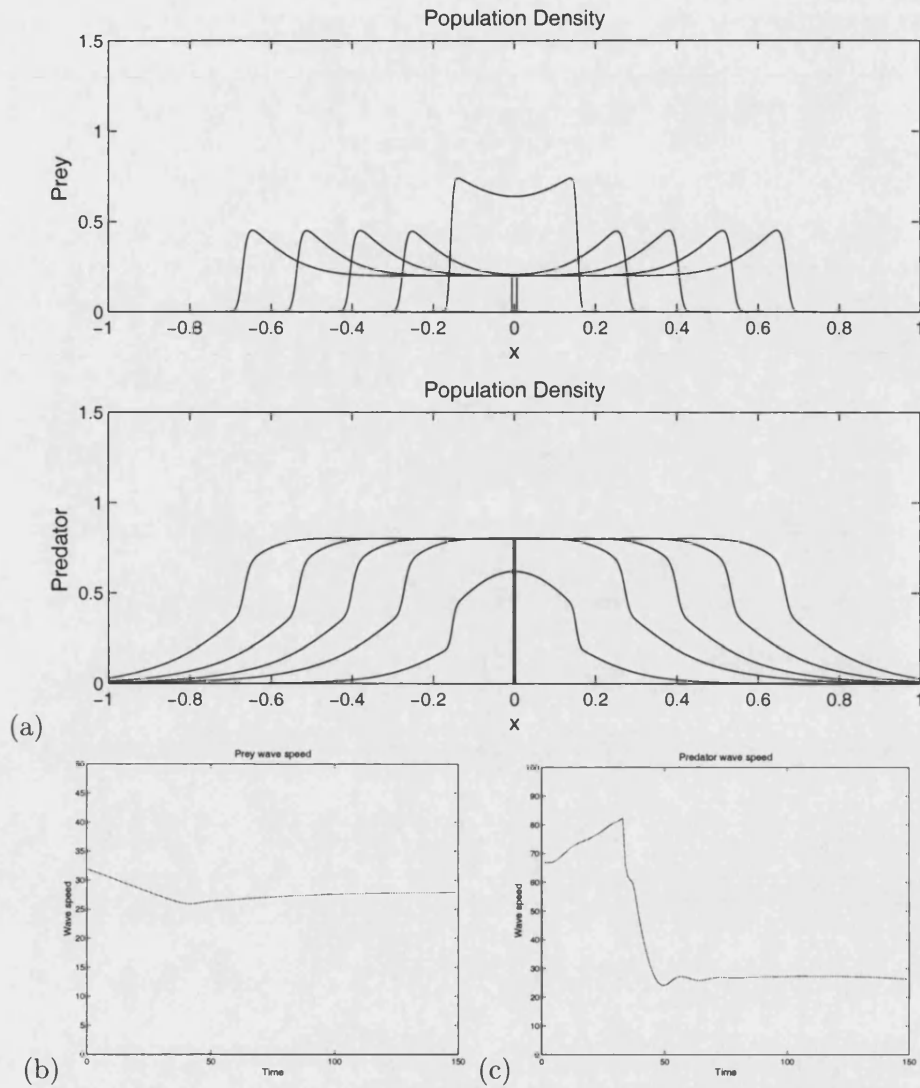
Figure 6-14: Plots show travelling waves and wave speeds when an invading predator can catch an advancing prey wave front in an integrodifference model. Figure (a) shows the travelling wave at 40 year intervals. Figure (b) shows the prey wave speed over time. Figures (c) shows the predator wave speed over time. Parameters are $r = 0.9; c = 1.0; \gamma = 0.8$; and dispersal coefficients $D_1 = 5\text{x}10^{-6}; D_2 = 5\text{x}10^{-3}$.

Here it is seen that after the predator catches the prey wave front the prey waves speed reduces. However unlike the reaction diffusion system the prey wave does not return to its original speed. Instead the speed increases slightly and then remains

119

constant at a lower speed than before. Hence the introduction of the predator, with faster diffusion than the prey, has unexpectedly caused the preys wave speed to reduce.

(a)   (b)
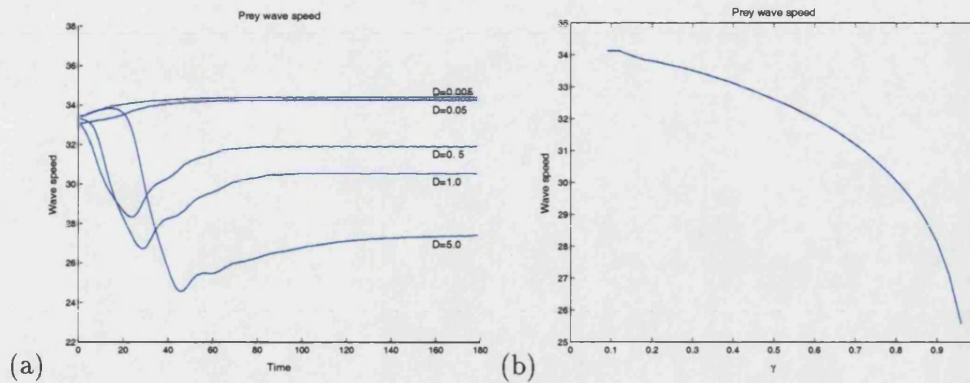
Figure 6-15: Plots show the changes in prey wave speed. Figure (a) shows the change in wave speed over time for $\gamma = 0.8$ and various dispersal rates. Figure (b) shows the change in wave speed over virus survival rates and $D_2 = 1.0$. Parameters are $r = 0.9; c = 1.0; \gamma = 0.8$; and dispersal coefficient $D_1 = 5 \times 10^{-6}$.

Figure 6-15(a) shows the wave speeds for a variety of diffusion rates for the predator. The figure shows that the more diffusive the predator becomes, the greater reduction occurs in the wave speed of the prey. Further to this, the survival rate of the predator, γ, also affects the wave speed. Figure 6-15(b) shows the wave speed against the survival rate, γ. For large γ there is a greater reduction in wave speed. As γ decreases the prey wave speed returns to a speed close to the original speed.

The same result occurs for other distribution kernels. Figure 6-16 shows the reduction in wave speed for Laplace distributions for the predator and the prey as well as a Gaussian distribution for the predator and Laplace distribution for the prey.
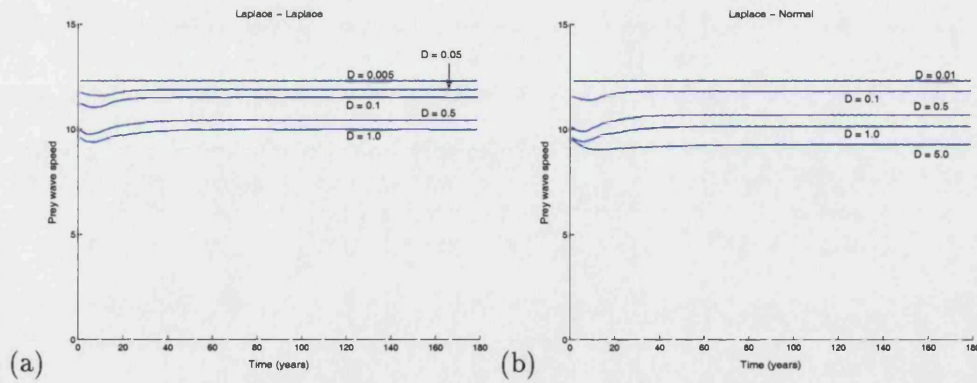
Figure 6-16: Plots show the change in wave speed for Laplace dispersal kernel for prey and Laplace dispersal kernel for predator (Figure (a)) and for Gaussian dispersal kernel for predator (Figure (b)). Parameters are $r = 0.9; c = 1.0; \gamma = 0.8;$ and dispersal coefficient $D_1 = 5 \times 10^{-6}$.

Therefore the travelling wave speed of the prey can be slowed when a predator disperses faster and catches the prey wave front. Surprisingly there is a distinct difference in results in constant speed travelling waves for predator prey systems between reaction diffusion and integrodifference models.

6.3   Slowing the spread of Gypsy moths

Gypsy moths are continuing to expand across the United States. Since their introduction in Massachusetts in the late 1860's gypsy moths have spread as far west as Wisconsin (1997) and as far south as the North Carolina - Virginia border. The spread has been relatively slow largely because the female gypsy moth is unable to fly. Liebhold, Halverson & Elmes (1992) estimated that the population should expand at 1.25 miles per year, however from 1960 to 1990, the population expanded at a rate of 13 miles per year. This increase in spread is most likely due to the accidental dispersion resulting from human activity. Consequently the USDA have acted by introducing the Slow The Spread (STS) project to reduce the expansion. The STS project began in 1999 and is based on mating disruption at the wave front.

In this section we begin by examining travelling waves and invasion rates of gypsy moths. We use the result from section 6.2, that a predator may reduce a prey's wave speed in an integrodifference model. We look at how fast dispersing NPV can slow the spread rate of gypsy moths. Based on this we propose an alternative method of slowing the spread by considering using NPV as a barrier. We first consider gypsy

121

moths invading an area where NPV levels are kept at a constant level to form a barrier in front of the advancing wave. This is achieved by applying Gypchek annually to maintain the NPV barrier. We investigate the reduction in wave speed of gypsy moths. Afterwards, we contemplate a more practical approach of spraying only the gypsy moth wave front each year. We look at how much and how far in front of the wave needs to be sprayed in order to reduce the invasion.

6.3.1 Travelling wave speeds and invasion rates for the gypsy moth model

The previous section showed that a predator population can slow a prey's wave speed in an integrodifference model if the predator disperses quicker than the prey. We now observe how much a travelling wave for gypsy moths is slowed by NPV. We let gypsy moths disperse via a Laplace distribution and NPV by either a Laplace or Gaussian distribution. From parameter estimates in Chapter 4 we show the reduction in gypsy moth wave speed as NPV dispersal increases. Figure 6-17(a) shows the travelling wave of gypsy moths and NPV over time using Laplace distributions. Figure 6-17(b) shows the reduction in wave speed for various NPV dispersal rates.
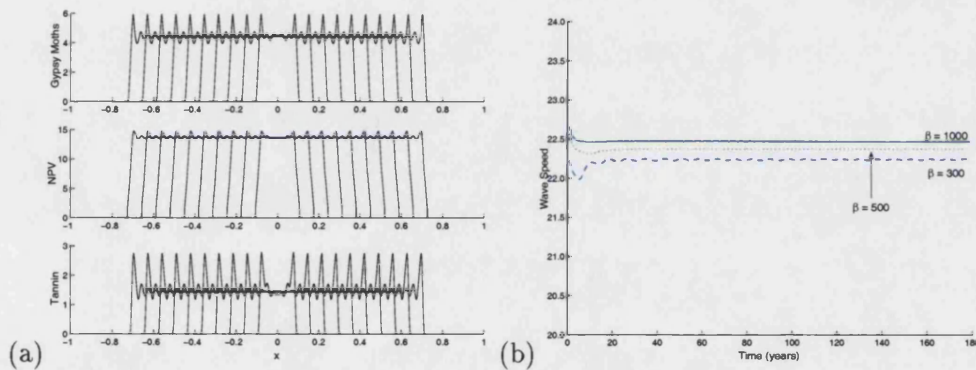
Figure 6-17: Plots show travelling wave solutions and wave speeds for Laplace dispersal kernels. Figure (a) shows the travelling wave for gypsy moth, NPV and tannin levels at 20 year intervals, $\beta = 500$. Figure (b) shows the reduction in wave speed for various NPV dispersal rates. Parameters are $a = 6.0; r = 0.0001; c = 0.1; d = 0.0067; q = 0.4; k = 20; b = 0.1; \lambda = 1.49; \sigma_v = 0.37; \sigma_t = 0.5; \rho = 0.6$ with dispersal coefficient $\alpha = 1000$.

In Figure 6-18 the Laplace distribution for NPV dispersal is replaced with the Gaussian distribution.

122
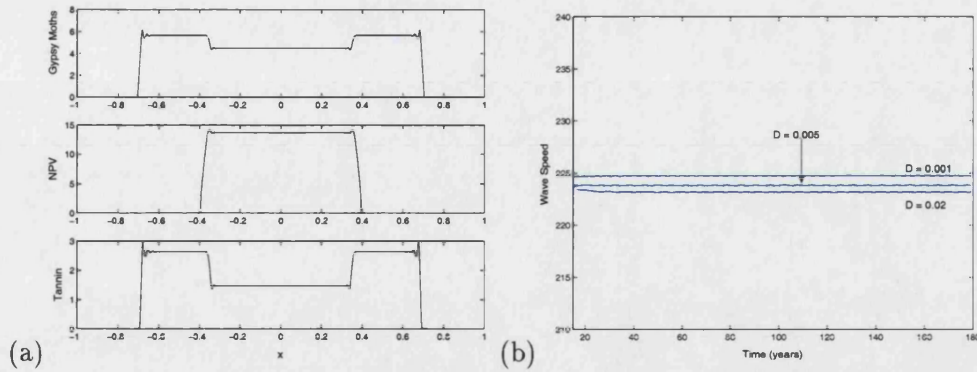
Figure 6-18: Plots show travelling wave solutions and wave speeds for Laplace dispersal kernel for gypsy moth and Gaussian dispersal kernel for NPV. Figure (a) shows the travelling wave for gypsy moth, NPV and tannin levels at 20 year intervals, $D = 0.001$. Figure (b) shows the reduction in wave speed for various NPV dispersal rates. Parameters are $a = 6.0; r = 0.0001; c = 0.1; d = 0.0067; q = 0.4; k = 20; b = 0.1; \lambda = 1.49; \sigma_v = 0.37; \sigma_t = 0.5; \rho = 0.6$ with dispersal coefficient $\alpha = 1000$.

We see, in both cases, that faster dispersing NPV causes a greater reduction in gypsy moth wave speed. In section 2, the amount of reduction in the wave speed of the prey depends not only on the dispersal of the predator but also its survival rate. In the case of gypsy moths the reduction in wave speed is seen to be less significant due to the low survival rate of NPV. However if this survival rate could be increased it would produce a greater reduction in the wave speed.

Travelling waves assume a constant stable coexisting population after the invasion, yet field data show cyclic behaviour of population levels. In this respect we consider an invasion where the population levels fluctuate. Figure 6-19 shows the behaviour of the invasion of gypsy moths and NPV. The dispersal rate of NPV is varied and plotted against wave speed in Figure 6-19.

123

(a)   (b)
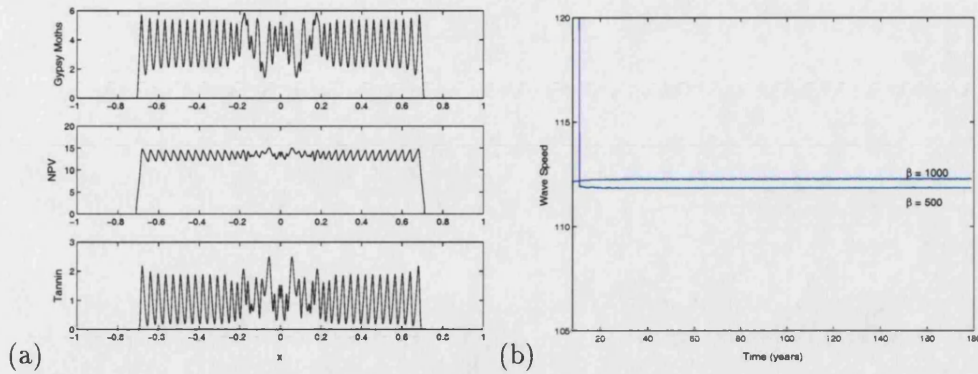
Figure 6-19: Plots show invasion and invasion rates for Laplace dispersal kernels. Figure (a) shows the travelling wave for gypsy moth, NPV and tannin levels, $\beta = 500$. Figure (b) shows the reduction in wave speed for various NPV dispersal rates. Parameters are $a = 6.0; r = 0.0001; c = 0.1; d = 0.0067; q = 0.4; k = 20; b = 0.1; \lambda = 1.49; \sigma_v = 0.37; \sigma_t = 0.4; \rho = 0.3$ with dispersal coefficient $\alpha = 1000$.

We see that a similar small reduction of wave speed is found for fast dispersing NPV. Therefore fast dispersing NPV alone can have little effect on reducing gypsy moth wave speed.

6.3.2   Slowing the spread of Gypsy moths by NPV barrier

Gypsy moths are well established in the United States and it is unlikely that their expansion can be completely stopped or reversed. For this reason the USDA have established a new strategy called Slow the Spread in an effort to control the gypsy moth population.

The critical component of the Slow the Spread program is the use of mating disruption. Mating disruption is a noninsecticidal treatment specific to the gypsy moth, which involves using controlled-release dispensers that emit animal pheromones. These pheromones hamper the ability of the males to find females to mate with, thus resulting in the females laying unfertilised eggs.

We propose an alternative method using Gypchek as a barrier to decrease the gypsy moth invasion rate. Initially we spray an uninvaded area and maintain this at a specific level, Q, of NPV to ascertain the affect when gypsy moths invade this area. Figure 6-20 shows how a large quantity of control, which is maintained causes the gypsy moth wave front to stop when reaching the sprayed area. Similarly in Figure 6-21 a smaller quantity of control is maintained and this results in the slowing down of the wave when it enters the controlled area.

124
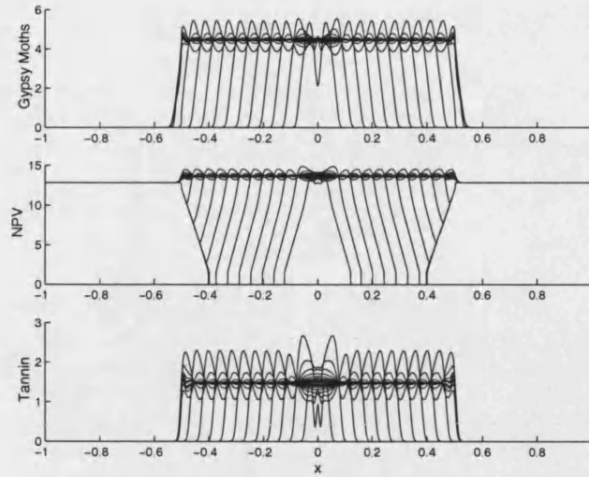
Figure 6-20: Plot shows the stopped wave from NPV barrier, $Q = 25$. Parameters are $a = 6.0; r = 0.0001; c = 0.1; d = 0.0067; q = 0.4; k = 20; b = 0.1; \lambda = 1.49; \sigma_v = 0.37; \sigma_t = 0.4; \rho = 0.6$ with dispersal coefficients $\alpha = 400$ and $\beta = 300$.
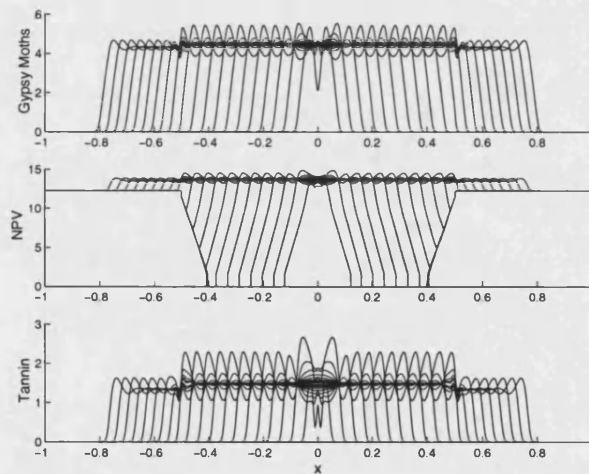
Figure 6-21: Plot shows the reduction in wave speed from NPV barrier, $Q = 5$. Parameters are $a = 6.0; r = 0.0001; c = 0.1; d = 0.0067; q = 0.4; k = 20; b = 0.1; \lambda = 1.49; \sigma_v = 0.37; \sigma_t = 0.4; \rho = 0.6$ with dispersal coefficients $\alpha = 400$ and $\beta = 300$.

Figure 6-22 shows the reduction in wave speed against the quantity of the control. Here the wave speed reduces quickly as the amount of control is increased. Although we do not see the reversal of the advancing front we see that it can be stopped for sufficiently large control levels. From this figure a relatively small increase in the

125

amount of control can have a large effect on reducing wave speed. However, it should be noted that a large amount of spray is initially required to cause any significant reduction in wave speed. Thus, it may not be practical to use such large quantities of control over such a wide area due to high costs or opposition by landowners. Consequently in the next section we look at specifically using the control only at the wave front.
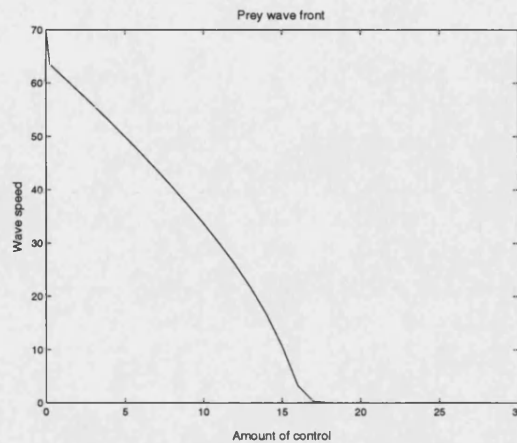
Figure 6-22: Plot shows the reduction in wave speed against the quantity of control. Parameters are $a = 6.0; r = 0.0001; c = 0.1; d = 0.0067; q = 0.4; k = 20; b = 0.1; \lambda = 1.49; \sigma_v = 0.37; \sigma_t = 0.4; \rho = 0.6$ with dispersal coefficients $\alpha = 400$ and $\beta = 300$.

6.3.3 Wave front spraying

We have seen that to cause any reduction in wave speed a large application of spray is needed. For large areas (as in the previous subsection) this can be impractical. However it may not be necessary to spray such large areas to significantly reduce wave speed. Here we look instead at only spraying just in front the wave front. By allowing the wave front to initially advance unhindered we then target the wave front by spraying the area just in front of the wave. We spray an interval from the gypsy moth wave front to a set distance ahead of the wave. Figure 6-23 shows how the wave speed differs for different lengths of intervals.
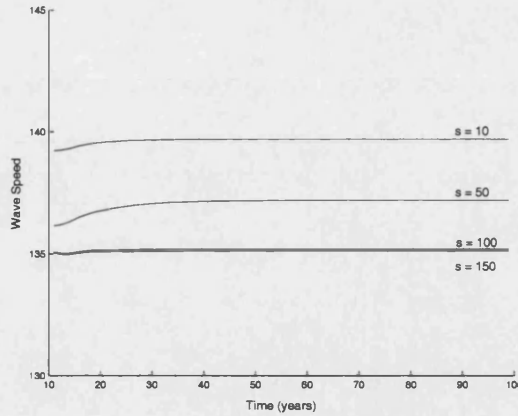
Figure 6-23: Plot shows the change in wave speed for various lengths of interval of spraying Gypchek, for $Q = 30$. Parameters are $a = 6.0; r = 0.0001; c = 0.1; d = 0.0067; q = 0.4; k = 20; b = 0.1; \lambda = 1.49; \sigma_v = 0.37; \sigma_t = 0.4; \rho = 0.6$ with dispersal coefficients $\alpha = 400$ and $\beta = 300$. s is the distance of the sprayed interval.

As the interval length increases the wave speed is reduced but as the interval increases further the reduction in the wave speed then becomes insignificant. Figure 6-24 illustrates this by plotting the length of the interval against wave speed.
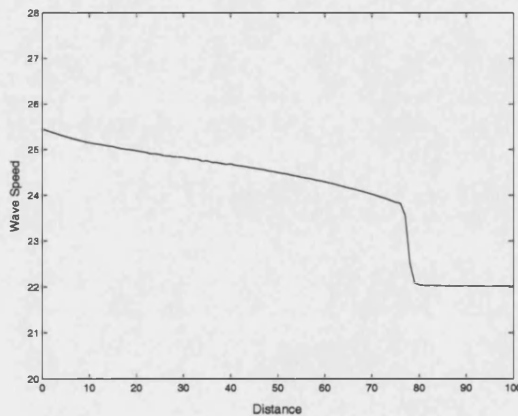
Figure 6-24: Plot shows wave speed against lengths of interval of spraying Gypchek, for $Q = 30$. Parameters are $a = 6.0; r = 0.0001; c = 0.1; d = 0.0067; q = 0.4; k = 20; b = 0.1; \lambda = 1.49; \sigma_v = 0.37; \sigma_t = 0.4; \rho = 0.6$ with dispersal coefficients $\alpha = 400$ and $\beta = 300$.

We see that an increase in the length of the interval has more of an effect when the

127

interval is originally small. As the interval gets larger there is a sudden drop in wave speed. Thereafter any further increases in the interval length have a negligible effect on the wave speed. Nevertheless a change in the quantity of spray per unit area will also cause a change in the speed. Figure 6-25 shows the reduction in wave speed for different quantities of spray for a set interval length.
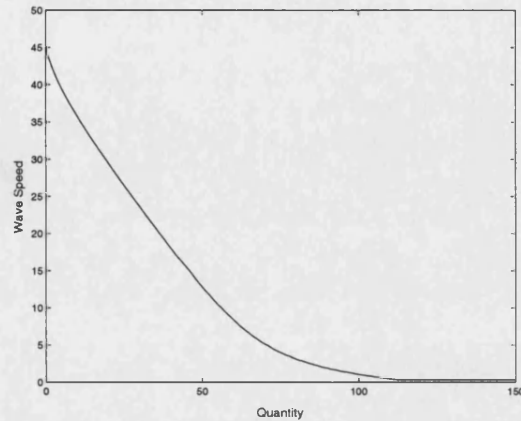
Figure 6-25: Plot shows wave speed against quantity of spray applied over an interval length of 80 units. Parameters are $a = 6.0; r = 0.0001; c = 0.1; d = 0.0067; q = 0.4; k = 20; b = 0.1; \lambda = 1.49; \sigma_v = 0.37; \sigma_t = 0.4; \rho = 0.6$ with dispersal coefficients $\alpha = 400$ and $\beta = 300$.

Therefore for the greatest effect of using Gypchek as a barrier method, the best application is to spray the interval from the wave front upto a distance 80 units in front of the wave (from Figure 6-24) with a quantity of 110 units of spray (from Figure 6-25). This will then cause the advancing wave front to considerably reduce to a fraction of the original wave speed. However this may not be practical and a shorter distance in front of the wave and a reduced level of application may be required. In this case the gypsy moths will continue to advance but at a reduced rate. This rate will depend on the exact amount of spray used and the distance from the wave front the application is applied.

6.4 Summary and discussion

Integrodifference models combine discrete population dynamics over a continuous spatial domain. This makes them ideally suited to spatially model gypsy moth populations. It is well documented that the dispersal of gypsy moths consists of short range dispersal, by crawling and ballooning of larvae, and long range dispersal by accidental human

128

movement. Accordingly their distribution is leptokurtic as this better accounts for the long range dispersal than the Gaussian distribution due to the distributions fatter tails. Using integrodifference equations has an advantage over conventional reaction diffusion models as different distributions can be chosen to more appropriately describe a species dispersal.

We began the chapter by introducing dispersal kernels for gypsy moths and NPV, to investigate spatially driven instabilities. We considered a spatially implicit steady state solution and found that this could be driven unstable in two ways. In a simplified version of the model, analysis was conducted which showed that two bifurcations may occur as dispersal coefficients were varied. We found that when dispersal of NPV was high, relative to gypsy moth dispersal, a plus-one bifurcation occurred giving rise to a spatially structured solution. Here gypsy moth population levels settled to remain constant over time but oscillatory over space. When dispersal of NPV is low relative to gypsy moth dispersal, a Hopf bifurcation occurred. This resulted in populations that were constant in space but cyclic in time. This is more realistic to observations in the field and therefore, slower dispersing virus may be a cause of the cyclic populations. The same behaviour was also observed in the complete model system.

Spatial patterning and dispersal driven instabilities are not the only matters to be considered from the inclusion of space. Spatial models are also used to predict or estimate speeds of invasion. In section 2 we studied a general predator-prey invasion and compared two different modelling techniques: reaction diffusion and integrodifference equations. We discovered that although a faster diffusing predator cannot slow the wave speed of the prey in a reaction diffusion model, it can in an integrodifference model. The reduction caused to the wave speed is dependent on the survival rate of the predator and its diffusion rate. Thus reductions in wave speed in integrodifference equations may not necessarily be caused by Allee effects as believed in reaction diffusion models. This is an important result as it demonstrates that different results can be obtained for different modelling techniques describing the same population systems.

In section 3 we used this finding to show how the gypsy moth wave speed may be reduced by fast diffusing NPV. Little is known about the dispersal of NPV, thus in this section we assumed that NPV was fast diffusing and investigated its affect on the spread rate of the gypsy moths. However we found that although the gypsy moth wave speed is reduced to some extent this reduction is only significant if NPV dispersal is exceptionally large. For smaller NPV dispersal the reduction in wave speed is very small. This is mainly due to the fairly low survival rate of NPV. As the majority of NPV is unable to survive outside the gypsy moth invaded area, the quantity is too small to significantly affect the gypsy moth wave speed. But if NPV survival rate could in

some way be increased, the wave speed could be considerably reduced as demonstrated in section 2.

In spite of the fact that fast dispersing NPV only causes small reductions in wave speed of gypsy moths, it could still be effective as a barrier in front of the advancing wave. The reduction in gypsy moth wave speed is only small due to the low survival rate of NPV. This can be overcome by adding and maintaining NPV in the form of Gypchek ahead of the gypsy moth advancing front. We therefore considered using Gypchek as a barrier in order to reduce gypsy moth wave speed. We began by spraying an entire area ahead of the gypsy moth wave front, maintaining the quantity of NPV each year. From this we saw that the gypsy moths wave speed reduced or even stopped when reaching the NPV barrier, although spraying large quantities of Gypchek in vast areas is unlikely to be realistic. We then explored a more practical method of only spraying a set distance in front of the wave. We found that, for large quantities of spray, only relatively small distances ahead of the wave needed to be sprayed to have a significant impact on the advancing wave front. Indeed the reduction can be substantial and can almost stop the wave from advancing. Small quantities and distances sprayed would still reduce the wave, but to a lesser extent. Therefore, a combination of mating disturbance and application of Gypchek as a barrier could further reduce the current invasion rate of gypsy moths.

Chapter 7

Spatial Optimal Control for the Gypsy Moth Model

Spatial optimal control techniques have been developed for continuous time partial differential equations (PDE's) by Lions (1971). Furthermore, the techniques for finding an optimal control solution have been extended to ecology by Lenhart & Bhat (1992) and Bhat et al. (1993). Management of pest populations can be an expensive process and bioeconomic models help provide information on cost effective control strategies. Lenhart & Bhat (1992) demonstrated this with a bioeconomic model for controlling beaver populations in New York. Yet optimal control for cost using bioeconomic models has not received significant attention in spatial ecological modelling.

Optimal control for hybrid systems such as integrodifference equations has not been developed. At present, there is no published research in this field, however work in this area by Joshi et al. (in press) is resolving this issue. They consider a one species system and we extend this technique to the spatial gypsy moth model system. This work is the first to examine optimal control in a discrete time integrodifference predator prey model.

In this chapter, we adapt the spatial integrodifference gypsy moth model presented in Chapter 6 to incorporate a control term. This control is the addition of NPV to the system in the form of the biocontrol agent Gypchek. As in Chapter 5 we seek an optimal control strategy that minimises the cost in a bioeconomic model. This bioeconomic model consists of the cost of damage caused by gypsy moths and the cost of control by Gypchek over the spatial domain.

We first show the set up of the bioeconomic model. We then prove the existence and uniqueness of the optimal control solution. Numerical simulations are given of optimal control strategies for different costs for the application of control.

7.1 Mathematical Analysis

We form a bioeconomic model, similar to that in Chapter 5, with the aim of optimising a total cost function (objective function) subject to constraints over a fixed time period. The objective function consists of the cost of biocontrol plus the cost of damage to society caused by gypsy moths. Therefore the objective function is given as

$$J(p) = \sum_{n=0}^{N} \int_{\Omega} \left[A_n M_n(x) + \frac{B_n}{2} p_n^2(x) \right] dx \tag{7.1}$$

where A_n is the cost of damage per gypsy moth, B_n is the cost parameter for the control and x is the spatial variable in a bounded domain $\Omega \subset \mathbb{R}^2$. $p_n(x)$ is the amount of spray of the biocontrol agent Gypchek used at location x for each generation. The objective function is subject to the constraints of the gypsy moth integrodifference model equations with control,

$$M_{n+1}(x) = \int_{\Omega} K_1(x-y) \frac{a}{1+dT_n(y)} \frac{k+(1-q)V_n(y)}{k+V_n(y)}$$
$$\exp\left(-rM_n(y) - \frac{bV_n(y)}{1+cT_n(y)}\right) M_n(y) dy \tag{7.2a}$$

$$V_{n+1}(x) = \int_{\Omega} K_2(x-y) \left[\sigma_v V_n(y) + \lambda \left(1 - \exp\left(\frac{-bV_n(y)}{1+cT_n(y)}\right)\right) \right.$$
$$\left. M_n(y)\right] dy + \int_{\Omega} K_3(x-y) p_n(y) dy \tag{7.2b}$$

$$T_{n+1}(x) = \rho M_n(x) + \sigma_t T_n(x) \tag{7.2c}$$

with the initial conditions

$$M_0(x) = M_{int}(x), \tag{7.3a}$$

$$V_0(x) = V_{int}(x), \tag{7.3b}$$

$$T_0(x) = T_{int}(x). \tag{7.3c}$$

where x is position and n is the generation. The states $M_n(x), V_n(x), T_n(x)$, dispersal kernels $K_1(x), K_2(x)$ and parameters are given in Chapter 6. When Gypchek is sprayed there is a narrow distribution given by kernel $K_3(x)$.

The set of controls is bounded at each spatial location $x \epsilon \Omega$ by

$$U = \{0 \le p_n(x) \le P_{max} | n = 0, 1, ..N - 1\} \tag{7.4}$$

where P_{max} is a maximum application at each spatial location for each generation.

132

Our goal is to find a control sequence p^* in the bounded set (7.4) such that

$$J(p^*) = \min_{p \epsilon U} J(p). \tag{7.5}$$

7.1.1 Optimal Control Existence

We begin, using a minimising sequence argument (Liang 1999), by verifying that there exists a solution to the optimal control problem (7.1-7.4). We prove this existence by following a similar method given by Joshi et al. (in press). Firstly, Lemma 7.1.1 shows that the states are bounded over a finite interval. This is followed by Theorem 7.1.1 which uses Lemma 7.1.1 to establish that an optimal control exists.

Lemma 7.1.1. *For all $n = 0, 1, 2...N$ states $M_n(x)$, $V_n(x)$, $T_n(x)$ are bounded at each $x \epsilon \Omega$.*

Proof. The state equations are invariant (i.e. given initial conditions M_0, V_0, T_0 (7.3) are non-negative then M_n, V_n, T_n are non-negative for all n), so therefore the states are bounded below by zero. So it remains to show the states are bounded above. Let, for each $x \epsilon \Omega$,

$$C_1^M \geq \frac{a}{1 + dT_0} \frac{k + (1-q)V_0}{k + V_0} \exp\left(-rM_0 - \frac{bV_0}{1 + cT_0}\right) M_0 \tag{7.6a}$$

$$\hat{C}_1^V \geq \sigma_v V_0 + \lambda \left(1 - \exp\left(\frac{-bV_0}{1 + cT_0}\right)\right) M_0 + p_0 \tag{7.6b}$$

$$C_1^T \geq \rho M_0 + \sigma_t T_0 \tag{7.6c}$$

Then substituting (7.6) into (7.2) we have

$$M_1(x) \leq C_1^M \int_\Omega k_1(x - y)dy \tag{7.7a}$$

$$V_1(x) \leq \hat{C}_1^V \int_\Omega k_2(x - y)dy + \int_\Omega k_3(x - y)p_0(y)dy \tag{7.7b}$$

$$T_1(x) \leq C_1^T \tag{7.7c}$$

Now as the kernels are redistributing kernels they have the property,

$$0 < \int_\Omega k_i(x - y)dy \leq 1 \quad i = 1, 2, 3$$

then from (7.7) and (7.4)

$$
\begin{aligned}
M_1(x) &\leq C_1^M \\
V_1(x) &\leq \hat{C}_1^V + P_{max} := C_1^V \\
T_1(x) &\leq C_1^T
\end{aligned}
$$

Therefore $M_1(x)$, $V_1(x)$, $T_1(x)$ are bounded above for each $x \epsilon \Omega$. Now as $M_1(x)$, $V_1(x)$, $T_1(x)$ are bounded then similarly there exist constants C_2^M, $\hat{C}_2^V$ and C_2^T such that

$$
\begin{aligned}
M_2(x) &\leq C_2^M \int_\Omega k_1(x-y)dy, \\
V_2(x) &\leq \hat{C}_2^V \int_\Omega k_2(x-y)dy + \int_\Omega k_3(x-y)p_1(y)dy, \\
T_2(x) &\leq C_2^T.
\end{aligned}
$$

Therefore we obtain the bounds

$$
\begin{aligned}
M_2(x) &\leq C_2^M, \\
V_2(x) &\leq \hat{C}_2^V + P_{max} := C_2^V, \\
T_2(x) &\leq C_2^T.
\end{aligned}
$$

Accordingly M_2, V_2, T_2 are bounded for all $x \epsilon \Omega$. Subsequently it follows iteratively that M_n, V_n, T_n for bounded for all $n = 0, 1 ... N$. $\qquad \square$

Theorem 7.1.1. *An optimal control $p^* \epsilon U$ exists such that the objective function $J(p)$ is minimised.*

Proof. Let $\{p^K\}_{K=1}^\infty$ be a minimising sequence for the objective functional J and $\{M^K\}_{K=1}^\infty$, $\{V^K\}_{K=1}^\infty$ and $\{T^K\}_{K=1}^\infty$ be the corresponding state sequences. As the sequences are bounded (Lemma 7.1.1) in $L^2(\Omega)$ then by Banach-Alaoglu theorem (Evans 1990) there exists a subsequence where

$$
\begin{aligned}
p_n^k &\rightharpoonup p_n^* \\
M_n^k &\rightharpoonup M_n^* \\
V_n^k &\rightharpoonup V_n^* \\
T_n^k &\rightharpoonup T_n^*
\end{aligned}
$$

with weak convergence in $L^2(\Omega)$. It is required to show that the states M^*, V^* and T^* correspond to the control p^*. Due to the fixed initial conditions (7.3) we have from

(7.2)

$$M_1(x) = \int_\Omega k_1(x-y) \frac{a}{1 + dT_0(y)} \frac{k + (1-q)V_0(y)}{k + V_0(y)}$$
$$\exp\left(-rM_0(y) - \frac{bV_0(y)}{1 + cT_0(y)}\right) M_0(y)dy$$

$$V_1^k(x) = \int_\Omega k_2(x-y)\left[\sigma_v V_n(y) + \lambda\left(1 - \exp\left(\frac{-bV_0(y)}{1 + cT_0(y)}\right)\right) M_0(y)\right] dy$$
$$+ \int_\Omega k_3(x-y)p_0^k(y)dy$$

$$T_1(x) = \rho M_0(x) + \sigma_t T_0(x)$$

Here M_1 and T_1 remain fixed however V_1^k is sequence dependent. By a further two iterations we see that M_3^k, V_3^k and T_3^k are all sequence dependent. Then as p_n^k converges weakly as $k \to \infty$ this forces M_n^k, V_n^k and T_n^k to converge pointwise. Hence $M^* = M(p^*)$, $V^* = V(p^*)$ and $T^* = T(p^*)$. Further to this

$$\min_{p\epsilon U} J(p) = \lim_{k\to\infty} \int_\Omega \sum_{n=0}^{N}\left(A_n M_n^k + \frac{B_n}{2}(p_n^k)^2\right) dx$$

$$\geq \int_\Omega \sum_{n=0}^{N} A_n \left(\lim_{k\to\infty} M_n^k\right) dx + \sum_{n=0}^{N} \frac{B_n}{2}\left(\liminf_{k\to\infty} \int_\Omega (p_n^k)^2\right) dx$$

$$\geq \int_\Omega \sum_{n=0}^{N}\left(A_n M_n^* + \frac{B_n}{2}(p_n^*)^2\right) dx$$

As the range of values for the control is a closed interval of the reals then $p^*\epsilon U$. Consequently an optimal control exists p^* with corresponding states M^*, V^* and T^*.

$\square$

7.1.2 Optimality system

In the previous section we proved the existence of an optimal control for minimising the objective functional (7.1) subject to the constraints (7.2). In order to find the optimal control we need to find the sensitivity and adjoint functions. The use of sensitivity and adjoint functions is a standard tool in optimal control theory of partial differential equations (Lions 1971, Li & Yong 1995). This model has similar features from a control viewpoint due to the continuous space variables. We will use the sensitivity and adjoint functions in a similar way as Joshi et al. (in press) to derive our control characterisation.

To characterise the optimal control we must differentiate the objective functional

at the minimising control

$$\frac{\partial J(p^*)}{\partial p} = \lim_{\varepsilon \to 0^+} \left(\frac{J(p^* + \varepsilon l) - J(p^*)}{\varepsilon} \right) \geq 0$$

where l is a directional vector and ε is small. However, to do this we must first be able to differentiate the states with respect to the control and show that these derivatives exist. The derivatives with respect to the control are the sensitivity functions.

Proposition 7.1.1. *Let $p \epsilon U$. Then the mappings*

$$p \to M = M(p), \quad p \to V = V(p), \quad p \to T = T(p)$$

are differentiable in the following sense

$$\frac{M_n(p + \varepsilon l, x) - M_n(p, x)}{\varepsilon} \rightharpoonup \psi_n^M(x)$$

$$\frac{V_n(p + \varepsilon l, x) - V_n(p, x)}{\varepsilon} \rightharpoonup \psi_n^V(x)$$

$$\frac{T_n(p + \varepsilon l, x) - T_n(p, x)}{\varepsilon} \rightharpoonup \psi_n^T(x)$$

weakly in $L^2(\Omega)$ as $\varepsilon \to 0^+$, for $0 < \varepsilon \ll 1$ such that $(p + \varepsilon l) \epsilon U$.

Proof. Consider the control maps

$$p + \varepsilon l \to M(p + \varepsilon l), \quad p + \varepsilon l \to V(p + \varepsilon l), \quad p + \varepsilon l \to T(p + \varepsilon l)$$

$$p \to M(p) \qquad p \to V(p) \qquad p \to T(p)$$

Definition 7.1.1. *For simplicity we define*

$$M^\varepsilon := M(p + \varepsilon l), \quad V^\varepsilon := V(p + \varepsilon l), \quad T^\varepsilon := T(p + \varepsilon l).$$

$$M := M(p), \qquad V := V(p), \qquad T := T(p).$$

Then since

$$M_{n+1}^\varepsilon(x) = \int_\Omega k_1(x-y)\frac{a}{1+dT_n^\varepsilon(y)}\frac{k+(1-q)V_n^\varepsilon(y)}{k+V_n^\varepsilon(y)}$$
$$\exp\left(-rM_n^\varepsilon(y)-\frac{bV_n^\varepsilon(y)}{1+cT_n^\varepsilon(y)}\right)M_n^\varepsilon(y)dy \qquad (7.8a)$$

$$V_{n+1}^\varepsilon(y) = \int_\Omega k_2(x-y)\left[\sigma_v V_n^\varepsilon(y)+\lambda\left(1-\exp\left(\frac{-bV_n^\varepsilon(y)}{1+cT_n^\varepsilon(y)}\right)\right)\right.$$
$$\left.M_n(x)\right]dy + \int_\Omega k_3(x-y)\left[p_n(y)+\varepsilon l_n(y)\right]dy \qquad (7.8b)$$

$$T_{n+1}^\varepsilon(x) = \rho M_n^\varepsilon(x)+\sigma_t T_n^\varepsilon(x) \qquad (7.8c)$$

Subtracting (7.2) from (7.8)

$$M_{n+1}^\varepsilon(x) - M_{n+1}(x) = \int_\Omega k_1(x-y)\left[\frac{a}{1+dT_n^\varepsilon(y)}\frac{k+(1-q)V_n^\varepsilon(y)}{k+V_n^\varepsilon(y)}\right.$$
$$\exp\left(-rM_n^\varepsilon(y)-\frac{bV_n^\varepsilon(y)}{1+cT_n^\varepsilon(y)}\right)M_n^\varepsilon(y)$$
$$-\frac{a}{1+dT_n(y)}\frac{k+(1-q)V_n(y)}{k+V_n(y)}$$
$$\left.\exp\left(-rM_n(y)-\frac{bV_n(y)}{1+cT_n(y)}\right)M_n(y)\right]dy \qquad (7.9a)$$

$$V_{n+1}^\varepsilon(x) - V_{n+1}(x) = \int_\Omega k_2(x-y)\left[\sigma_v V_n^\varepsilon(y)\right.$$
$$+\lambda\left(1-\exp\left(\frac{-bV_n^\varepsilon(y)}{1+cT_n^\varepsilon(y)}\right)\right)M_n^\varepsilon(x)-\sigma_v V_n(y)$$
$$\left.-\lambda\left(1-\exp\left(\frac{-bV_n(y)}{1+cT_n(y)}\right)\right)M_n(y)\right]dy$$
$$+\int_\Omega k_3(x-y)\left[p_n(y)+\varepsilon l_n(y)-p_n(y)\right]dy \qquad (7.9b)$$

$$T_{n+1}^\varepsilon(x) - T_{n+1}(x) = \rho M_n^\varepsilon(x)+\sigma_t T_n^\varepsilon(x)-\rho M_n(x)-\sigma_t T_n(x) \qquad (7.9c)$$

Substituting the initial conditions (7.3) into (7.9) we find,

$$M_1^\varepsilon(x)-M_1(x) = 0 \qquad (7.10a)$$

$$|V_1^\varepsilon(x)-V_1(x)| = 0+\int_\Omega k_3(x-y)\varepsilon|l_n(y)|dy$$
$$\leq \varepsilon C_1^V \qquad (7.10b)$$

$$T_1^\varepsilon(x)-T_1(x) = 0 \qquad (7.10c)$$

From these bounds we have the existence of the sensitivities and the following bounds

$$\psi_1^M = 0$$
$$|\psi_1^V| \leq C_1^V$$
$$\psi_1^T = 0$$

and the first set of sensitivities exist and are bounded. For the second set of sensitivities

$$
\begin{aligned}
M_2^\varepsilon(x) - M_2(x) &= \int_\Omega k_1(x-y) \left[\frac{a}{1+dT_1^\varepsilon(y)} \frac{k+(1-q)V_1^\varepsilon(y)}{k+V_1^\varepsilon(y)} \right. \\
&\qquad \exp\left(-rM_1^\varepsilon(y) - \frac{bV_1^\varepsilon(y)}{1+cT_1^\varepsilon(y)} \right) M_1^\varepsilon(y) \\
&\qquad - \frac{a}{1+dT_1(y)} \frac{k+(1-q)V_1(y)}{k+V_1(y)} \\
&\qquad \left. \exp\left(-rM_1(y) - \frac{bV_1(y)}{1+cT_1(y)} \right) M_1(y) \right] dy \qquad (7.11a)
\end{aligned}
$$

$$
\begin{aligned}
V_2^\varepsilon(x) - V_2(x) &= \int_\Omega k_2(x-y) \left[\sigma_v V_1^\varepsilon(y) \right. \\
&\qquad + \lambda \left(1 - \exp\left(\frac{-bV_1^\varepsilon(y)}{1+cT_1^\varepsilon(y)} \right) \right) M_1^\varepsilon(x) - \sigma_v V_1(y) \\
&\qquad \left. - \lambda \left(1 - \exp\left(\frac{-bV_1(y)}{1+cT_1(y)} \right) \right) M_1(y) \right] dy \\
&\qquad + \int_\Omega k_3(x-y)\varepsilon l_1(y) dy \qquad (7.11b)
\end{aligned}
$$

$$T_2^\varepsilon(x) - T_2(x) = \rho M_1^\varepsilon(x) + \sigma_t T_1^\varepsilon(x) - \rho M_1(x) - \sigma_t T_1(x) \qquad (7.11c)$$

From (7.10a) and (7.10c) we find that (7.11a) can be rewritten

$$
\begin{aligned}
M_2^\varepsilon(x) - M_2(x) &= \int_\Omega k_1(x-y) \left[\frac{a}{1+dT_1(y)} \frac{k+(1-q)V_1^\varepsilon(y)}{k+V_1^\varepsilon(y)} \right. \\
&\qquad \exp\left(-rM_1(y) - \frac{bV_1^\varepsilon(y)}{1+cT_1(y)} \right) M_1(y) \\
&\qquad - \frac{a}{1+dT_1(y)} \frac{k+(1-q)V_1(y)}{k+V_1(y)} \\
&\qquad \left. \exp\left(-rM_1(y) - \frac{bV_1(y)}{1+cT_1(y)} \right) M_1(y) \right] dy \qquad (7.12)
\end{aligned}
$$

Dividing through by ε (> 0) and adding and subtracting a term into (7.12) then this

138

becomes,

$$\frac{M_2^\varepsilon(x) - M_2(x)}{\varepsilon} = \frac{1}{\varepsilon} \int_\Omega k_1(x-y) \frac{a}{1+dT_1(y)} M_1(y)$$

$$\left[\frac{k+(1-q)V_1^\varepsilon(y)}{k+V_1^\varepsilon(y)} \exp\left(-rM_1(y) - \frac{bV_1^\varepsilon(y)}{1+cT_1(y)} \right) \right.$$

$$- \frac{k+(1-q)V_1^\varepsilon(y)}{k+V_1^\varepsilon(y)} \exp\left(-rM_1(y) - \frac{bV_1(y)}{1+cT_1(y)} \right)$$

$$+ \frac{k+(1-q)V_1^\varepsilon(y)}{k+V_1^\varepsilon(y)} \exp\left(-rM_1(y) - \frac{bV_1(y)}{1+cT_1(y)} \right)$$

$$\left. - \frac{k+(1-q)V_1(y)}{k+V_1(y)} \exp\left(-rM_1(y) - \frac{bV_1(y)}{1+cT_1(y)} \right) \right] dy$$

Furthermore as $\varepsilon \to 0$,

$$\psi_2^M = \lim_{\varepsilon \to 0^+} \left(\frac{M_2^\varepsilon(x) - M_2(x)}{\varepsilon} \right)$$

$$= \int_\Omega k_1(x-y) \left(\frac{qk}{(k+V_1)^2} - \frac{b}{1+cT_1} \frac{k+(1-q)V_1}{k+V_1} \right)$$

$$\frac{a}{1+dT_1} M_1 \exp\left(-rM_1 - \frac{bV_1}{1+cT_1} \right) \psi_1^V(y) dy$$

$$|\psi_2^M| \le C^M \int_\Omega k_1(x-y)\psi_1^V(y) dy$$

$$\le C_2^M.$$

Therefore ψ_2^M exists and is bounded. Similarly for (7.11b) and (7.11c) we obtain the existence and boundedness of ψ_2^V and ψ_2^T.

$$\psi_2^V = \lim_{\varepsilon \to 0} \left(\frac{V_2^\varepsilon(x) - V_2(x)}{\varepsilon} \right)$$

$$= \int_\Omega k_2(x-y) \left(\sigma_v + \frac{\lambda b}{1+cT_1} \exp\left(\frac{-bV_1}{1+cT_1} \right) \right) M_1 \psi_1^V(y) dy$$

$$+ \int_\Omega k_3(x-y) l_n(y) dy$$

$$|\psi_2^V| \le C^V \int_\Omega k_2(x-y)\psi_1^V(y) dy + C^p$$

$$\le C_2^V$$

$$\psi_2^T = \lim_{\varepsilon \to 0} \left(\frac{T_2^\varepsilon(x) - T_2(x)}{\varepsilon} \right)$$

$$= 0$$

139

Continuing iteratively it follows that

$$|\psi_n^M| \le C_n^M$$
$$|\psi_n^V| \le C_n^V$$
$$|\psi_n^T| \le C_n^T$$

Hence the sensitivities exist and are bounded. $\qquad\square$

Proposition 7.1.2. *The sensitivities ψ satisfy the following system*

$$
\begin{aligned}
\psi_{n+1}^M &= \int_\Omega k_1(x-y)\left[\frac{a}{1+dT_n}\frac{k+(1-q)V_n}{k+V_n}\exp\left(-rM_n-\frac{bV_n}{1+cT_n}\right)\right.\\
&\quad (1-rM_n)\psi_n^M(y) + \left(\frac{qk}{(k+V_n)^2}-\frac{b}{1+cT_n}\frac{k+(1-q)V_n}{k+V_n}\right)\\
&\quad \frac{a}{1+dT_n}M_n\exp\left(-rM_n-\frac{bV_n}{1+cT_n}\right)\psi_n^V(y)\\
&\quad -\left(\frac{cbV_n}{(1+cT_n)^2}\frac{a}{1+dT_n}+\frac{ad}{1+dT_n}\right)\frac{k+(1-q)V_n}{k+V_n}\\
&\quad \left. M_n\exp\left(-rM_n-\frac{bV_n}{1+cT_n}\right)\psi_n^T(y)\right]dy &(7.13a)\\
\psi_{n+1}^V &= \int_\Omega k_2(x-y)\left[\lambda\left(1-\exp\left(\frac{-bV_n}{1+cT_n}\right)\right)\psi_n^M(y)\right.\\
&\quad +\left(\sigma_v+\frac{\lambda b}{1+cT_n}\exp\left(\frac{-bV_n}{1+cT_n}\right)\right)M_n\psi_n^V(y)\\
&\quad \left. -\frac{\lambda cbV_n}{(1+cT_n)^2}M_n\exp\left(\frac{-bV_n}{1+cT_n}\right)\psi_n^T(y)\right]dy\\
&\quad +\int_\Omega k_3(x-y)l_n(y)dy &(7.13b)\\
\psi_{n+1}^T &= \rho\psi_n^M+\sigma_t\psi_n^T &(7.13c)
\end{aligned}
$$

Proof. The proof follows ideas from the proof of Proposition 7.1.1. $\qquad\square$

Theorem 7.1.2. *Suppose there exists a set of optimum controls p^* with corresponding solutions M^*, V^*, T^* that minimises the objective function $J(p)$ over the control set U_p. Then there exists adjoint variables q^M, q^V, q^T such that the adjoint variables satisfy the system*

$$
\begin{aligned}
q_{n-1}^M(x) &= (1-rM_n)\frac{a}{1+dT_n}\frac{k+(1-q)V_n}{k+V_n}\exp\left(-rM_n-\frac{bV_n}{1+cT_n}\right)\\
&\quad \int_\Omega k_1(x-y)q_n^M(y)dy+\lambda\left(1-\exp\left(\frac{-bV_n}{1+cT_n}\right)\right)
\end{aligned}
$$

$$\int_{\Omega} k_2(x-y)q_n^V(y)dy + \rho q_n^T(x) + A_n \tag{7.14a}$$

$$
\begin{aligned}
q_{n-1}^V(x) =\ & \left(\frac{qk}{(k+V_n)^2} - \frac{b}{1+cT_n}\frac{k+(1-q)V_n}{k+V_n}\right)\frac{a}{1+dT_n}M_n \\
& \exp\left(-rM_n - \frac{bV_n}{1+cT_n}\right)\int_{\Omega} k_1(x-y)q_n^M(y)dy \\
& + \left(\sigma_v + \frac{\lambda bM_n}{1+cT_n}\exp\left(\frac{-bV_n}{1+cT_n}\right)\right)\int_{\Omega} k_2(x-y)q_n^V(y)dy \tag{7.14b}
\end{aligned}
$$

$$
\begin{aligned}
q_{n-1}^T(x) =\ & \left(\frac{cbV_n}{(1+cT_n)^2}\frac{a}{1+dT_n} + \frac{ad}{1+dT_n}\right)\frac{k+(1-q)V_n}{k+V_n}M_n \\
& \exp\left(-rM_n - \frac{bV_n}{1+cT_n}\right)\int_{\Omega} k_1(x-y)q_n^M(y)dy \\
& - \frac{\lambda cbV_n}{(1+cT_n)^2}\exp\left(\frac{-bV_n}{1+cT_n}\right)M_n\int_{\Omega} k_2(x-y)q_n^V(y)dy \\
& + \sigma_t q_n^T(x) \tag{7.14c}
\end{aligned}
$$

with the transversality conditions

$$q_N^M = 0 \tag{7.15a}$$

$$q_N^V = 0 \tag{7.15b}$$

$$q_N^T = 0 \tag{7.15c}$$

Furthermore the optimal control is given by

$$p_n^* = \max\left(0, \min\left(-\frac{\int_{\Omega} k_3(x-s)q_n^V(x)dx}{B_n}, P_{max}\right)\right) \tag{7.16}$$

Proof. We start by taking the directional derivative of the objective function. Then for $\varepsilon > 0$ and directional vector l,

$$
\begin{aligned}
0 \leq\ & \frac{\partial(J(p^*))}{\partial p} \tag{7.17} \\
=\ & \lim_{\varepsilon \to 0^+}\left(\frac{J(p^* + \varepsilon l) - J(p^*)}{\varepsilon}\right) \\
=\ & \lim_{\varepsilon \to 0^+}\frac{1}{\varepsilon}\left[\sum_{n=0}^{N}\int_{\Omega}\left(A_n M_n^\varepsilon + \frac{B_n}{2}(p_n^{*\varepsilon})^2\right)dx\right] \\
& - \lim_{\varepsilon \to 0^+}\frac{1}{\varepsilon}\left[\sum_{n=0}^{N}\int_{\Omega}\left(A_n M_n - \frac{B_n}{2}(p_n^*)^2\right)dx\right] \\
=\ & \sum_{n=0}^{N}\int_{\Omega}\left[A_n \lim_{\varepsilon \to 0^+}\left(\frac{M_n^\varepsilon - M_n}{\varepsilon}\right)\right.
\end{aligned}
$$

141

$$+ \frac{B_n}{2} \lim_{\varepsilon \to 0^+} \left(\frac{(p_n^{*\varepsilon})^2 - (p_n^*)^2}{\varepsilon} \right) \Bigg] dx$$

$$= \sum_{n=0}^{N} \int_\Omega \left[A_n \psi_n^M + B_n p_n^* l_n \right] dx \qquad (7.18)$$

where

$$
\begin{aligned}
p^\varepsilon(x) &= p(x) + \varepsilon l(x) \\
M^\varepsilon(x) &= M(p(x) + \varepsilon l(x)) \\
V^\varepsilon(x) &= V(p(x) + \varepsilon l(x)) \\
T^\varepsilon(x) &= T(p(x) + \varepsilon l(x))
\end{aligned}
$$

and from Proposition 7.1.1

$$\frac{M^\varepsilon(x) - M(x)}{\varepsilon} \to \psi^M(x)$$

Note also from Proposition 7.1.1

$$\frac{V^\varepsilon(x) - V(x)}{\varepsilon} \to \psi^V(x)$$

$$\frac{T^\varepsilon(x) - T(x)}{\varepsilon} \to \psi^T(x)$$

To solve the optimal control we need to replace ψ_n^M in (7.18) with parameters from the original problem. To do this we need to find the adjoint equations. The adjoint equations can be found as demonstrated from the following sensitivity equations. From Proposition 7.1.2 we have the system of sensitivities (7.11a)

$$\psi_{n+1}^M = \int_\Omega k_1(x - y) \left[\frac{\partial F}{\partial M_n} \psi_n^M + \frac{\partial F}{\partial V_n} \psi_n^V + \frac{\partial F}{\partial T_n} \psi_n^T \right] dy \qquad (7.19a)$$

$$\psi_{n+1}^V = \int_\Omega k_2(x - y) \left[\frac{\partial G}{\partial M_n} \psi_n^M + \frac{\partial G}{\partial V_n} \psi_n^V + \frac{\partial G}{\partial T_n} \psi_n^T \right] dy \qquad (7.19b)$$

$$\psi_{n+1}^T = \rho \psi_n^M + \sigma_t \psi_n^T \qquad (7.19c)$$

where

$$
\begin{aligned}
F &= \frac{a}{1 + dT_n(y)} \frac{k + (1 - q)V_n(y)}{k + V_n(y)} \\
&\quad \exp\left(-rM_n(y) - \frac{bV_n(y)}{1 + cT_n(y)} \right) M_n(y) \\
G &= \sigma_v V_n(y) + \lambda \left(1 - \exp\left(\frac{-bV_n(y)}{1 + cT_n(y)} \right) \right) M_n(y)
\end{aligned}
$$

Then we let

$$
S = \int_\Omega \sum_{n=0}^{N-1} \begin{pmatrix} q_n^M & q_n^V & q_n^T \end{pmatrix} \begin{pmatrix} \psi_{n+1}^M - \int_\Omega k_1(x-y) \left[\frac{\partial F}{\partial M_n} \psi_n^M + \frac{\partial F}{\partial V_n} \psi_n^V + \frac{\partial F}{\partial T_n} \psi_n^T \right] dy \\ \psi_{n+1}^V - \int_\Omega k_2(x-y) \left[\frac{\partial G}{\partial M_n} \psi_n^M + \frac{\partial G}{\partial V_n} \psi_n^V + \frac{\partial G}{\partial T_n} \psi_n^T \right] dy \\ \psi_{n+1}^T - \rho \psi_n^M - \sigma_t \psi_n^T \end{pmatrix} dx
$$

$$
= \int_\Omega \sum_{n=0}^{N-1} \begin{pmatrix} q_n^M & q_n^V & q_n^T \end{pmatrix} \begin{pmatrix} \psi_{n+1}^M \\ \psi_{n+1}^V \\ \psi_{n+1}^T \end{pmatrix}
$$

$$
- \begin{pmatrix} q_n^M & q_n^V & q_n^T \end{pmatrix} \begin{pmatrix} \int_\Omega k_1(x-y) \left[\frac{\partial F}{\partial M_n} \psi_n^M + \frac{\partial F}{\partial V_n} \psi_n^V + \frac{\partial F}{\partial T_n} \psi_n^T \right] dy \\ \int_\Omega k_2(x-y) \left[\frac{\partial G}{\partial M_n} \psi_n^M + \frac{\partial G}{\partial V_n} \psi_n^V + \frac{\partial G}{\partial T_n} \psi_n^T \right] dy \\ \rho \psi_n^M + \sigma_t \psi_n^T \end{pmatrix} dx
$$

$$
= \sum_{n=1}^N \int_\Omega \begin{pmatrix} \psi_n^M & \psi_n^V & \psi_n^T \end{pmatrix} \begin{pmatrix} q_{n-1}^M \\ q_{n-1}^V \\ q_{n-1}^T \end{pmatrix} dx
$$

$$
- \sum_{n=1}^N \begin{pmatrix} \int_\Omega \int_\Omega k_1(x-y) q_n^M \left[\frac{\partial F}{\partial M_n} \psi_n^M + \frac{\partial F}{\partial V_n} \psi_n^V + \frac{\partial F}{\partial T_n} \psi_n^T \right] dydx \\ + \int_\Omega \int_\Omega k_2(x-y) q_n^V \left[\frac{\partial G}{\partial M_n} \psi_n^M + \frac{\partial G}{\partial V_n} \psi_n^V + \frac{\partial G}{\partial T_n} \psi_n^T \right] dydx \\ + \int_\Omega q_n^T \left[\rho \psi_n^M + \sigma_t \psi_n^T \right] dx \end{pmatrix}
$$

Note the initial conditions for the sensitivities $\begin{pmatrix} \psi_0^M & \psi_0^V & \psi_0^T \end{pmatrix}$ are all zero (as $M_0^\varepsilon = M_0$ etc). Therefore we exclude that term from the second sum. Then we force the terminal conditions for the adjoint variables $\begin{pmatrix} q_N^M & q_N^V & q_N^T \end{pmatrix}$ to be zero (7.15) and include this term in the second sum. We also renumber the indices of the first sum in order to match that of the second. Hence

$$
S = \sum_{n=1}^N \int_\Omega \begin{pmatrix} \psi_n^M & \psi_n^V & \psi_n^T \end{pmatrix} \begin{pmatrix} q_{n-1}^M \\ q_{n-1}^V \\ q_{n-1}^T \end{pmatrix} dx
$$

$$
- \sum_{n=1}^N \begin{pmatrix} \int_\Omega \left[\frac{\partial F}{\partial M_n} \psi_n^M + \frac{\partial F}{\partial V_n} \psi_n^V + \frac{\partial F}{\partial T_n} \psi_n^T \right] \int_\Omega k_1(x-y) q_n^M \, dxdy \\ + \int_\Omega \left[\frac{\partial G}{\partial M_n} \psi_n^M + \frac{\partial G}{\partial V_n} \psi_n^V + \frac{\partial G}{\partial T_n} \psi_n^T \right] \int_\Omega k_2(x-y) q_n^V \, dxdy \\ + \int_\Omega q_n^T \left[\rho \psi_n^M + \sigma_t \psi_n^T \right] dx \end{pmatrix}
$$

Then by changing the order of integration,

$$
= \sum_{n=1}^{N} \int_{\Omega} \begin{pmatrix} \psi_n^M & \psi_n^V & \psi_n^T \end{pmatrix} \begin{pmatrix} q_{n-1}^M \\ q_{n-1}^V \\ q_{n-1}^T \end{pmatrix} dx
$$

$$
- \sum_{n=1}^{N} \int_{\Omega} \begin{pmatrix} \left[\frac{\partial F}{\partial M_n} \psi_n^M + \frac{\partial F}{\partial V_n} \psi_n^V + \frac{\partial F}{\partial T_n} \psi_n^T \right], \\ \left[\frac{\partial G}{\partial M_n} \psi_n^M + \frac{\partial G}{\partial V_n} \psi_n^V + \frac{\partial G}{\partial T_n} \psi_n^T \right], \\ \left[\rho \psi_n^M + \sigma_t \psi_n^T \right] \end{pmatrix} \begin{pmatrix} \int_{\Omega} k_1(x-y) q_n^M \, dx \\ \int_{\Omega} k_2(x-y) q_n^V \, dx \\ q_n^T \end{pmatrix} dy
$$

By a change of variable

$$
= \int_{\Omega} \sum_{n=1}^{N} \begin{pmatrix} \psi_n^M & \psi_n^V & \psi_n^T \end{pmatrix} \begin{pmatrix} q_{n-1}^M \\ q_{n-1}^V \\ q_{n-1}^T \end{pmatrix}
$$

$$
- \begin{pmatrix} \left[\frac{\partial F}{\partial M_n} \psi_n^M + \frac{\partial F}{\partial V_n} \psi_n^V + \frac{\partial F}{\partial T_n} \psi_n^T \right], \\ \left[\frac{\partial G}{\partial M_n} \psi_n^M + \frac{\partial G}{\partial V_n} \psi_n^V + \frac{\partial G}{\partial T_n} \psi_n^T \right], \\ \left[\rho \psi_n^M + \sigma_t \psi_n^T \right] \end{pmatrix} \begin{pmatrix} \int_{\Omega} k_1(x-s) q_n^M \, dx \\ \int_{\Omega} k_2(x-s) q_n^V \, dx \\ q_n^T \end{pmatrix} ds
$$

$$
= \int_{\Omega} \sum_{n=1}^{N} \begin{pmatrix} \psi_n^M & \psi_n^V & \psi_n^T \end{pmatrix} \begin{pmatrix} q_{n-1}^M \\ q_{n-1}^V \\ q_{n-1}^T \end{pmatrix}
$$

$$
- \begin{pmatrix} \psi_n^M & \psi_n^V & \psi_n^T \end{pmatrix} \begin{pmatrix} \frac{\partial F}{\partial M_n} & \frac{\partial G}{\partial M_n} & \rho \\ \frac{\partial F}{\partial V_n} & \frac{\partial G}{\partial V_n} & 0 \\ \frac{\partial F}{\partial T_n} & \frac{\partial G}{\partial T_n} & \sigma_t \end{pmatrix} \begin{pmatrix} \int_{\Omega} k_1(x-s) q_n^M \, dx \\ \int_{\Omega} k_2(x-s) q_n^V \, dx \\ q_n^T \end{pmatrix} ds
$$

Therefore the adjoint system is

$$
q_{n-1}^M = \frac{\partial F}{\partial M_n} \int_{\Omega} k_1(y-x) q_n^M \, dy + \frac{\partial G}{\partial M_n} \int_{\Omega} k_2(y-x) q_n^V \, dy + \rho q_n^T \quad (7.20a)
$$

$$
q_{n-1}^V = \frac{\partial F}{\partial V_n} \int_{\Omega} k_1(y-x) q_n^M \, dy + \frac{\partial G}{\partial V_n} \int_{\Omega} k_2(y-x) q_n^V \, dy \quad (7.20b)
$$

$$
q_{n-1}^T = \frac{\partial F}{\partial T_n} \int_{\Omega} k_1(y-x) q_n^M \, dy + \frac{\partial G}{\partial T_n} q_n^T + \sigma_t q_n^T \quad (7.20c)
$$

We can replace (7.19a) with (7.20b) in (7.18) as,

$$
\sum_{n=1}^{N} [A_n \psi_n^M] = \sum_{n=0}^{N-1} \left[q_n^V \int_{\Omega} k_3(x-y) l_n(y) dy \right] \quad (7.21)
$$

Hence from (7.18)

$$
\begin{aligned}
0 \;\leq\; & \frac{\partial (J(p^*))}{\partial p} \\
=\; & \int_\Omega \sum_{n=0}^{N} [A_n \psi_n^M(x) + B_n p_n^*(x) l_n(x)] dx \\
=\; & \int_\Omega A_0 \psi_0^M(x) + \sum_{n=1}^{N} \left[A_n \psi_n^M(x) \right] \\
& + \sum_{n=0}^{N-1} [B_n p_n^*(x) l_n(x)] + B_N p_N^*(x) l_N(x) dx \\
=\; & \int_\Omega \sum_{n=1}^{N} \left[A_n \psi_n^M(x) \right] + \sum_{n=0}^{N-1} [B_n p_n^*(x) l_n(x)] \, dx \\
=\; & \int_\Omega \sum_{n=0}^{N-1} \left[q_n^V \int_\Omega k_3(x-y) l_n(y) dy + B_n p_n^*(x) l_n(x) \right] dx
\end{aligned}
$$

Then by a further change of order of integration we have

$$
\begin{aligned}
0 \;\leq\; & \frac{\partial (J(p^*))}{\partial p} \\
=\; & \sum_{n=0}^{N-1} \left[\int_\Omega l_n(s) \int_\Omega k_3(x-s) q_n^V dx ds + \int_\Omega B_n p_n^*(s) l_n(s) ds \right] dx \\
=\; & \sum_{n=0}^{N-1} \left[\int_\Omega l_n(s) \left[\int_\Omega k_3(x-s) q_n^V(x) dx + B_n p_n^*(s) \right] ds \right]
\end{aligned}
$$

So for a minimum to occur

$$
p_n^* = \begin{cases}
0 & \text{if} \quad 0 \leq \int_\Omega k_3(x-s) q_n^V(x) dx \\
-\frac{\int_\Omega k_3(x-s) q_n^V(x) dx}{B_n} & \text{if} \quad -B_n P_{max} \leq \int_\Omega k_3(x-s) q_n^V(x) dx \leq 0 \\
P & \text{if} \quad \int_\Omega k_3(x-s) q_n^V(x) dx \leq -B_n P_{max}
\end{cases}
$$

Therefore

$$
p_n^* = \max \left(0, \min \left(-\frac{\int_\Omega k_3(x-s) q_n^V(x) dx}{B_n}, P_{max} \right) \right)
$$

and we get the system as originally stated (7.14)-(7.1.2). $\qquad \square$

7.1.3 Uniqueness of the Optimal Control

Theorem 7.1.3. *The optimal control is unique if B_n are sufficiently large for $n=0,1...N$.*

Proof. We prove a uniqueness result by showing the objective functional J(p) is strictly convex (Rockafellar 1970). We begin by defining the function

$$
\begin{aligned}
g(\varepsilon) &= J((1-\varepsilon)p + \varepsilon l) \\
&= J(p + \varepsilon(l - p))
\end{aligned}
\tag{7.22}
$$

For convexity we need to show that the second derivative of (7.22) is strictly positive

$$
g''(\varepsilon) > 0
\tag{7.23}
$$

The first derivative of (7.22) gives

$$
\begin{aligned}
g'(\varepsilon) &= \lim_{\tau \to 0}\left(\frac{J(p + (\tau + \varepsilon(l-p))) - J(p + \varepsilon(l-p))}{\tau} \right) \\
&= \lim_{\tau \to 0}\sum_{n=0}^{N}\int_{\Omega} A_n \left(\frac{M_n^{\tau+\varepsilon}(x) - M_n^{\varepsilon}(x)}{\tau} \right) \\
&\quad + \frac{B_n}{2}\left(\frac{[p_n + (\tau + \varepsilon)(l_n - p_n)]^2(x) - [p_n + \varepsilon(l_n - p_n)]^2}{\tau} \right) dx \\
&= \sum_{n=0}^{N}\int_{\Omega} A_n \psi_n^{M,\varepsilon} + B_n(l_n - p_n)[p_n + \varepsilon(l_n - p_n)]dx
\end{aligned}
\tag{7.24}
$$

We now define

$$
\sigma_{n+1}^{M,\varepsilon} := \lim_{\tau \to 0}\left(\frac{\psi_{n+1}^{M,\tau+\varepsilon}(x) - \psi_{n+1}^{M,\varepsilon}(x)}{\tau} \right)
\tag{7.25a}
$$

$$
\sigma_{n+1}^{V,\varepsilon} := \lim_{\tau \to 0}\left(\frac{\psi_{n+1}^{V,\tau+\varepsilon}(x) - \psi_{n+1}^{V,\varepsilon}(x)}{\tau} \right)
\tag{7.25b}
$$

$$
\sigma_{n+1}^{T,\varepsilon} := \lim_{\tau \to 0}\left(\frac{\psi_{n+1}^{T,\tau+\varepsilon}(x) - \psi_{n+1}^{T,\varepsilon}(x)}{\tau} \right)
\tag{7.25c}
$$

Then by a similar result to Proposition 7.1.2 we have

$$
\psi_{n+1}^{M,\varepsilon}(x) = \int_{\Omega} k_1(x - y)\left[\frac{\partial F}{\partial M_n^{\varepsilon}}\psi_n^{M,\varepsilon} + \frac{\partial F}{\partial V_n^{\varepsilon}}\psi_n^{V,\varepsilon} + \frac{\partial F}{\partial T_n^{\varepsilon}}\psi_n^{T,\varepsilon} \right] dy
\tag{7.26a}
$$

$$
\psi_{n+1}^{V,\varepsilon}(x) = \int_{\Omega} k_2(x - y)\left[\frac{\partial G}{\partial M_n^{\varepsilon}}\psi_n^{M,\varepsilon} + \frac{\partial G}{\partial V_n^{\varepsilon}}\psi_n^{V,\varepsilon} + \frac{\partial G}{\partial T_n^{\varepsilon}}\psi_n^{T,\varepsilon} \right] dy
\tag{7.26b}
$$

$$
\psi_{n+1}^{T,\varepsilon}(x) = \rho\psi_n^{M,\varepsilon} + \sigma_t\psi_n^{T,\varepsilon}
\tag{7.26c}
$$

146

where

$$F = \frac{a}{1 + dT_n^\varepsilon(y)} \frac{k + (1-q)V_n^\varepsilon(y)}{k + V_n^\varepsilon(y)}$$
$$\exp\left(-rM_n^\varepsilon(y) - \frac{bV_n^\varepsilon(y)}{1 + cT_n^\varepsilon(y)}\right) M_n^\varepsilon(y)$$

$$G = \sigma_v V_n^\varepsilon(y) + \lambda\left(1 - \exp\left(\frac{-bV_n^\varepsilon(y)}{1 + cT_n^\varepsilon(y)}\right)\right) M_n^\varepsilon(y)$$

Then (7.26) combined with (7.25) yields

$$
\begin{aligned}
\sigma_{n+1}^{M,\varepsilon}(x) &= \int_\Omega k_1(x-y)\left[\frac{\partial F}{\partial M_n^\varepsilon}\sigma_n^{M,\varepsilon}(y) + \frac{\partial^2 F}{\partial M_n^{\varepsilon 2}}(\psi_n^{M,\varepsilon}(y))^2\right] dy \\
&+ \int_\Omega k_1(x-y)\left[\frac{\partial F}{\partial V_n^\varepsilon}\sigma_n^{V,\varepsilon}(y) + \frac{\partial^2 F}{\partial V_n^{\varepsilon 2}}(\psi_n^{V,\varepsilon}(y))^2\right] dy \\
&+ \int_\Omega k_1(x-y)\left[\frac{\partial F}{\partial T_n^\varepsilon}\sigma_n^{T,\varepsilon}(y) + \frac{\partial^2 F}{\partial T_n^{\varepsilon 2}}(\psi_n^{T,\varepsilon}(y))^2\right] dy \quad (7.27a)
\end{aligned}
$$

$$
\begin{aligned}
\sigma_{n+1}^{V,\varepsilon}(x) &= \int_\Omega k_2(x-y)\left[\frac{\partial G}{\partial M_n^\varepsilon}\sigma_n^{M,\varepsilon}(y) + \frac{\partial^2 G}{\partial M_n^{\varepsilon 2}}(\psi_n^{M,\varepsilon}(y))^2\right] dy \\
&+ \int_\Omega k_2(x-y)\left[\frac{\partial G}{\partial V_n^\varepsilon}\sigma_n^{V,\varepsilon}(y) + \frac{\partial^2 G}{\partial V_n^{\varepsilon 2}}(\psi_n^{V,\varepsilon}(y))^2\right] dy \\
&+ \int_\Omega k_2(x-y)\left[\frac{\partial G}{\partial T_n^\varepsilon}\sigma_n^{T,\varepsilon}(y) + \frac{\partial^2 G}{\partial T_n^{\varepsilon 2}}(\psi_n^{T,\varepsilon}(y))^2\right] dy \quad (7.27b)
\end{aligned}
$$

$$\sigma_{n+1}^{T,\varepsilon}(x) = \rho\sigma_n^{M,\varepsilon} + \sigma_t\sigma_n^{T,\varepsilon} \quad (7.27c)$$

Now the initial sensitivities are all zero, $\psi_0^{M,\varepsilon} = 0$, $\psi_0^{V,\varepsilon} = 0$ and $\psi_0^{T,\varepsilon} = 0$. Then using (7.26) we calculate the next sensitivities. Next

$$
\begin{aligned}
\psi_1^{M,\varepsilon} &= 0 \\
\psi_1^{V,\varepsilon} &= \int_\Omega k_3(x-y)(l_o - p_o) dy \\
\psi_1^{T,\varepsilon} &= 0
\end{aligned}
$$

Continuing this process iteratively we find the following expression

$$|\psi_{n+1}^{M,\varepsilon}| \le \sum_{j=0}^n C_j^M \int_\Omega k_3(x-y)(l_n - p_n) dy$$

$$|\psi_{n+1}^{V,\varepsilon}| \le \sum_{j=0}^n C_j^V \int_\Omega k_3(x-y)(l_n - p_n) dy$$

$$|\psi_{n+1}^{T,\varepsilon}| \le \sum_{j=0}^n C_j^T \int_\Omega k_3(x-y)(l_n - p_n) dy$$

Also note that $\sigma_0^{M,\varepsilon} = 0$, $\sigma_0^{V,\varepsilon} = 0$ and $\sigma_0^{T,\varepsilon} = 0$. Using the result for $f_1, f_2 \epsilon L^2$ (see Appendix B2)

$$\int_\Omega f_1(x)f_2(x)dx \geq \frac{-1}{2} \int_\Omega \left(f_1^2(x) + f_2^2(x)\right) dx \qquad (7.28)$$

we can compute the successive values from (7.27)

$$|\sigma_{n+1}^{M,\varepsilon}| \leq \sum_{j=0}^{n} C_j^M \int_\Omega k_3(x-y)(l_{n-j} - p_{n-j})^2 dy,$$

$$|\sigma_{n+1}^{V,\varepsilon}| \leq \sum_{j=0}^{n} C_j^V \int_\Omega k_3(x-y)(l_{n-j} - p_{n-j})^2 dy,$$

$$|\sigma_{n+1}^{T,\varepsilon}| \leq \sum_{j=0}^{n} C_j^T \int_\Omega k_3(x-y)(l_{n-j} - p_{n-j})^2 dy.$$

So

$$\sum_{i=0}^{n} \int_\Omega |\sigma_{i+1}^{M,\varepsilon}| dy \geq \sum_{j=0}^{n} C_M \int_\Omega (l_{n-j} - p_{n-j})^2 dy \qquad (7.29a)$$

$$\sum_{i=0}^{n} \int_\Omega |\sigma_{i+1}^{V,\varepsilon}| dy \geq \sum_{j=0}^{n} C_V \int_\Omega (l_{n-j} - p_{n-j})^2 dy \qquad (7.29b)$$

$$\sum_{i=0}^{n} \int_\Omega |\sigma_{i+1}^{T,\varepsilon}| dy \geq \sum_{j=0}^{n} C_T \int_\Omega (l_{n-j} - p_{n-j})^2 dy \qquad (7.29c)$$

We can now take the second derivative of the function g. Hence differentiating (7.24) and using the bound (7.29a)

$$
\begin{aligned}
g''(\varepsilon) &= \sum_{n=0}^{N} \int_\Omega A_n \lim_{\tau \to 0} \left(\frac{\psi_n^{M,\varepsilon+\tau} - \psi_n^{M,\varepsilon}}{\tau} \right) + B_n(l_n - p_n) \\
&\qquad \lim_{\tau \to 0} \left(\frac{[p_n + (\varepsilon + \tau)(l_n - p_n)] - [p_n + \varepsilon(l_n - p_n)]}{\tau} \right) dx \\
&= \sum_{n=0}^{N} \int_\Omega A_n \sigma_n^{M,\varepsilon} + B_n(l_n - p_n)^2 dx \\
&\geq \sum_{n=0}^{N} \int_\Omega (B_n - \hat{C})(l_n - p_n)^2 dx \\
&> 0
\end{aligned}
$$

So for sufficiently large B_n's the function is convex. Hence the optimal control is unique. □

148

7.2 Numerical results

We now demonstrate three cases where the optimal control problem is applied. These three cases are when population levels are at a spatially uniform stable steady state, spatially uniform but periodic in time or a spatially patterned stable population. We use an iterative method to find the optimal solution, which involves solving state and adjoint equations using Fast Fourier Transforms (FFT's) for the convolution integrals on a spatial domain of size 2^{11}. Also dispersal kernels are chosen to be Laplace distributions for gypsy moths and NPV dispersal with a narrow Gaussian distribution for the control.

We first find a suitable set of initial conditions by solving the spatial state equations over 1,000 generations without control. These initial conditions are then used with arbitrary values of $p_n(x)$ to solve the state equations giving estimates for $M_n(x)$, $V_n(x)$, $T_n(x)$ for $n = 1...N$. Using these estimates together with the transversality conditions, the adjoint equations are solved. From the adjoint variables, new control values $p_n(x)$ are calculated which are compared with the original control values. If the difference between control values do not agree to the specified tolerance (0.0001) at each spatial location $x\epsilon\Omega$ and in each generation, then the new $p_n(x)$ values are used with the initial conditions to find new estimates for $M_n(x)$, $V_n(x)$, $T_n(x)$ for $n = 1...N$. Subsequently, the adjoint variables are found and in turn control values $p_n(x)$. Comparisons are again made between the latest control values and the previous $p_n(x)$ values. The process continues iteratively until the tolerance is met. This process was further described in Chapter 5 and similarly in Hackbusch (1978). We now look at the optimal solutions applied to the three cases.

7.2.1 Case i: Spatially Uniform Steady State

We consider a spatially uniform steady state solution to the integrodifference model and add a control term to the equation describing NPV population levels. Due to difficulties in convergence of the optimal system, we replace the linear term for the production of tannin by the bounded function $\rho M_n(x)/(1 + \tau M_n(x))$. We then look at the optimal control strategy over a 15 year period at a particular cost of damage, A_n, and cost of control, B_n. Figure 7-1 demonstrates the behaviour.

149

Figure 7-1: Plots show the population levels for the optimal solution when $A = 10$ and $B = 2$ over 15 generations (gypsy moth - blue line, NPV - green line, tannin - aqua line, control - red line). Parameters are $a = 6.0, r = 0.0001, c = 0.1, d = 0.067, q = 0.4, k = 3, b = 0.1, \lambda = 1.49, \sigma_v = 0.37, \sigma_t = 0.1, \rho = 0.01, \tau = 1.2$ with dispersal coefficients $\alpha = 100, \beta = 100$ and $D = 10^{-6}$.

We see that the optimal solution is to apply the control periodically. Due to the periodic application of the control, the population levels begin to fluctuate in time. After the first application of control in years 3 and 4, further control is used when virus levels diminish in years 8 and 9 and again in years 13 and 14. This causes the virus levels to continue to fluctuate resulting in oscillatory gypsy moth populations. As no spatial variation occurs, we look at how the populations change over time at one location point for various costs of control, B.

Figure 7-2: Plots show population levels over time with $A = 10$. Figure(a) cost of control, B=50, Figure(b) B=10, Figure(c) B=2, Figure(d) B=1, Figure(e) B=0.5, Figure(f) B=0.01. Parameters are $a = 6.0, r = 0.0001, c = 0.1, d = 0.067, q = 0.4, k = 3, b = 0.1, \lambda = 1.49, \sigma_v = 0.37, \sigma_t = 0.1, \rho = 0.01, \tau = 1.2$ with dispersal coefficients $\alpha = 100, \beta = 100$ and $D = 10^{-6}$.

Figure 7-2 shows the population levels at a particular location in the middle of the spacial domain over 25 generations. In Figures 7-2(a)&(b), the cost of control is high and therefore little control is used. Thus we see that the population levels begin to fluctuate, but this is very small. In Figures 7-2(c)&(d), the cost of control has

decreased, resulting in more control being used in the optimal solution. This causes fluctuations in the population levels to appear. However, the fluctuating population of gypsy moths always remain lower than the original population level (with no control). Finally, Figures 7-2(e)&(f) show the control reaching maximum levels. We see that the control remains periodic flipping between the maximum amount of control in some years and no control in other years. Here, gypsy moth populations are further reduced but the fluctuations still remain.

We also look at how the total cost of the optimal strategy changes as the cost of the control is varied. Figure 7-3 plots the cost of control, B, against the total cost.

Figure 7-3: Plot shows the total cost against the cost of the control, B_n. Parameters are $A = 10$, $a = 6.0$, $r = 0.0001$, $c = 0.1$, $d = 0.067$, $q = 0.4$, $k = 3$, $b = 0.1$, $\lambda = 1.49$, $\sigma_v = 0.37$, $\sigma_t = 0.1$, $\rho = 0.01$, $\tau = 1.2$ with dispersal coefficients $\alpha = 100$, $\beta = 100$ and $D = 10^{-6}$.

As in Chapter 5, we see a critical range where a small change in the cost of control, B, causes a large reduction in the total cost. Therefore, a slight reduction in the cost of control in the range [0.1,10], will be economically beneficial. Moreover, management strategists may see substantial savings in the total cost of the optimal solution by investing in initiatives to reduce the cost of control.

7.2.2 Case ii: Oscillatory Populations

Using the bounded function $\rho M_n(x)/(1 + \tau M_n(x))$ for the production rate of tannin, we look at an optimal control strategy for a spatially uniform oscillatory population. Figure 7-4 shows the population levels for an optimal control strategy when the cost of control B=0.5.
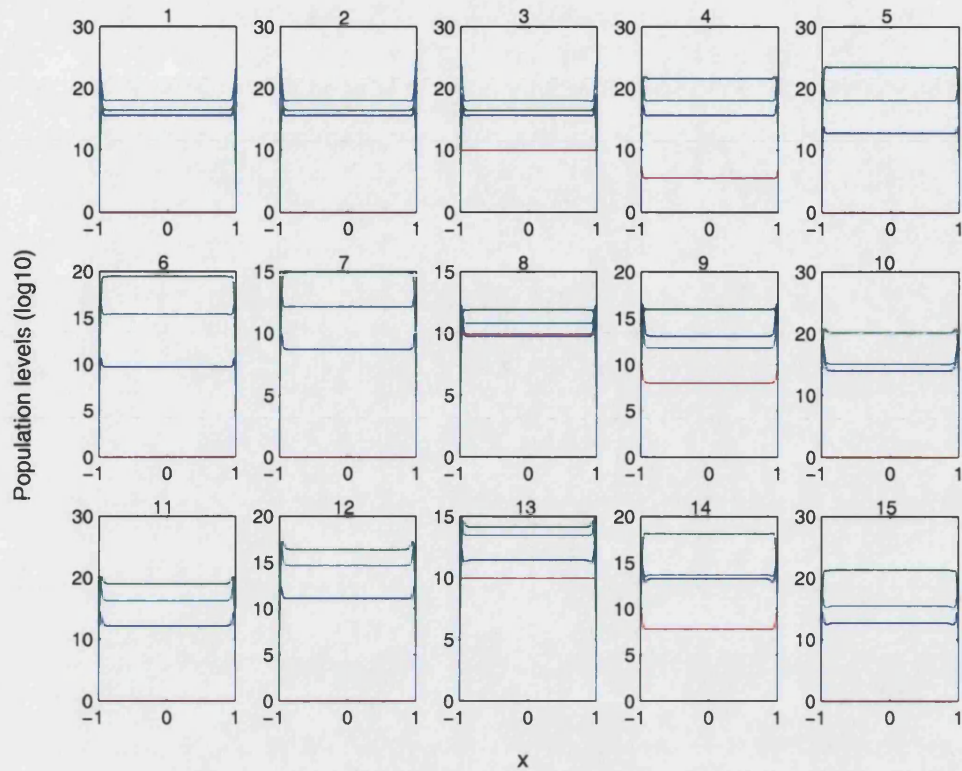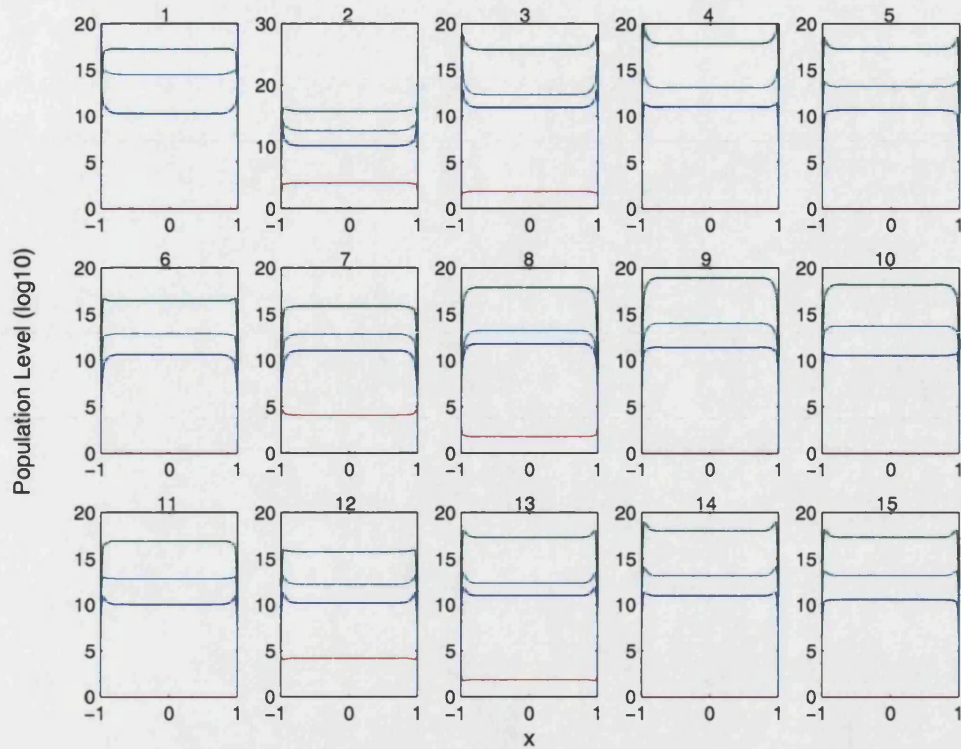
Figure 7-4: Plots show the population levels for the optimal solution when $A = 10$ and $B = 2$ over 15 generations (gypsy moth - blue line, NPV - green line, tannin - , control - red line). Parameters are $a = 6.0, r = 0.0001, c = 0.1, d = 0.067, q = 0.4, k = 3, b = 0.1, \lambda = 1.49, \sigma_v = 0.37, \sigma_t = 0.1, \rho = 0.01, \tau = 1.2$ with dispersal coefficients $\alpha = 100$, $\beta = 1200$ and $D = 10^{-6}$.

As in the case of the stable steady state, we see that the control is added periodically. We again look at one of the locations in the centre of the spatial domain and consider what happens to the population levels over time as cost of control varies.
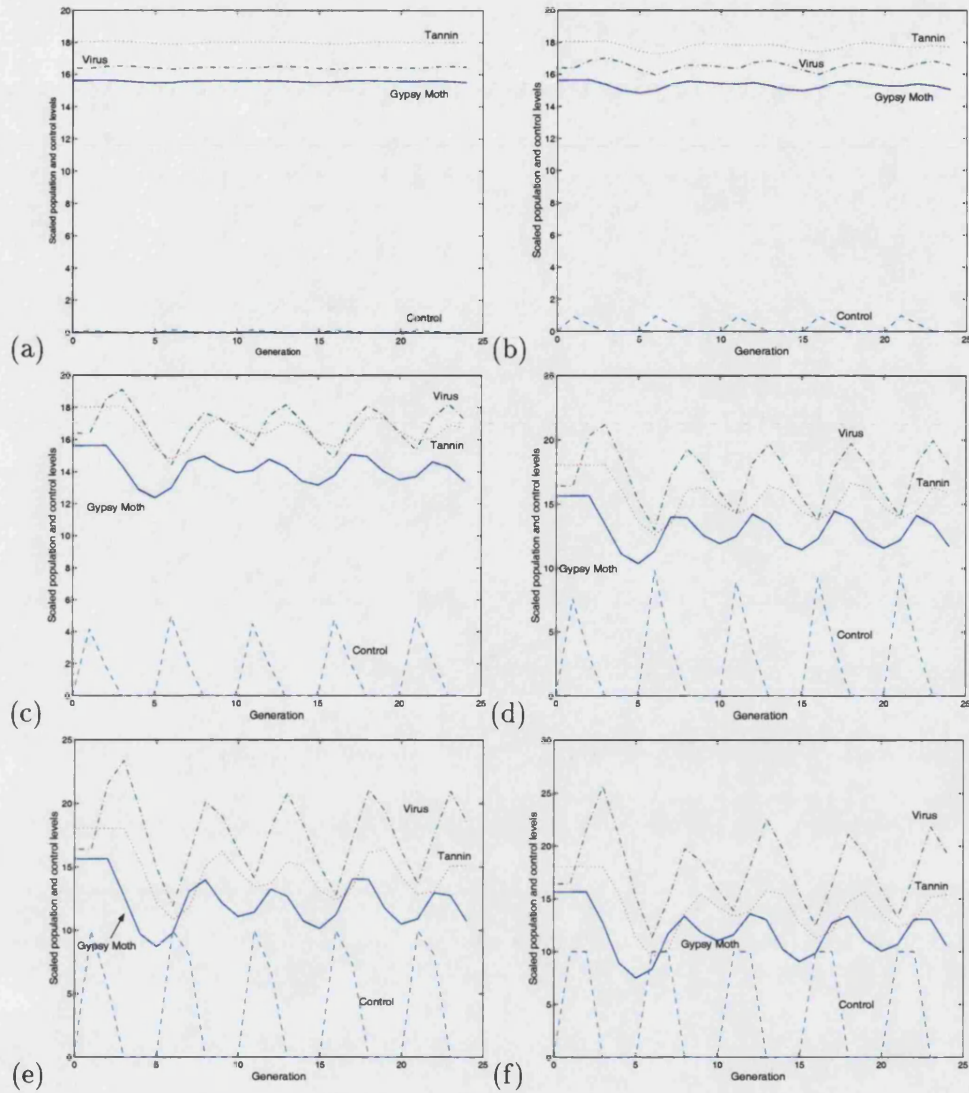
153
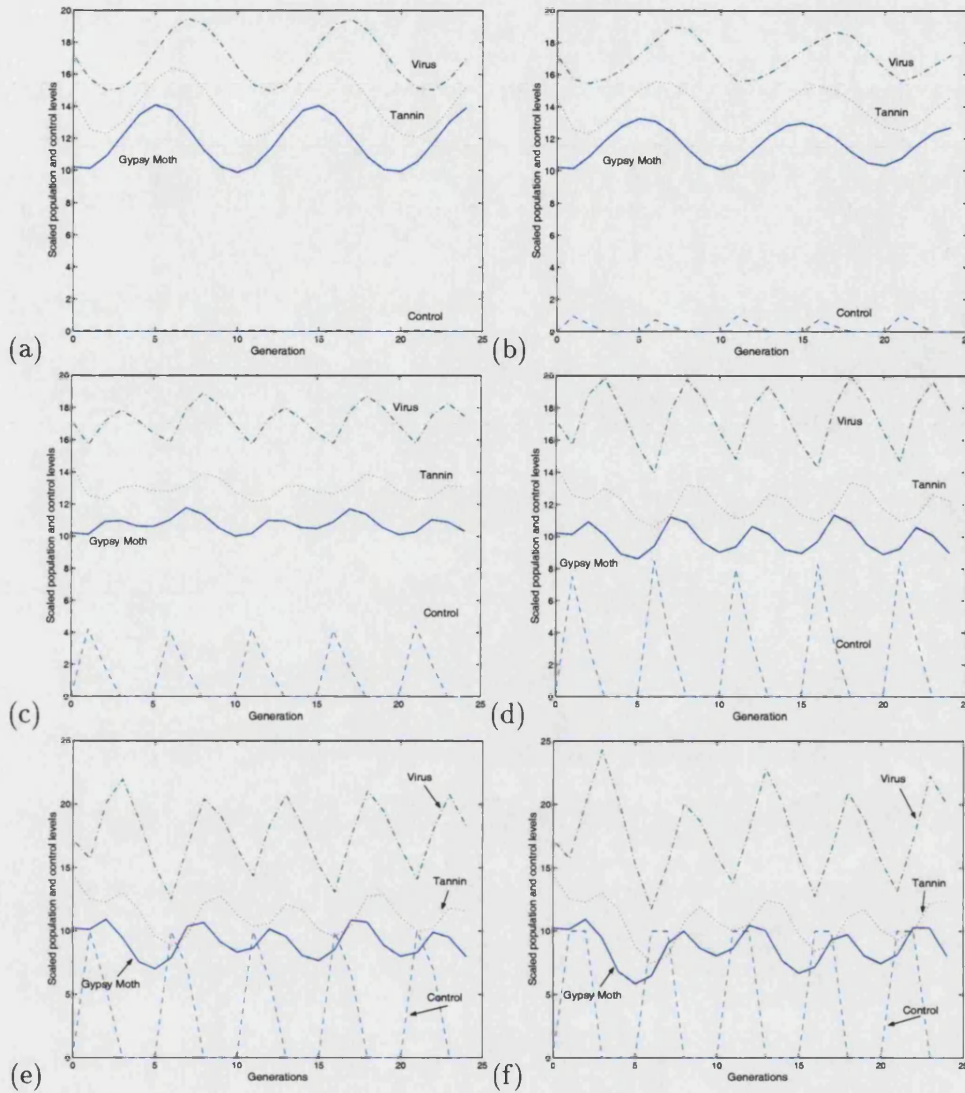
Figure 7-5: Plots show population levels over time with $A = 10$. Figure(a) cost of control, B=100, Figure(b) B=10, Figure(c) B=2, Figure(d) B=1, Figure(e) B=0.5, Figure(f) B=0.01. Parameters are $a = 6.0, r = 0.0001, c = 0.1, d = 0.067, q = 0.4, k = 3, b = 0.1, \lambda = 1.49, \sigma_v = 0.37, \sigma_t = 0.1, \rho = 0.01, \tau = 1.2$ with dispersal coefficients $\alpha = 100, \beta = 1200$ and $D = 10^{-6}$.

In Figures 7-5(a)&(b), the cost of the control is high, thus little control is used and the populations remain oscillatory, although a slight reduction in the fluctuations has occurred in Figure 7-5(b). From Figures 7-5(c)&(d), the reduction in cost of control has caused an increase in the use of control in the optimum strategy. We see that the

154

control is applied periodically in time. This has caused the populations to fluctuate more frequently in time but with less amplitude. The height at which gypsy moth populations reach is considerably less than seen in Figures 7-5(a)&(b). Further, we see in Figures 7-5(e)&(f), the use of control is increased. The application of control still remains periodic in time, varying from no control to the maximum use of control. The gypsy moth populations have reduced further, now with maximum levels only reaching as high as minimum levels when no control is applied. Also, we see that there has been no further increase in the number of fluctuations yet the amplitude of the fluctuation has grown with minimum levels significantly lower than seen in Figures 7-5(c)&(d).

Plotting the total cost against cost of control, the behaviour is similar to the steady state optimal control. We see a critical region ($B = 0.1 - 10$) where small reductions in the cost of control have a considerable effect on the total cost for the optimal solution. We point out that there is a difference in the total cost of the oscillatory optimal control compared with the steady state optimal control, which is slightly lower. This difference in total cost occurs over the whole range of B.
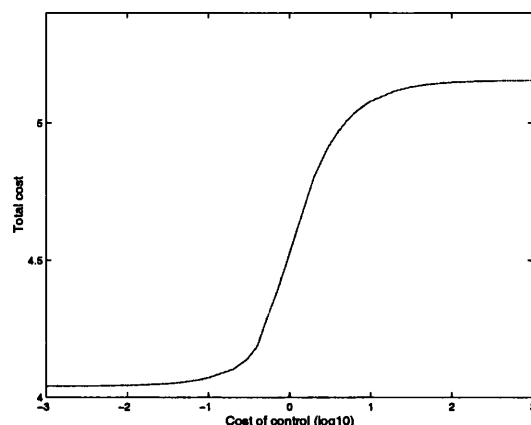

Figure 7-6: Plot shows the total cost against the cost of the control, B_n. Parameters are $A = 10$, $a = 6.0, r = 0.0001, c = 0.1, d = 0.067, q = 0.4, k = 3, b = 0.1, \lambda = 1.49, \sigma_v = 0.37, \sigma_t = 0.1, \rho = 0.01, \tau = 1.2$ with dispersal coefficients $\alpha = 100$, $\beta = 1200$ and $D = 10^{-6}$.

7.2.3   Case iii: Stable spatial patterning

We now consider an optimal control strategy for a spatially periodic environment. In this case, we use the function $\rho M_n(x)$ as the production rate of tannin as we find that there is no issue with convergence. Figures 7-7 & 7-8 show the behaviour of gypsy moth populations and the amount of control applied when the costs of control are low

and high (B=0.5, B=2).

In Figure 7-7(a), we see that for high cost of control, gypsy moth populations are reduced and begin to fluctuate over time. However, the spatial pattern remains the same, although the amplitude of the oscillation has decreased. We see from Figure 7-7(b) that the control is applied periodically in time. Also, levels of control marginally vary in time with troughs in synchrony, with the troughs of the gypsy moth population.
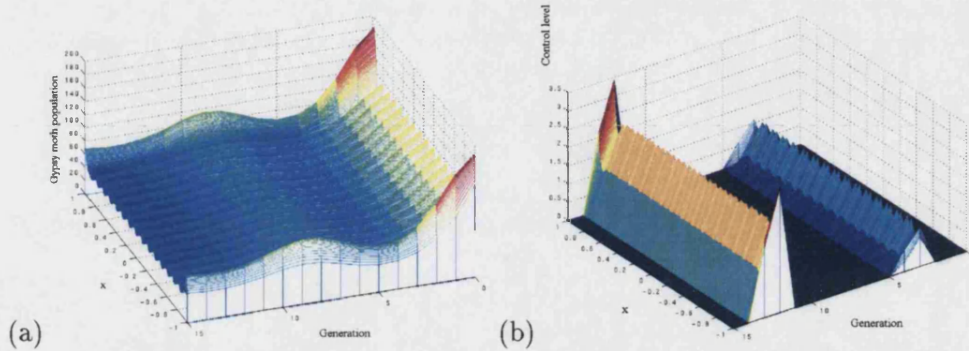
Figure 7-7: Plots show the optimal control applied to gypsy moth populations which are spatially patterned. Figure (a) shows the population of gypsy moths over time and space. Figure (b) shows the level of control applied over time and space. Parameters are $A = 10, B = 2.0, a = 6.0, r = 0.0001, c = 0.1, d = 0.067, q = 0.4, k = 3, b = 0.1, \lambda = 1.49, \sigma_v = 0.37, \sigma_t = 0.5, \rho = 0.6$ with dispersal coefficients $\alpha = 100, \beta = 30$ and $D = 10^{-6}$.

In Figure 7-8, we see similar reductions in gypsy moth populations for low cost of control. The gypsy moth population again begins to fluctuate in time with the spatial patterning remaining the same. Although for low cost of control, gypsy moth populations reduce further than in Figure 7-8(a). Similarly, control is periodic but now varies between no control to maximum levels. However, we observe that during this first application of control, an extra year of control occurs only if a trough in gypsy moth population is present. Therefore, the application of control is also periodic in space in that year. Interestingly, the control is applied at the troughs in gypsy moth populations rather than its peaks. This maybe due to the low gypsy moth population causing tannin levels to be lower thus making the gypsy moth more susceptible to virus infection.

(a)   (b)
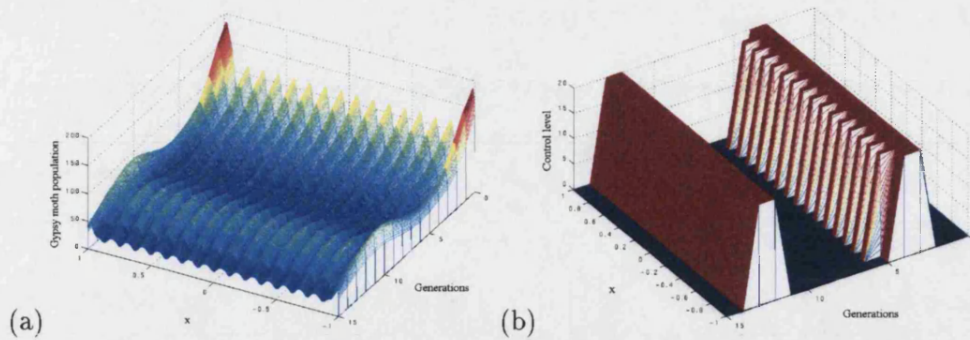
Figure 7-8: Plots show the optimal control applied to gypsy moth populations which are spatially patterned. Figure (a) shows the population of gypsy moths over time and space. Figure (b) shows the level of control applied over time and space. Parameters are $A = 10, B = 0.5, a = 6.0, r = 0.0001, c = 0.1, d = 0.067, q = 0.4, k = 3, b = 0.1, \lambda = 1.49, \sigma_v = 0.37, \sigma_t = 0.5, \rho = 0.6$ with dispersal coefficients $\alpha = 100, \beta = 30$ and $D = 10^{-6}$.

We again plot the total cost against cost of control. We see a slight increase in the critical region of cost of control to the interval $[0.01, 10]$ and also a rise in the value of the total cost. This is likely to be due to the change in function for the production rate of tannin.
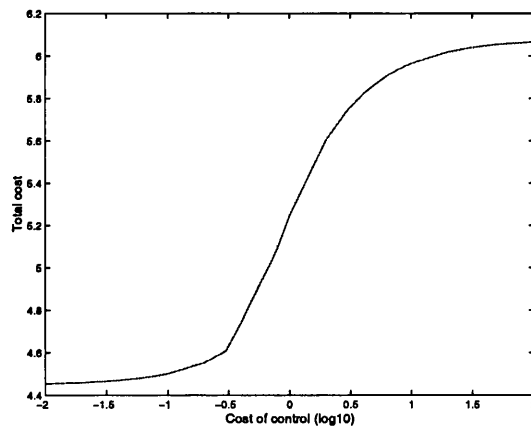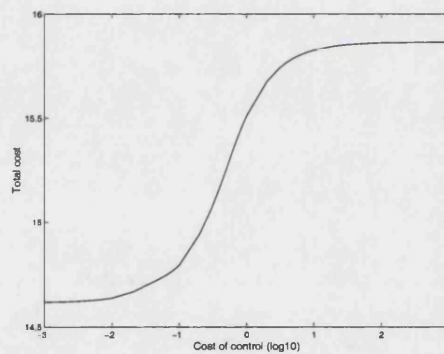

Figure 7-9: Plot shows the total cost against the cost of the control, B_n. Parameters are $A = 10, a = 6.0, r = 0.0001, c = 0.1, d = 0.067, q = 0.4, k = 3, b = 0.1, \lambda = 1.49, \sigma_v = 0.37, \sigma_t = 0.5, \rho = 0.6$ with dispersal coefficients $\alpha = 100, \beta = 30$ and $D = 10^{-6}$.

157

7.3 Summary and Discussion

In this chapter, we have solved an optimal control problem for a system of integrodifference equations. A bioeconomic model is formed with the objective to minimise costs in pest control of gypsy moths over a spatial domain. Currently, only optimal control for a single species exists for integrodifference models and this chapter has extended this theory to multiple species integrodifference model. We have shown the characterisation of an optimal control by finding the adjoint system. We have proved that an optimal control exists and that it is unique under the condition that the cost of control is sufficiently large.

Numerical simulations were presented to demonstrate optimal solutions for the three cases; stable spatially uniform steady states, spatially uniform but oscillatory in time and spatially patterned constant in time populations. For the spatially uniform stable steady state and the spatially uniform oscillatory populations, control was found to be added periodically in the optimal strategies. This caused fluctuations for the steady state case and a change in frequency and amplitude in fluctuations in the oscillatory case. As the cost of control became cheaper, this caused the populations to reduce. Also, the total cost of the optimal strategy reduced as the cost of control decreased. Furthermore, we found a range of the cost of control where a small reduction significantly decreases the total cost. However, outside this range the cost of control caused a negligible decrease when reduced.

Optimal control was also applied to a patchy gypsy moth population where populations were oscillatory in space and constant in time. It was found that the population levels reduced but remained periodic, however the amplitude of the oscillations did decrease. The control was added periodically, thus causing the populations to fluctuate in time. More interestingly, we found that for the cost of control $B = 0.5$, the first application of control occurred for 2 years in locations where gypsy moth populations were high and 3 years where gypsy moth populations were low. Therefore, an extra year of Gypchek was required to be applied periodically over the spatial domain in low gypsy moth population areas. This could be due to the higher probability of infection in these gypsy moth populations because of lower tannin levels.

Chapter 8

Conclusions and Future work

This thesis has presented a mathematical model to describe the tritrophic interactions of gypsy moths, NPV and tannin. There is strong evidence that tannin plays a critical role in the interaction of gypsy moths and NPV, and that tannin levels change depending on the plants defoliation due to gypsy moths. This study differs from previous research as it considers a dynamic system where gypsy moth populations, NPV and tannin levels are time dependent and their interactions cause changes in population levels. Earlier work had only considered either gypsy moth and NPV interactions without the influence of tannin or gypsy moth and NPV interactions at several different tannin levels held constant over time. The thesis also takes a different approach to model gypsy moth populations using discrete time difference equations rather than continuous time ODE's, used in previous studies.

In Chapter 3, we considered adapting previous gypsy moth modelling to include tannin as a dynamic variable. We found that the addition of tannin could cause a stabilisation effect on gypsy moth NPV interactions. It had previously been thought (Foster et al. 1992) that any inclusion of tannin was likely to produce a destabilising effect due to the decrease in susceptibility of gypsy moths to NPV infection caused by high tannin levels (Schultz et al. 1990). However, even with the inclusion of tannin, the typical behaviour of oscillatory population cycles that are found in the field, were also displayed in the model, as they were in Foster et al. (1992) model.

Chapter 4 extended gypsy moth modelling further by considering a discrete time approach, which is deemed to be more appropriate for modelling gypsy moths due to their distinct non-overlapping stages in their life cycle. From the discrete time model, we saw the same stabilisation phenomenon as discovered in Chapter 3. We also saw oscillatory cycles of populations that resembled the behaviour in the field. So the discrete modelling gave similar behaviour to the continuous time model and,

furthermore, matches the field data. Due to the life cycle of gypsy moths, the discrete time model more realistically reflects the gypsy moth population dynamics and forms the base model used in subsequent chapters.

We then considered whether spatial differences in population levels of gypsy moths can occur. In Chapter 6 we found that dispersal driven instabilities of a stable nontrivial steady state can result in spatial patterning. Moreover, cyclic populations may also result from dispersal driven instabilities. This occurs when NPV dispersal is small relative to gypsy moth dispersal whereas spatial patterning is formed when NPV dispersal is faster than gypsy moth dispersal. In field data, cyclic populations are observed, thus indicating that NPV dispersal is likely to be smaller than gypsy moth dispersal. Intuitively, since gypsy moths can travel long distances due to human intervention, then it is more likely that gypsy moths dispersal will be greater than NPV dispersal. Therefore, dispersal alone could be a reason for the large fluctuations found in gypsy moth population levels over time.

In addition, we have also looked at the optimal control of a bioeconomic model to control gypsy moth levels whilst minimising cost. This model is formed by summing a damage cost caused to the economy by gypsy moths together with the cost of using a biocontrol agent, Gypchek. In the nonspatial model in Chapter 5, we found that as the cost of the control reduced, so did the gypsy moth population and the total cost of the optimal solution. In stable populations, the optimal strategy was to apply control to reduce gypsy moth levels whilst not allowing the populations to fluctuate. In oscillatory populations, the optimal strategy was to dampen the oscillations by spraying Gypchek in years when virus populations were low. We also found a critical area for the cost of control where small reductions in cost of the control could significantly reduce the total economic cost. Thus, advancements in reducing the cost of the control using Gypchek can provide substantial savings in this range. Practical approaches for spraying Gypchek were considered and compared with the optimal strategy. It was found that although gypsy moth population levels were reduced, the methods were far from cost effective in comparison to the optimal control.

In Chapter 7, we considered a spatial bioeconomic model. We looked at the optimal control solution applied to three different environments of gypsy moth populations. We found that optimal strategies applied the biocontrol agent periodically. This caused stable steady state gypsy moth populations to fluctuate in time and oscillatory populations to fluctuate more frequently, but with less amplitude. In a patchy, environment control was also found to be applied periodically, causing the population to fluctuate in time and the amplitude in spatial oscillations to decrease. Also, in some cases, extra control was applied to gypsy moth populations in areas which were smaller in popu-

lation size than neighbouring areas. This is thought to be due to the higher infection rate of gypsy moths as a result of lower tannin levels in these areas.

In Chapter 6, we also studied the spread of gypsy moths and whether this spread can be reduced. We found that fast dispersing NPV may slow the gypsy moth wave speed. However, this reduction was small and only occurred when NPV over-dispersal was large. The reduction in speed is small mainly due to the low survival rate of NPV. We then look at reducing wave speed by the use of Gypchek as a barrier. We found that for extremely large quantities of spray over vast areas, gypsy moth wave speed could be drastically reduced and even stopped by the Gypchek barrier. Moreover, more practical applications still showed a reduction in gypsy moth wave speed with the reduction dependent on the exact quantity of spray used and how far ahead from the wave front the spraying was applied. Therefore, Gypchek may well be effective in the fight to control the advancing front of gypsy moths in combination with the current methods of mating disruption in the Slow-The-Spread project.

This thesis has progressed research in optimal control in bioeconomic models for hybrid systems. The bioeconomic model presented in Chapter 7 is specific for the dynamics of the gypsy moth model, however the optimal control technique can be applied to any set of integrodifference equations. Thus, in Chapter 7, we have extended a single species spatial optimal control problem to a multi-species optimal control problem where currently no published work exists in this area. Also in Chapter 6, we discovered that integrodifference systems differ to reaction diffusion systems when considering wave speeds in predator prey models. We found that, unlike a reaction diffusion system, a predator can reduce the wave speed of the prey in a integrodifference model if the predator advances faster than the prey and catches the prey wave front. This reduction in prey wave speed depends on the survival rate of the predator and how fast it disperses. This, however, is not possible in reaction diffusion models and it has been proven that a predator cannot reduce a prey's wave speed unless there is an Allee effect (Owen & Lewis 2001). But in integrodifference models, an Allee effect is not necessary to reduce prey wave speed thus this restriction is not required.

8.1   Future work

Chapter 5 and Chapter 7 presented an optimal control strategy to minimise the total cost in a bioeconomic model. The economic cost consisted of a damage cost caused by gypsy moths and the cost of spray to reduce gypsy moth numbers. The cost of damage was assumed to linearly increase with the amount of gypsy moths and the cost of control was assumed to increase quadratically with respect to the amount of control

required. However, other terms could be considered to make this more realistic. Other bioeconomic models have also considered this simplification and in order to make the models more realistic and practical, these cost functions need to be chosen based on available data. Also, the cost of damage and spray may vary each year depending on changes in the economy, land use and the cost of production of Gypchek.

Furthermore, the inclusion of space in Chapter 7 creates more variation. We may now see that costs of damage and spray could vary spatially, as some areas may suffer economically more than others from gypsy moth outbreaks and applying control in some areas may be more expensive. Further, the maximum application of control may vary spatially with reduced levels of spray in recreation or urban areas.

At present, virus control is the most common and effective method in the attempt to reduce gypsy moths and hence reduce the damage they cause. In the thesis, we have discussed the large costs involved, not only in damage, but also in the cost of controlling gypsy moths. However, more recent investigations have focused on controlling tree tannin levels. Gypchek works much more effectively when tree tannin levels are low. This is due to the reduction in susceptibility of gypsy moths to virus infection at high tannin levels. Hence, if a control strategy could reduce tannin then less Gypchek may be required to control gypsy moths. Although this work is at a preliminary stage, two enzymes have been identified that inhibit or promote tannin. Therefore, we can form an optimal control strategy seeking an optimal pair of solutions using the two controls, virus and tree tannin controls. A similar method, for seeking an optimal pair of controls in an ODE system has been investigated by (Joshi 2002). The advantage of controlling tannin would allow less virus spraying in urban areas reducing the irritating effect on humans.

162

Appendix

A.1 Routh-Hurwitz criteria for cubics

If J is a Jacobian matrix of a 3rd order system

$$J = \begin{pmatrix} J_{11} & J_{12} & J_{13} \\ J_{21} & J_{22} & J_{23} \\ J_{31} & J_{32} & J_{33} \end{pmatrix}.$$

then the characterisic polynomial of $det(J - \chi I)$ is the cubic expression

$$P(\chi) = \chi^3 + a\chi^2 + b\chi + c = 0.$$

The Routh-Hurwitz stability conditions for the cubic expression $P(\chi)$ are given by

$$a > 0, c > 0 \quad \text{and} \quad ab - c > 0. \tag{1}$$

From Chapter 3, section 3.1.3 the first two Routh-Hurwitz conditions give

$$b + \alpha + u + vH^* > 0 \tag{2}$$

$$\frac{d(W^*)^2 + k(a - b)}{k + W^*} u(b + \alpha) > 0 \tag{3}$$

As H^*, W^* and all parameters are positive then the conditions (2), (3) hold. Thus, the stability depends only on the third condition.

B.1 Bound for uniqueness proof in Chapter 5

For $a, b \epsilon \mathbb{R}$, then

$$0 \leq \frac{1}{2}(a+b)^2$$
$$-\frac{1}{2}a^2 - \frac{1}{2}b^2 \leq ab.$$

This provides a bound using in the uniqueness proof in Chapter 5.

B.2 Bound for uniqueness proof in Chapter 7

For functions $f_1(x), f_2(x) \epsilon L^2$, we have

$$0 \leq \int_\Omega \frac{1}{2}(f_1(x)+f_2(x))^2 dx < \infty$$
$$-\frac{1}{2}\int_\Omega f_1^2(x)dx - \frac{1}{2}\int_\Omega f_2^2(x)dx \leq \int_\Omega f_1(x)f_2(x)dx.$$

This provides a bound using in the uniqueness proof in Chapter 7.

Bibliography

Andersen, M. (1991), 'Properties of some density-dependent integrodifference equation population models', *Mathematical Biosciences* **104**, 135–157.

Anderson, R. M. & May, R. M. (1981), 'The population dynamics of microparasites and their invertebrate hosts', *Philosophical Transactions of the Royal Society of London, Series B* **291**, 452–524.

Bess, H. A. (1961), 'Population ecology of the gypsy moth, porthetria dispar (l.)', *Connecticut Agricultural Experiment Station Bulletin* **646**.

Bess, H. A., Spurr, S. H. & Littlefield, E. W. (1947), 'Forest site conditions and the gypsy moth', *Harvard Forest Bulletin* **22**, 56.

Bhat, M. G., Huffaker, R. G. & Lenhart, S. M. (1993), 'Controlling forest damage by dispersive beaver populations: Centralized optimal management strategy', *Ecological Applications* **3**(3), 518–530.

Bowers, R. G. & Begon, M. (1991), 'A host-host-pathogen model with free-living infective stages, applicable to microbial pest control', *Journal of Theoretical Biology* **148**, 305–329.

Campbell, R. W. (1981), The gypsy moth, Technical report, USDA.

Clark, C. (1976), *Mathematical Bioeconomics*, Wiley-Interscience, NY.

Clark, C. (1990), *Mathematical Bioeconomics: The Optimal Management of Renewable Resources*, 2nd edn, Wiley.

Clark, J. S. (1998), 'Why trees migrate so fast: confronting theory with dispersal biology and the paleorecord', *American Naturalist* **152**, 204–224.

Conway, E. D. (1984), Diffusion and predator-prey interaction: pattern in closed systems, *in* 'Partial differential equations and dynamical systems', Vol. 101 of *Res. Notes in Math.*, Pitman, Boston, MA, pp. 85–133.

D'Amico, V., Elkinton, J. S., Dwyer, G., Willis, R. B. & Montgomery, M. E. (1998), 'Foliage damage does not affect within-season transmission of an insect virus', *Ecology* **79**(3), 1104–1110.

DeBach, P. (1974), *Biological Control by Natural Enemies*, Cambridge University Press.

Doane, C. C. (1970), 'Primary pathogens and their role in the development of an epizootic in the gypsy moth', *Journal of Invertebrate Pathology* **15**, 21–33.

Dobson, A. P. (1985), 'The population dynamics of competition between parasites', *Parasitology* **91**, 317–347.

Dobzhansky, T. & Wright, S. (1943), 'Genetics of natural populations, x. dispersion rates in drosphila pseudoobscura', *Genetics* **28**, 304–340.

Dunbar, S. R. (1983), 'Travelling wave solutions of diffusive Lotka-Volterra equations', *J. Math. Biol.* **17**(1), 11–32.

Dwyer, G. (1991), 'The roles of density stage and patchiness in the transmission of an insect virus', *Ecology* **72**, 559–574.

Dwyer, G., Dushoff, J., Elkinton, J. S. & Levin, S. A. (2000), 'Pathogen-driven outbreaks in forest defoliators revisited: Building models from experimental data', *American Naturalist* **156**(2), 105–120.

Dwyer, G. & Elkinton, J. S. (1993), 'Using simple models to predict virus epizootics in gypsy moth populations', *Journal of Animal Ecology* **62**, 1–11.

Dwyer, G. & Elkinton, J. S. (1995), 'Host dispersal and the spatial spread of insect pathogens', *Ecology* **76**(4), 1262–1275.

Edel'man, N. M. (1963), 'Effect of the biochemical composition of food on growth changes in the physiological conditions of insects. questions of ecology', *Vysshaya Skkola* **7**, 211–213.

Elkinton, J. S., Healy, W. M., Buonaccorsi, J. P., Boettner, G. H., Hazzard, A. M., Smith, H. R. & Leibhold, A. M. (1996), 'Interactions among gypsy moth white footed mice and acorns', *Ecology* **77**(8), 2332–2342.

Evans, L. C. (1990), *Weak Convergence Methods for Nonlinear Partial Differential Equation(s)*, AMS, Providence.

Fisher, R. A. (1937), 'The wave of advance of advantageous genes', *Annals of Eugenics* **7**, 355–369.

Fister, R. (1997), 'Optimal control of harvesting in a predator-prey parabolic system', *Houston Journal of Mathematics* **23**(2), 341–355.

Foster, M. A., Schultz, J. C. & Hunter, M. D. (1992), 'Modelling gypsy moth-virus-leaf chemistry interactions: implications of plant quality for pest and pathogen dynamics', *Journal of Animal Ecology* **61**, 509–520.

Freedman, H. I. (1980), *Deterministic Mathematical Models in Population Biology*, Marcel-Dekker, NY.

Hackbusch, W. (1978), 'A numerical method for solving parabolic equations with opposite orientations', *Computing* **20**(3), 229–240.

Hallam, T. G. & Levin, S. A. (1986), *Mathematical Ecology: An Introduction*, Springer-Verlag, Berlin Heidelburg.

Hardin, D. P., Takáč, P. & Webb, G. F. (1988a), 'Asymptotic properties of a continuous-space discrete-time population model in a random environment', *J. Math. Biol.* **26**(4), 361–374.

Hardin, D. P., Takáč, P. & Webb, G. F. (1988b), 'A comparison of dispersal strategies for survival of spatially heterogeneous populations', *SIAM J. Appl. Math.* **48**(6), 1396–1423.

Hardin, D. P., Takáč, P. & Webb, G. F. (1990), 'Dispersion population models discrete in time and continuous in space', *J. Math. Biol.* **28**(1), 1–20.

Hassell, M. P. (1978), *The dynamics of arthropod predator-prey systems*, Vol. 13 of *Monographs in Population Biology*, Princeton University Press, Princeton, N.J.

Hastings, A. (1997), *Population Biology: Concepts and Models*, Springer-Verlag, NY.

Hochberg, M. E., Hassell, M. P. & May, R. M. (1990), 'The dynamics of host-parasitoid-pathogen interactions', *American Naturalist* **135**, 74–94.

Hochberg, M. E. & Holt, R. D. (1990), 'The coexistence of competing parasites. 1. the role of cross-species infection', *American Naturalist* **136**, 517–541.

Holt, R. D. & Pickering, J. (1985), 'Infectious disease and species coexistence: a model in lokta-volterra form', *American Naturalist* **126**, 196–211.

Hough, J. A. & Pimental, D. (1978), 'Influence of host foliage on development, survival, and fecundity of gypsy moth', *Environmental Entomology* **7**, 97–102.

Joshi, H. R. (2002), 'Optimal control of an HIV immunology model', *Optimal Control Appl. Methods* **23**(4), 199–213.

Joshi, H. R., Lenhart, S. M. & Gaff, H. (in press), 'Optimal harvesting in an integro-difference population model', *Discrete and Continuous Dynamical Systems* .

Jung, E., Lenhart, S. & Feng, Z. (2002), 'Optimal control of treatments in a two-strain tuberculosis model', *Discrete Contin. Dyn. Syst. Ser. B* **2**(4), 473–482.

Kaya, H. K. (1976), *Insect pathogens in natural and microbial control of forest defoliators*, Academic Press Inc. NY, chapter Perspectives in Forest Entomology, pp. 251–263.

Keating, S. T., Hunter, M. D. & Schultz, J. C. (1990), 'Leaf phenolic inhibition of the gypsy moth nuclear polyhedrosis virus: the role of the polyhedral inclusion body aggregation', *Journal of Chemical Ecology* **16**, 1445.

Keating, S. T. & Yendol, W. G. (1987), 'Influence of selected host plants on gypsy moth larval mortality caused by a baculovirus', *Environmental Entomology* **16**, 459–462.

Keating, S. T., Yendol, W. G. & Schultz, J. C. (1988), 'Relationship between susceptibility of gypsy moth (lepidoptera: Lymantriidae) to a baculovirus and host-plant foliage constituents', *Environmental Entomology* **17**, 952–958.

Kot, M. (1992), 'Discrete-time travelling waves: ecological examples', *J. Math. Biol.* **30**(4), 413–436.

Kot, M. (2002), 'Do invading organisms do the wave?', *Can. Appl. Math. Q.* **10**(1), 139–170.

Kot, M., Lewis, M. A. & van den Driessche, P. (1996), 'Dispersal data and the spread of invading organisms', *Ecology* **77**(7), 2027–2042.

Kot, M. & Schaffer, W. M. (1986), 'Discrete-time growth-dispersal models', *Math. Biosci.* **80**(1), 109–136.

Lauterschlager, R. A. & Podewaite, J. D. (1977), 'Passage of infectious nuclear polyhedrosis virus through the alimentary tracts of two small mammal predators of the gypsy moth, lymantria dispar', *Environmental Entomology* **6**, 737–738.

Lenhart, S. & Liang, M. (2000), 'Bilinear optimal control for a wave equation with viscous damping', *Houston Journal of Mathematics* **26**, 575–595.

Lenhart, S. M. & Bhat, M. G. (1992), 'Application of distributed parameter control model in wildlife damage management', *Mathematical Models and Methods in Applied Sciences* **2**(4), 423–439.

Levin, S. A. (1992), 'The problem of pattern and scale in ecology', *Ecology* **73**, 1943–1967.

Levin, S. A. & Segel, L. A. (1976), 'Hypothesis for the origin of planktonic patchiness', *Nature* **259**, 659.

Lewis, M. A. (1997), *Spatial Ecology: The role of space in population dynamics and interspecific interactions*, Princeton University Press, chapter Variability, patchiness, and jump dispersal in the spread of an invading population, pp. 46–69.

Li, X. & Yong, J. (1995), *Optimal Control Theory for Infinite Dimensional Systems*, Birkhauser.

Liang, M. (1999), 'Bilinear optimal control of a wave equation', *Mathematical Models and Methods in Applied Sciences* **9**, 45–68.

Liebhold, A. M., Halverson, J. & Elmes, G. (1992), 'Quantitative analysis of the invasion of gypsy moth in north america', *Journal of Biogeograph* .

Lions, J. L. (1971), *Optimal control of systems governed by partial differential equations*, Springer-Verlag, New York.

Ludwig, D. (1974), *Stochastic Population Theories*, Springer-Verlag, Heidelberg.

Mackas, D. L. & Boyd, C. M. (1979), 'Spectral analysis of zooplankton spatial hetrogeneity', *Science* **204**, 62–64.

Macki, J. & Strauss, A. (1982), *Introduction to Optimal Control Theory*, Springer-Verlang.

May, R. M. (1976), *Theoretical Ecology Principles and Applications*, Saunders PA Blackwell Oxford.

Murray, J. D. (2002), *Mathematical biology. I*, Vol. 17 of *Interdisciplinary Applied Mathematics*, third edn, Springer-Verlag, New York. An introduction.

Murray, J. D. (2003), *Mathematical biology. II*, Vol. 18 of *Interdisciplinary Applied Mathematics*, third edn, Springer-Verlag, New York. Spatial models and biomedical applications.

Murray, K. D. & Elkinton, J. S. (1989), 'Environmental contamination of egg mass as major component of transgenerational transmission of gypsy moth nuclear polyhedrosis virus (ldmnpv)', *Journal of Invertebrate Pathology* **53**, 324–334.

Neubert, M. G. (2003), 'Marine reserves and optimal harvesting', *Ecology Letters* **6**, 843–849.

Neubert, M. G., Kot, M. & Lewis, M. A. (1995), 'Dispersal and pattern formation in a discrete-time predator-prey model', *Theoretical Population Biology* **48**, 7–43.

Nicholson, A. J. & Bailey, V. A. (1935), 'The balance of animal populations', *Proceedings of the Zoological Society of London* **3**, 551–598.

Okubo, A. (1980), *Diffusion and ecological problems: mathematical models*, Vol. 10 of *Biomathematics*, Springer-Verlag, Berlin. An extended version of the Japanese edition, *Ecology and diffusion*, Translated by G. N. Parker.

Owen, M. R. & Lewis, M. A. (2001), 'How predation can slow, stop or reverse a prey invasion', *Bulletin of Mathematical Biology* **63**(4), 655–684.

Regniere, J. (1984), 'Vertical transmission of diseases and population dynamics of insects with discrete generations: a model', *Journal of Theoretical Biology* **107**, 287–301.

Renshaw, E. (1991), *Modelling Biological Population in Space and Time*, Cambridge University Press.

Ricker, W. E. (1954), 'Stock and recruitment', *Journal of the Fisheries Research Board of Canada* **11**, 559–623.

Rockafellar, R. T. (1970), *Convex Analysis*, Princeton.

Rossiter, M. C., Schultz, J. C. & Baldwin, I. T. (1988), 'Relationships among defoliation, red oak phenolics, and gypsy moth growth and reproduction', *Ecology* **69**, 267–277.

Schultz, J. C., Foster, M. A. & Montgomery, M. E. (1990), *Population Dynamics of Forest Insects*, Intercept Ltd, Andover, chapter Host-plant-mediated impacts of baculovirus on gypsy moth populations.

Segel, L. A. & Jackson, J. L. (1972), 'Dissipative structure: An explanation and an ecological example', *Journal of Theoretical Biology* **37**, 545–559.

Segel, L. A. & Levin, S. A. (1976), Application of nonlinear stability theory to the study of the effects of diffusion on predator-prey interactions, *in* 'Topics in statistical mechanics and biophysics: a memorial to Julius L. Jackson', Amer. Inst. Phys., New York, pp. 123–152. AIP Conf. Proc., No. 27.

Sethi, S. P. & Thompson, G. L. (2000), *Optimal Control Theory: Application to Management Science and Economics*, Kluwer.

Shapiro, M., Presler, H. K. & Robertson, J. L. (1987), 'Enhancement of baculovirus activity on gypsy moth (lepidoptera: Lymantriidae) by chitinase', *Journal of Economic Entomology* **80**, 1113–1116.

Skellam, J. G. (1951), 'Random dispersal in theoretical populations', *Biometrika* **38**, 196–218.

Taylor, R. A. J. (1978), 'The relationship between density and distance of dispersing insects', *Ecological Entomology* **3**, 63–70.

Turing, A. (1952), 'The chemical basis of morphogenesis', *Philosofical Trans Royal Society London B* **237**, 37–72.

Van Den Bosch, F., Hengeveld, R. & Metz, J. A. J. (1992), 'Analyzing the velocity of animal range expansion', *Journal of Biogeography* **19**(2), 135–150.

Veit, R. R. & Lewis, M. A. (1996), 'Dispersal, population growth and the allee effect: Dynamics of the house finch invasion of eastern north america', *The American Naturalist* **148**(2), 255–274.

Wade, W. R. (2000), *An Introduction to Analysis*, Prentice Hall.

Weinberger, H. F. (1978), Asymptotic behavior of a model in population genetics, *in* 'Nonlinear partial differential equations and applications (Proc. Special Sem., Indiana Univ., Bloomington, Ind., 1976–1977)', Springer, Berlin, pp. 47–96. Lecture Notes in Math., Vol. 648.

White, K. A. J. & Wilson, K. (1999), 'Modelling density-dependent resistance in insect-pathogen interactions', *Theoretical Population Biology* **56**, 163–181.

Woods, S. A. & Elkinton, J. S. (1987), 'Bimodal patterns of mortality from nuclear polyhedrosis virus in gypsy moth (lymntria dispar) populations', *Journal on Invertebrate Pathology* **50**, 151–157.

Woods, S. A., Elkinton, J. S. & Podgewaite, J. D. (1989), 'Acquisition of nuclear polyhedrosis virus from tree stems by newly emerged gypsy moth (lepidoptera: Lymantriidae) larvae', *Enviromental Entomology* **18**, 298–301.